Annual Report 2022

Oregon State University
College of Forestry

Swiss Needle Cast Cooperative

Oregon State University | College of Forestry

Members of the Swiss Needle Cast Cooperative

Cascade Timber Consulting

Greenwood Resources, Inc. Lewis & Clark Tree Farms, LLC

Oregon Department of Forestry

Starker Forests

Stimson Lumber

USDA Forest Service

Weyerhaeuser Corporation

Swiss Needle Cast Cooperative Staff

Dave Shaw – Director and Associate Professor of Forest Health

Adam Carson – Associate Director and Faculty Research Assistant

SNCC Income Sources and Expenditures: 2022

Income	
Membership dues	*84,000*
Oregon State Legislature	*95,000*
Carry-over	*88,873*
Total 2022 Income	**$267,873**
Expenditures	
Salaries and wages	*36,539*
Travel	*3,819*
Operating expenses	*16,464*
Materials and Supplies	*0*
Indirect Costs (@17.5%)	*9,944*
Total 2022 Expenditures	**$66,766**
Balance	**$201,107**

SNCC Background and Organization

A major challenge to intensive management of Douglas fir in Oregon and Washington is the current Swiss needle cast (SNC) epidemic. Efforts to understand the epidemiology, symptoms, and growth losses from SNC have highlighted gaps in our knowledge of basic Douglas-fir physiology, growth, and silviculture. The original mission of the Swiss Needle Cast Cooperative (SNCC), formed in 1997, was broadened in 2004 to include research aiming to ensure that Douglas-fir remains a productive component of the Coast Range forests. The SNCC is located in the Department of Forest Engineering, Resources and Management within the College of Forestry at Oregon State University. The Membership is comprised of private, state, and federal organizations. Private membership dues are set at a fixed rate. An annual report, project reports, and newsletters are distributed to members each year. Our objective is to carry out projects in cooperation with members on their land holdings.

SNCC Mission

To conduct research on enhancing Douglas-fir productivity and forest health in the presence of Swiss needle cast and other diseases in coastal forests of Oregon and Washington.

SNCC Objectives

(1) Understand the epidemiology of Swiss needle cast and the basic biology of the causal fungus, *Nothophaeocryptopus gaeumannii*.

(2) Design silvicultural treatments and regimes to maximize Douglas-fir productivity and ameliorate disease problems in the Coast Range of Oregon and Washington.

(3) Understand the growth, structure, and morphology of Douglas-fir trees and stands as a foundation for enhancing productivity and detecting and combating various diseases of Douglas-fir in the Coast Range of Oregon and Washington.

Oregon State University

Department of Forest Engineering, Resources and Management
Oregon State University
216 Peavy Forest Science Complex
Corvallis, Oregon 97331

P 541-737-4952
F 541-737-4316
ferm.forestry.oregonstate.edu

2/16/2023

To: Swiss Needle Cast Cooperative Members
From: David Shaw, Director, SNCC
Re: Annual Report

Dear SNCC Membership,

Thanks again for your support for the Swiss Needle Cast Cooperative. I believe we are making a significant contribution to our understanding and management of Swiss needle cast. The Coop is in a state of transition; Gabi is now working for the Oregon Department of Forestry as the state Forest Pathologist, and we have hired Adam Carson as our new SNCC Faculty Research Assistant. Adam began work January 1, 2023, and is catching on quickly.

I will be stepping down June 30, 2023 (and retiring at the end of the year) and Jared LeBoldus will be taking over as the Director of the SNCC. Jared has established an exceptional forest pathology laboratory split between the Department of Forest Engineering, Resources, and Management (FERM) and the Department of Botany and Plant Pathology (BPP). The SNCC will remain within the College of Forestry, and Adam is a FERM appointed FRA.

We saved significant funds in 2022 because we went the entire year without an FRA. Luckily, remeasurement of the SNCC Coastal Research and Monitoring Plot Network was not scheduled for 2022, but we also delayed implementing the spore dispersal project. The coop will have a bit more room for additional research due to this savings. We look forward to 2023 and Adam will be busy. We plan to re-install the Cascades SNC Monitoring plot network this spring/early summer, restart the spore dispersal study with collaboration from an international forest pathologist, and begin remeasurement of the SNC Coastal Research and Monitoring Plot Network in the fall.

It has been a honor to be Director of the SNCC, and a real joy to work with on-the-ground foresters to determine research needs and continue inquiry into this complex disease of Douglas-fir. I feel the coops are unique because foresters interact with scientists directly.

Sincerely,

David C. Shaw

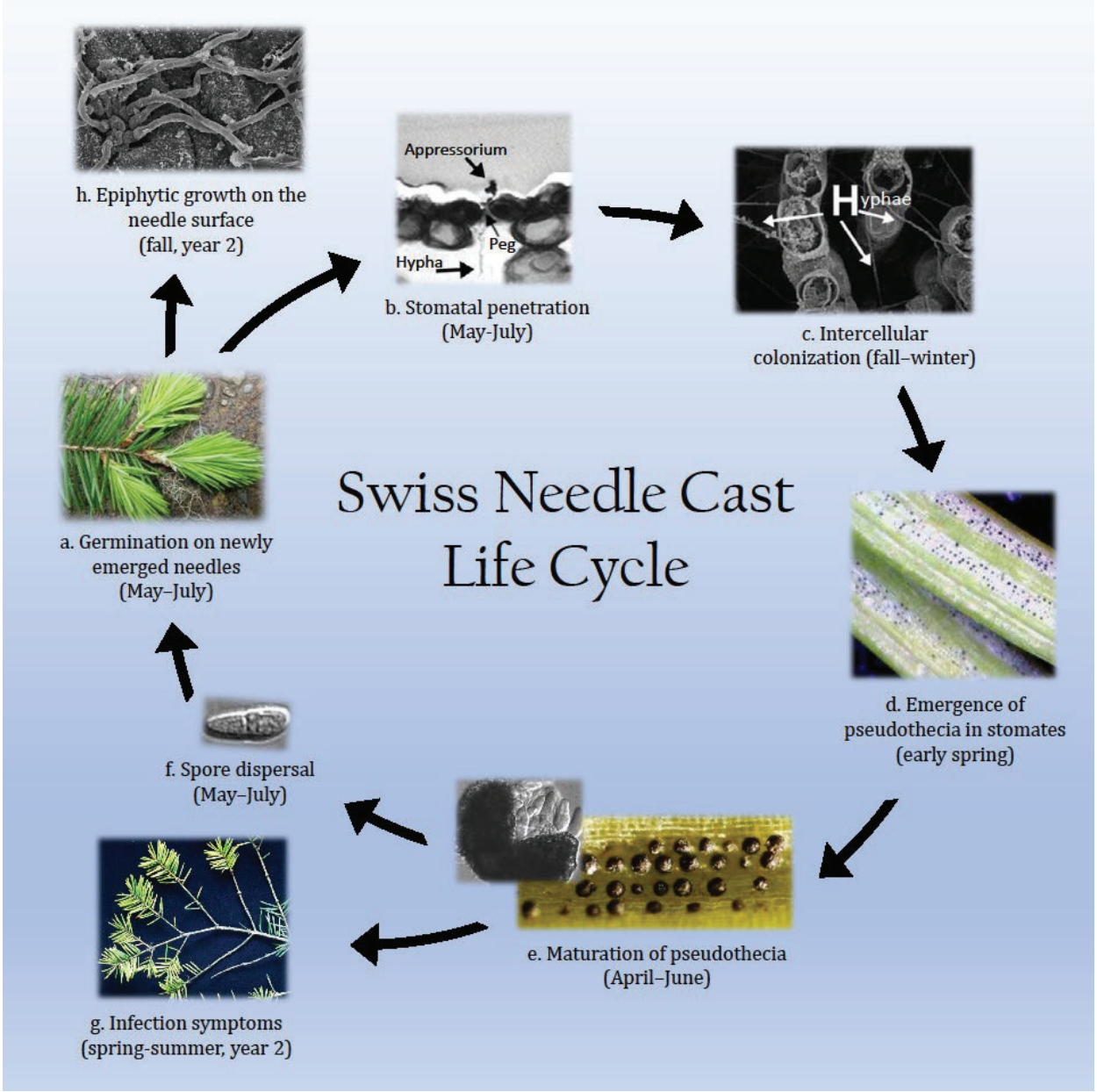

Spore dispersal during humid and wet weather begins the life cycle of *Nothophaeocryptopus gaeumannii*. New infections occur primarily on first-year (current year) needles and coincides with bud break and shoot elongation between May and July (a). Upon contacting a stoma, the germinating ascospore produces an appressorium from which a penetration peg is formed leading to needle penetration via the stomatal opening (b). The intercellular tissue of the needle is colonized in the fall and winter (c) and gives rise to pseudothecia, which can begin to emerge in the early spring depending on geographic location and environmental conditions (d). The fruiting bodies mature throughout the spring (e) and release ascospores between May and July (possibly into August and September) (f). Symptoms of infection can arise in second year (1-year-old) needles and older (g) and include premature needle loss (due to stomatal occlusion from pseudothecia), chlorotic foliage, and thin crowns. During the fall of the second year, epiphytic hyphae emerge from the base of pseudothecia (h) and grow along the surfaces of the needles. This epiphytic growth can result in the penetration of unoccupied stomata and might aid in expanding intercellular colonization. The development of *N. gaeumannii* within needles and the timing of pseudothecia development varies depending on geographic location, winter temperature, and periods of leaf wetness.

2022 Swiss Needle Cast Aerial Survey

Gabriela Ritóková and Harold Stevens

Oregon Department of Forestry

Survey procedures:

The observation plane flew at 1,500 to 2,000 feet above the terrain, following north-south lines separated by 2 miles. Observers looked for areas of Douglas-fir forest with obvious yellow to yellow-brown foliage, a symptom of Swiss needle cast (SNC). Patches of forests with these symptoms (patches are referred to as polygons) were sketched onto computer touchscreens displaying topographic maps or ortho-photos and the position of the aircraft. Each polygon was classified for a degree of discoloration as either "S" (severe) or "M" (moderate). Polygons classified as "S" had very sparse crowns and brownish foliage, while those classified as "M" were predominantly yellow to yellow-brown foliage with slightly denser crowns than those classified as "S". The survey area extended from the Columbia River in Oregon south to the north border of Port Orford, and from the coastline eastward until obvious symptoms were no longer visible.

Oregon utilized the national standard Digital Mobile Sketch Mapper for the SNC survey in 2022. The system syncs the data directly to a national database housed in the USDA Forest Service and makes for an easily consumable and robust system for collecting aerial survey data. With this new system, the area is recorded in much the same way as the previous digital system but incorporates some important changes, one being the metric used to record survey information. For defoliators such as SNC, we gain the area of the treed area affected in addition to the intensity of defoliation. This means that we can now record the intensity (severe or moderate) and the amount of the stand/polygon/area of interest that has damage. This is very useful for mixed stands with host and non-host species.

Results:

The survey was flown on June 1, 2, and 8, 2022, and covered 3,692,653 acres in the Oregon Coast Range (figure 1). Bud break was later than normal because of colder weather conditions, but the survey was delayed until much later than planned because of a staffing shortage, technical and administrative difficulties related to the aircraft, and contract delays. Despite this, symptoms remained visible to observers well after bud-break and into June. Despite this, symptoms remained visible to observers well after bud-break and into June.

The survey showed an increase in the area of forest with symptoms of Swiss needle cast compared to the previous 5 years, reaching an all-time high with 657,376 acres of Douglas-fir forests with obvious symptoms of Swiss needle cast (figure 2). As has been the case for the past several years, the easternmost area with obvious SNC symptoms was approximately 28 miles inland from the coast in the Highway 20 corridor, but most of the area with symptoms occurred within 18 miles of the coast. Figures 3 and 4 show the trend in damage from 1996 through 2022.

The Swiss needle cast aerial survey provides a conservative estimate of damage because observers can map only those areas where disease symptoms have developed enough to be visible from the air. We know Swiss needle cast occurs throughout the survey area, but discoloration often is not severe enough to enable aerial detection. The total area of forest affected by Swiss needle cast is far greater than

indicated by the aerial survey. The aerial survey does, however, provide a reasonable depiction of the extent of moderate and severe damage and coarsely documents trends in damage over time.

Acknowledgements:

The survey was conducted by the Oregon Department of Forestry Forest Health and Air Operations sections and was funded by the Oregon State University Swiss Needle Cast Cooperative, the USDA Forest Service Forest, and the Oregon Department of Forestry. Dan McCarron (ODF) piloted the plane. Christine Buhl (ODF) is the survey coordinator and primary observer. Other aerial observers were Sarah Navarro (USFS) and Gabriela Ritokova (ODF).

Additional Notes:

We appreciate any information regarding the accuracy or usefulness of the maps. If you have a chance to look at some of the mapped areas on the ground, please let us know what you observe. Please call Gabi Ritokova (503-978-2404) or Harold Stevens (503-302-4259) if you have questions, suggestions, or comments.

The GIS data and a .pdf file can be accessed via the ODF web page at:
http://tinyurl.com/ODF-ForestHealth

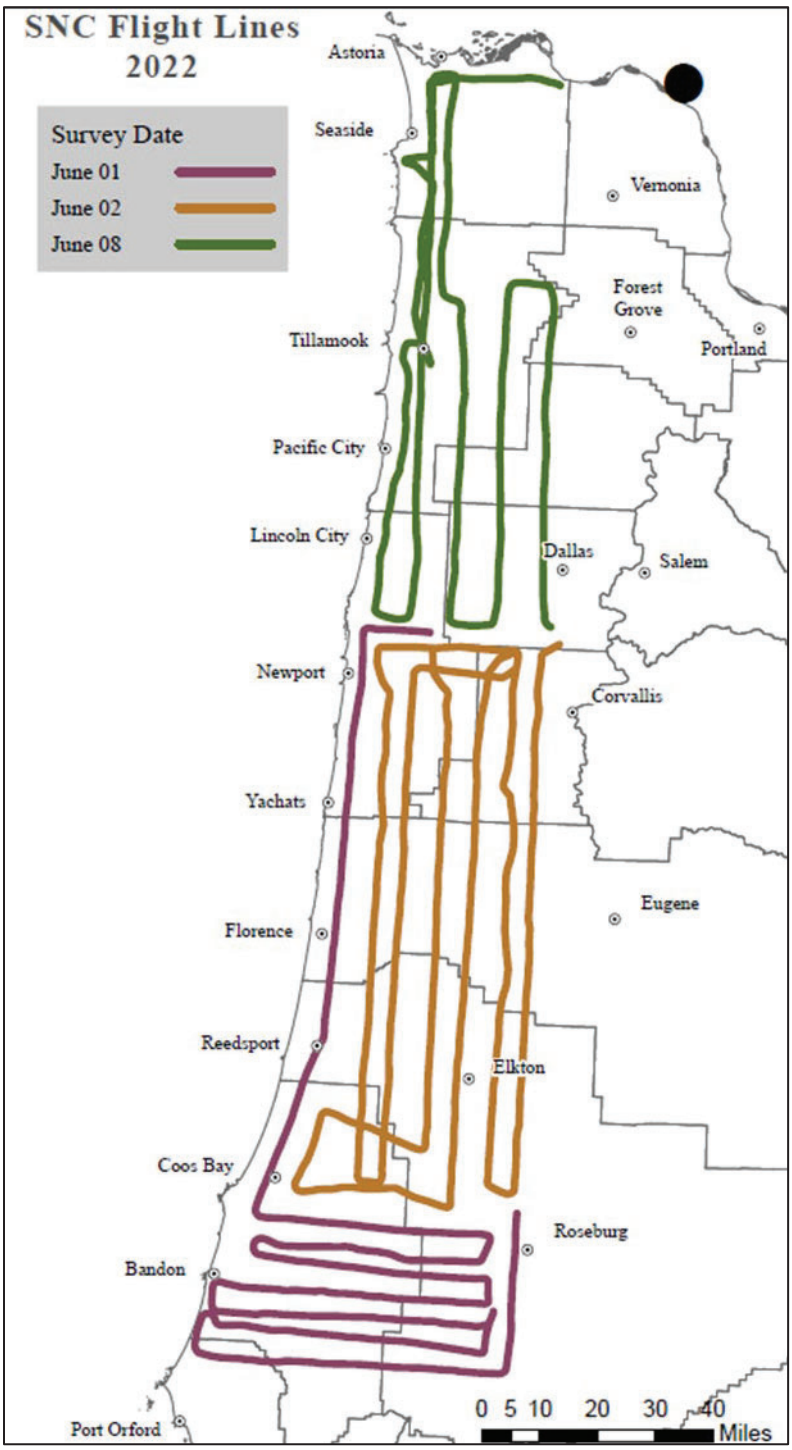

Figure 1. Area surveyed for Swiss needle cast symptoms, 2022. Flight lines are approximately two miles apart.

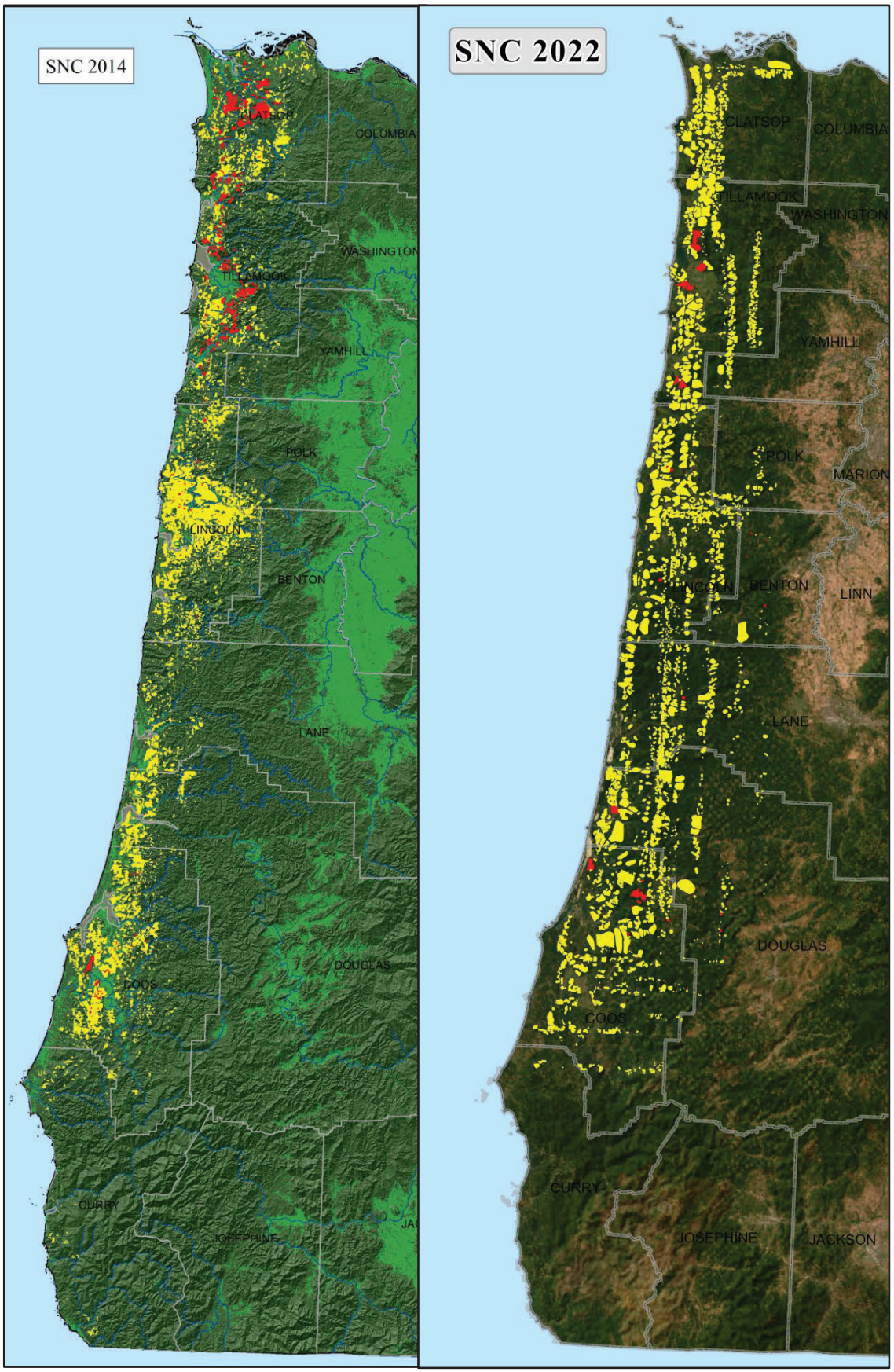

Figure 2. Areas of Douglas-fir forest with symptoms of Swiss Needle Cast detected in the 2014 and 2022 aerial surveys, Coast Range, Oregon.

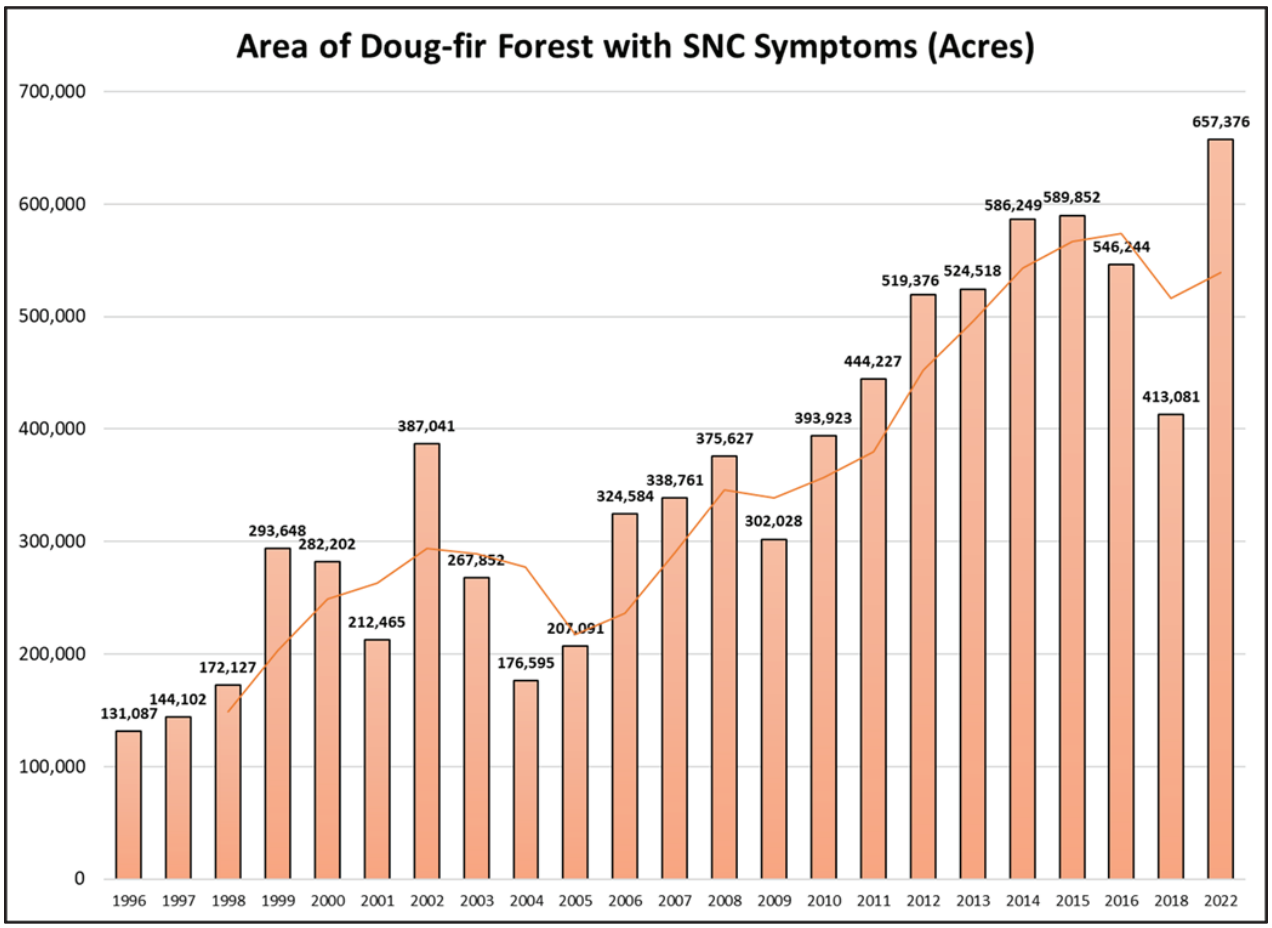

Figure 3. Area of Douglas-fir forest in western Oregon with symptoms of Swiss needle cast detected during aerial surveys conducted in April-June, 1996-2022. Trend line is 3-year rolling average. Coast Range, Oregon.

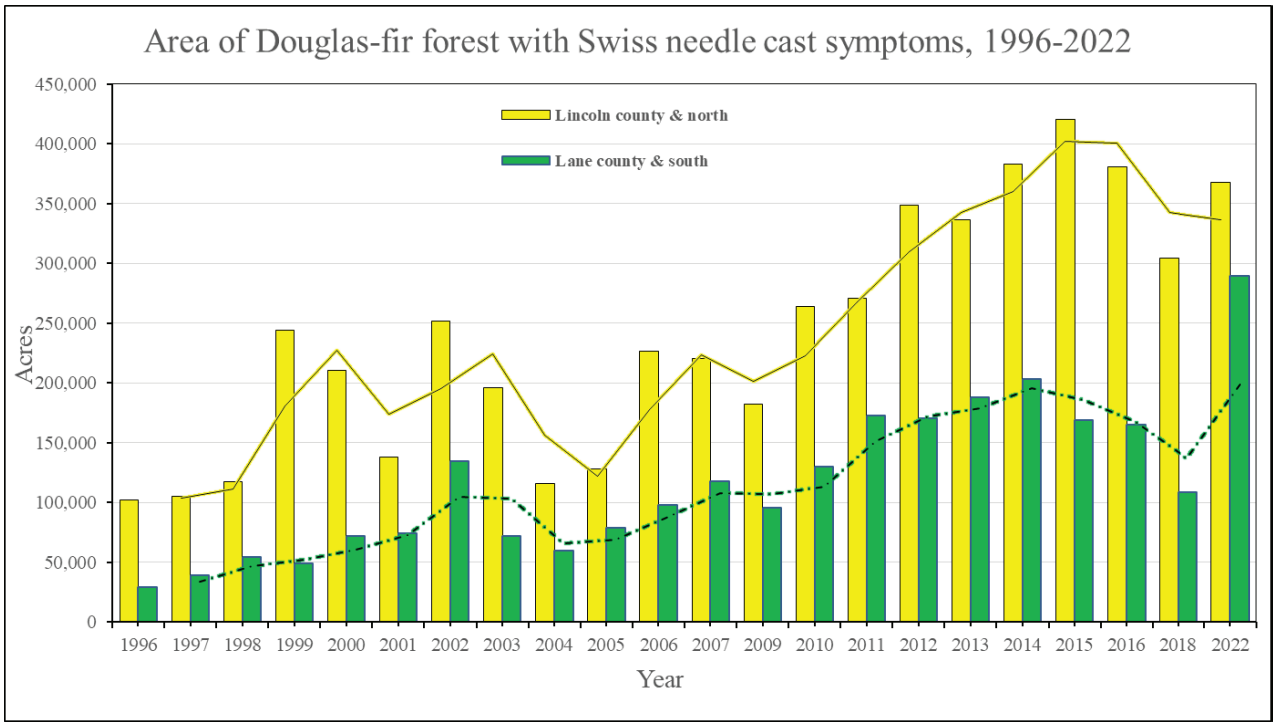

Figure 4. Area of Douglas-fir forest in western Oregon with symptoms of Swiss needle cast detected during aerial surveys conducted in April-June, 1996-2022; north and south halves of survey area. Trend line is 3-year rolling average. Coast Range, Oregon.

Western Washington Swiss Needle Cast Aerial and Ground Surveys, 2021 - 2022

Swiss needle cast is a native fungal foliar disease of Douglas-fir, often associated with Pacific NW coastal forests. Impacts of infection may include:

- Discoloration
- Premature needle loss
- Reduced growth
- Alteration of wood properties
- Stand structure and forest development changes

Discolored yellow-brown Douglas-fir stand (left) and normal-colored dark-green Douglas-fir stand (right). Lighter trees scattered throughout are red alder.

Aerial Survey

- Completed May 2022
- 2.0 million acres surveyed
- 115,000 acres displaying symptoms were mapped, representing almost 6% of the total area surveyed
- Acreages mapped are within the range of previous measurements
- Aerial surveys detect discoloration in trees, not necessarily SNC severity or impacts

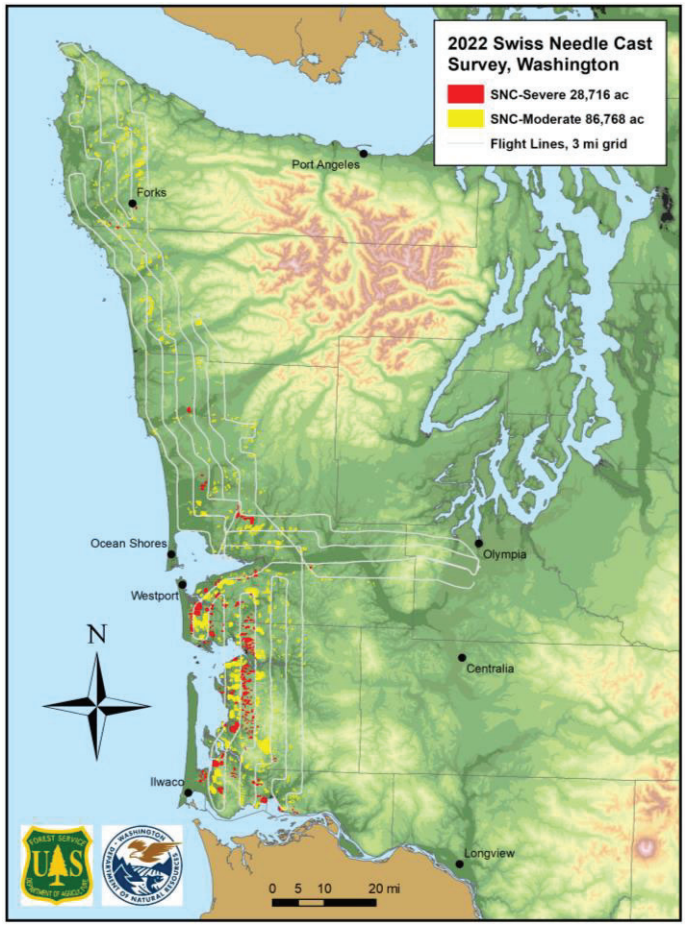

Map of 2022 Swiss needle cast aerial survey data.

Ground Survey

- Conducted spring 2021 & spring 2022
- Assessed 128 ground plots, representing over 3 million acres, along the coast and in the NW region
- In the coastal region, similar or lower needle retention and SNC fungal counts were measured compared to previous observations
- SNC fungal counts and needle retention measurements were higher in the NW region than in the coastal region
- Correlations between needle retention and fungal counts were inconsistent, possibly signifying other stressors may contribute to needle loss

Surveys Conducted by:

Washington Department of Natural Resources, USDA Forest Service, and Washington Department of Fish and Wildlife

Western Washington Swiss Needle Cast Aerial and Ground Survey, 2021-2022

Rachel Brooks[1], Dan Omdal[1], Isaac Davis[1], Glenn Kohler[1], Justin Hof[2], Marty Kimbrel[3], Connie Okasaki[4]

[1]Washington Department of Natural Resources, Forest Health Program, Olympia, WA
[2]USDA Forest Service, Forest Health Protection, Sandy, OR
[3]Washington Department of Fish and Wildlife, Olympia, WA
[4]University of Washington, Seattle, WA

Abstract

Swiss needle cast (SNC; caused by the native fungus *Nothophaeocryptopus gaeumannii*) is a foliar disease of Douglas-fir (*Pseudotsuga menziesii*) often associated with Pacific Northwest coastal forests. This disease may lead to foliage discoloration, foliage loss, and reduced growth in Douglas-fir. In May 2022, an aerial survey covering 2.0 million acres was flown to map the distribution of discolored Douglas-fir trees associated with SNC in coastal Washington forests. Just over 115,000 acres of symptomatic Douglas-fir were mapped, which is within range of measurements taken in previous years. In support of the aerial survey, 96 ground locations across the range of the aerial survey, along the coast of Washington, were assessed in spring 2021 and 2022. SNC severity (percent of stomata blocked by fungal fruiting bodies on two-year-old needles) and needle retention (amount of needles from previous years still present on a limb) were estimated at each location. An average of 2.5 (2021) and 2.1 (2022) years of needle retention and 21.1 (2021) and 8.9 (2022) percent SNC severity were measured at these coastal plots, numbers similar or lower than in previous years surveys. Additionally, during the same time period, 32 ground plots were surveyed in the NW Region in an area where monitoring had not occurred before. An average of 2.9 (2022) and 2.4 (2021) years of foliage and 35.9 (2021) and 25.6 (2022) percent occluded stomata were measured. These numbers are significantly higher than those measured along the coast during the same time period. The correlation between SNC severity and needle retention was not significant in all locations and years except for the NW Region in 2022. This lack of consistent correlation may indicate other factors are driving needle retention, such as drought, heat, site quality, or other foliar diseases.

Introduction

The fungus that causes Swiss needle cast (SNC), Notho*phaeocryptopus gaeumannii*, is found everywhere its only host, Douglas-fir (*Pseudostuga menziesii*), is grown. This foliar disease rarely causes tree mortality, but can cause premature needle loss and foliar discoloration that results in reduced growth, altered wood properties, and stand structure and development changes (Shaw et. al. 2021). This native pathogen became a priority in the coastal forests of Washington and Oregon in the 1990s, and more recently has impacted forests in British Columbia (Shaw et al. 2021). These areas have likely seen high SNC levels due to the fungi-favorable topographic and climatic conditions (such as mild winters and wet springs), historical plantings using off-site Douglas-fir seed sources, and increases in Douglas-fir numbers due to forest management practices (Shaw et. al. 2021). Monitoring SNC and its symptoms along the Pacific NW coast from the air and on the ground have become common practices in Washington and Oregon, with British Columbia recently also starting to monitor the disease.

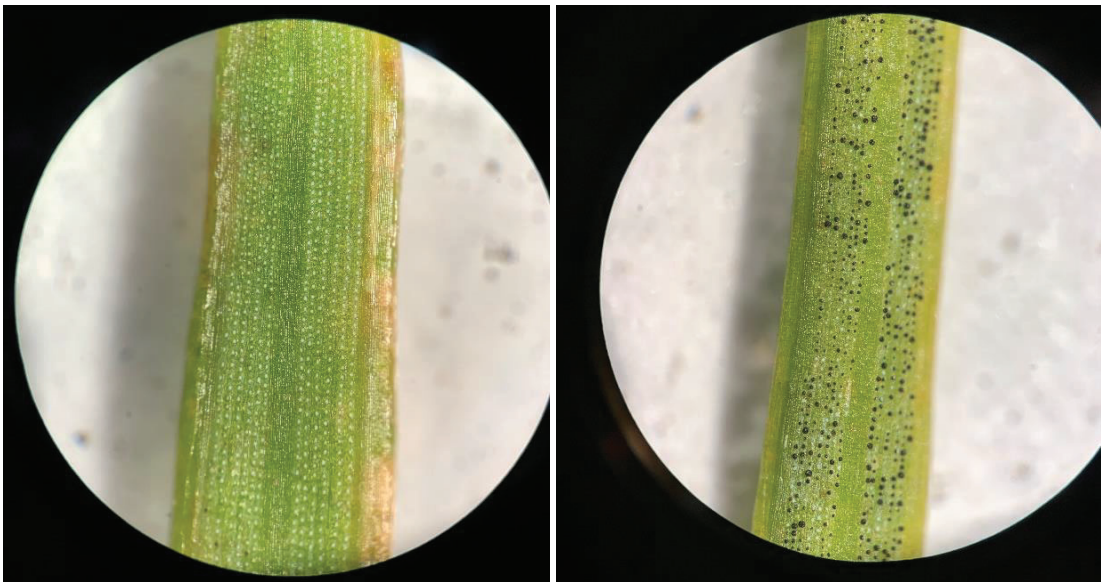

Figure 1: The underside of two-year old needles collected during SNC ground plot monitoring showing an uninfected needle (left) and an infected needle with about a 70% SNC severity rating (right). Unobstructed stomata are seen as white dots in vertical rows while SNC fruiting body occluded stomata are seen as black dots.

Figure 2: A Douglas-fir tree with poor needle retention (needles retained are almost exclusively one-year old, with very few older needles) causing the tree's canopy to look sparse (left). Douglas-fir stands displaying yellow-brown discoloration associated with high SNC impact (right).

In Oregon, where the disease is most severe, an aerial survey has been conducted most years since 1996, with roughly 300,000 acres of symptomatic Douglas-fir mapped yearly along the coast (https://sncc.forestry.oregonstate.edu/survey-maps). In Washington, an aerial survey along the coast was completed in 1998, 1999, 2000, 2012, 2015, 2016, and 2018, with mapped symptomatic acres ranging between 44,000 to over 400,000 (Ramsey, et al. 2018). In both Oregon, Washington, and recently in British Columbia, ground plots have been used to support aerial surveys and help correlate the observed discoloration with fungal signs and impact to trees. In Washington, ground surveys have been conducted most years since 1997.

The Washington State Legislature provided funding in the 2019-2021 biennium to conduct aerial and ground surveys in Washington's coastal forests (hereafter 'Coastal Region'), representing the area that has been previously monitored. After being delayed by COVID-19 operating restrictions, an aerial survey was completed in

Washington in spring 2022. To support this aerial survey, ground surveys throughout the Coastal Region were also completed in spring 2021 and 2022.

In addition to the Coastal Region, an area in the NW Region representing the active timberlands between the cities of Mount Vernon, Darrington, Concrete, Bellingham, and Sumas was also ground surveyed (hereafter 'NW Region'). This region represents an area not previously surveyed, and was included in the ground survey due to its proximity to British Columbia where SNC has been reported as a growing concern (Shaw et. al. 2021).

Methods

The 2022 aerial survey was conducted during May for the Coastal Region of Washington covering 2.0 million acres (Figure 3). This survey is timed to occur after crown discoloration symptoms have developed, but before new foliage has emerged (bud break). The survey area extended from the Columbia River north to the Strait of Juan de Fuca, and from the coastline eastward. The observation aircraft flew at 1,500 to 2,000 feet above ground level, following north-south or east-west lines separated by 3 miles. Observers on both sides of the aircraft looked for areas of Douglas-fir forest with apparent yellow-brown foliage, a rather generic symptom that is considered to be indicative of moderate to severe SNC disease. Patches of forest with these symptoms were sketched onto touch-screen tablets displaying topographic maps or ortho-photos and the position of the aircraft. Each polygon was classified for degree of yellow-brown discoloration as either severe or moderate.

During the spring of 2021 and 2022, ground surveys were conducted throughout the two selected study areas (the Coastal Region and the NW Region), representing 2.4 million acres and 0.7 million acres respectively (Figure 4). Ground sampling locations in each of these areas, and for each year, were separately selected with a uniform spatial weighting function using a Balanced Acceptance Sampling method (Robertson et al., 2013). Based on time availability, 50 sampling locations were randomly selected in the Coastal Region and 17 selected in the NW Region each year. Each selected point was visited once between March and May 2021 or 2022 where an accessible and appropriate stand (dominated by suitably-sized Douglas-firs) no greater than four miles away from the random point was chosen for sampling. Points that had no appropriate or accessible sites within four miles were excluded. In total, the Coastal Region had 48 sites assessed each year and the NW Region had 17 sites assessed in 2021 and 15 sites assessed in 2022.

At each ground survey location, 10 Douglas-fir trees were selected for sample collection and measurements. Needle retention (the number of cohorts on a branch still retaining needles) was visually estimated on each tree. Two-year-old foliage was collected from the fifth whirl of branches of each tree and taken back to the lab for examination under a microscope. SNC severity (percent stomata obstructed by the fungal fruiting bodies called pseudothecia) was determined by counting the number of pseudothecia in 300 stomata on each of ten needles for each tree. Due to differences in sampling density of the two areas, summary calculations for each site were determined separately prior to comparison using a t-test. To account for the site selection method, standard errors were calculated using appropriate design-based estimators (Kincaid et al. 2019). Correlation between needle retention and severity were assessed for each region each year.

Results & Discussion

The aerial survey covered 2.0 million acres in the Coastal Region on May 4 and 31, 2022, totaling 8.6 hours of flying time. SNC associated symptomatic stands were detected on just over 115,000 acres, representing almost 6% of the total acres surveyed. This represents a slight increase from the previous survey conducted in 2018, but a decrease from earlier surveys (Table 1). Severely symptomatic stands were generally located between Westport and Ilwaco, while moderately symptomatic stands were found scattered throughout the region (Figure 3).

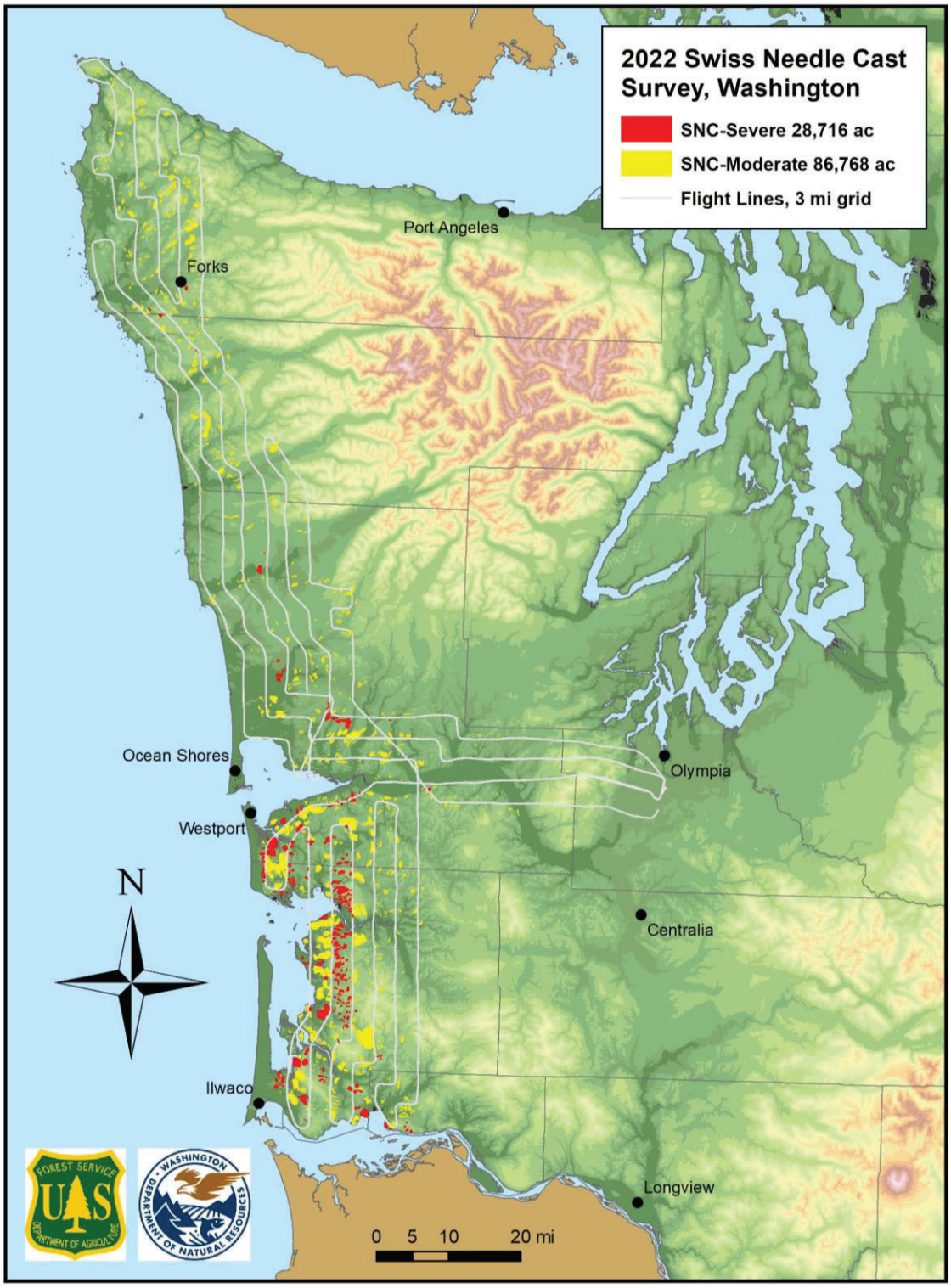

Figure 3: Washington 2022 Swiss needle cast aerial survey map showing the flight path and the mapped SNC severe and moderate stands.

Table 1: The 2022 aerial survey results compared to previous years of SNC aerial survey results in the coastal region of Washington (Ramsey et al. 2018).

	severe SNC symptoms		moderate SNC symptoms		total SNC symptoms		area flown
year	% of total acres	severe SNC acres	% of total acres	moderate SNC acres	% of total acres	total SNC acres	acres in millions
2022	1%	29,000	4%	87,000	6%	115,000	2.0
2018	< 1%	6,000	3%	73,000	3%	79,000	2.7
2016	< 1%	14,000	10%	234,000	10%	248,000	2.4
2015	1%	19,000	13%	332,000	14%	351,000	2.6
2012	< 1%	6,000	8%	222,000	9%	228,000	2.7

The 2021 and 2022 ground surveys found that SNC severity and needle retention varied between site, regions, and by year. In the Coastal Region, an average of 2.5 (2021) and 2.1 (2022) years of foliage (needle retention) and 21.1 (2021) and 8.9 (2022) percent occlusion (SNC severity) was measured at each site. 2021 measurements were similar to previous measurements, while 2022 measurements were lower (Table 2). In the NW Region, an average of 2.9 (2021) and 2.4 (2022) years of foliage (needle retention) and 35.9 (2021) and 25.6 (2022) percent occlusion (SNC severity) were measured at sites. The NW Region's needle retention and SNC severity measurements were significantly higher than those measured in the Coastal Region (t-test, $p<0.001$). Overall, these numbers varied greatly between sites, with average needle retention ranging from 1.2 to 3.3 years and SNC severity ranging from 0.3 to 62.6 percent.

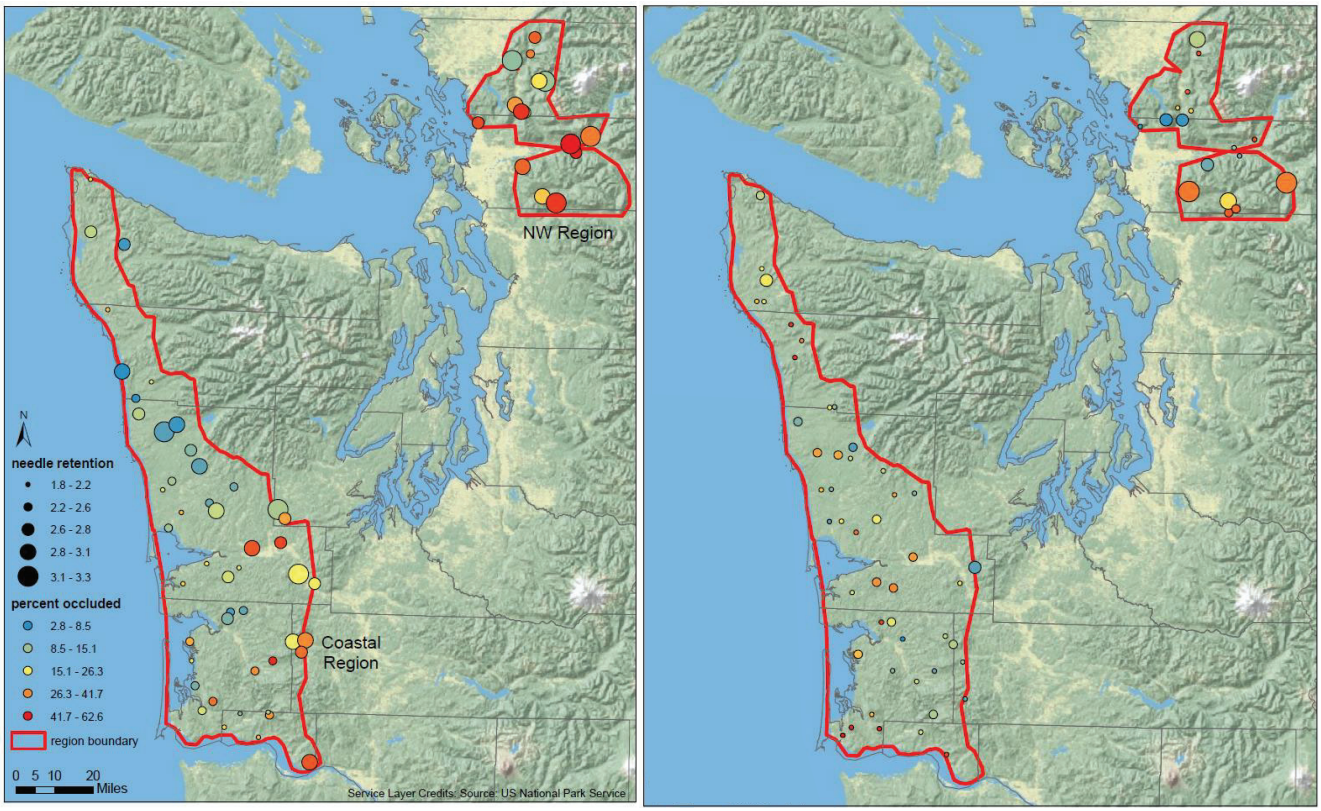

Figure 4: SNC ground survey plot results in 2021 (left) and 2022 (right). Surveyed regions are outlined in red with points representing sampled plots locations. Point size indicates average needle retention measured and point color represents SNC severity (% occluded) measured.

Table 2: Number of sites, average percentage of occluded stomata on two-year-old needles, and average foliar retention (0 indicates there were no needles retained and 3.6 indicates full retention of 4-years of foliate) for each region surveyed since 2012.

region	year	number of sites	average pseudothecia density (%)	average foliar retention
Coastal	2022	48	8.9	2.1
	2021	48	21.1	2.5
	2018	26	16.0	2.3
	2016	63	22.1	2.4
	2015	47	22.5	2.3
	2012	75	15.5	2.2
NW	2022	17	25.6	2.4
	2021	15	35.9	2.9

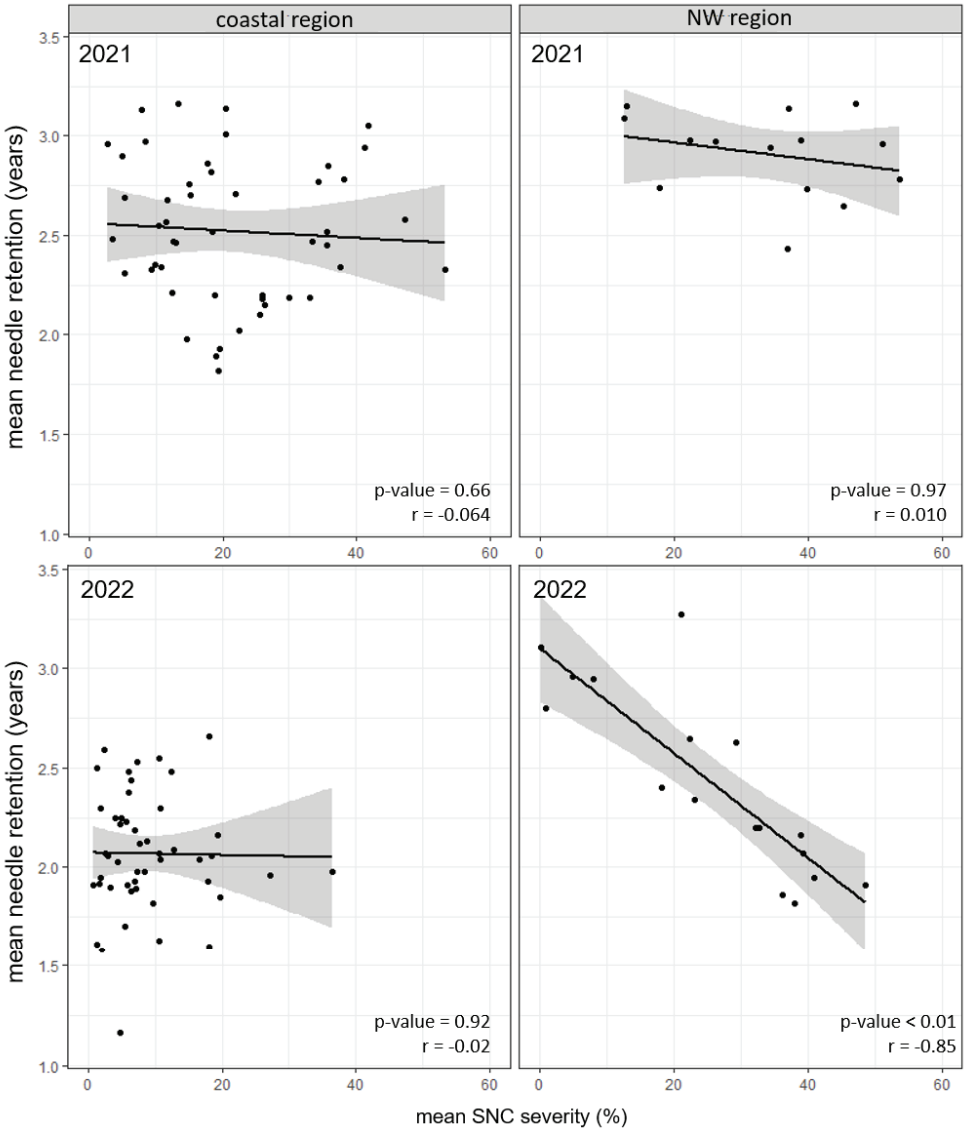

Figure 5: Correlations between mean SNC severity (% stomata occluded on two-year old needles) and mean needle retention (years retained) split by region (columns) and year (rows). Associated p-values and r values are shown on each graph.

Within regions each year, the correlation between SNC severity and needle retention was not significant in all locations and years, except for the NW Region in 2022 (Figure 5), which was the only region that displayed the expected correlation between high SNC severity and low needle retention. This overall lack of correlation between high SNC severity and low needle retention is of note, since stomata are responsible for gas and water exchange within a needle, and significant obstruction of these features often results in needle loss. Therefore, this may indicate that other factors besides SNC are driving needle loss in Douglas-fir forests in both the Coastal and NW Regions most years. Other factors that influence needle retention can include drought, heat, site quality, and other diseases.

Both surveys indicate that there has been no substantial increase in the severity of SNC over the past decade in coastal Washington, as acreage mapped during the aerial survey and SNC ratings from the ground survey are well within the range of measurements observed in previous years' surveys. Results from the NW Region are inconclusive, as they indicate Douglas-fir have better levels of needle retention than the Coastal Region, despite having higher SNC severity measurements.

Caution should be advised when interpreting this data. The SNC aerial survey maps symptoms (discoloration) visible from air. As SNC observers can only map areas where symptoms are visible from 1,000+ feet, aerial survey data can only be used to coarsely document trends over time. Therefore, while the aerial survey and randomly selected ground points can be used as a guide for identifying areas impacted by SNC, site specific ground surveys should be conducted in stands of interest before SNC mitigating management decisions are made. In particular, if less than three years of foliage are being retained on Douglas-fir branches, then growth loss may occur. Given that Douglas-fir is the only host of SNC, forest managers with impacted sites may select for or plant other tree species, such as red alder, western redcedar, western white pine, Sitka spruce, or western hemlock. For a more detailed management discussion, refer to the "Silvicultural decision guide for Swiss needle cast in coastal Oregon and Washington" (Ritóková et al. 2022) available online at: extension.oregonstate.edu/pub/em-9352

Acknowledgements

The survey was conducted by the Washington Department of Natural Resources Forest Resilience Division and the Washington Department of Fish and Wildlife (WDFW) Aviation Section. Marty Kimbrel (WDFW) piloted the aircraft. Funding for the survey was provided by the Washington State Legislature, Washington Department of Natural Resources, and the USDA Forest Service, an equal opportunity employer.

Contact Us

Rachel Brooks (Rachel.Brooks@dnr.wa.gov) or Dan Omdal (Daniel.Omdal@dnr.wa.gov)

References

Kincaid, T.M., Olsen, A.R., and Weber, M.H. 2019. Spsurvey: Spatial survey design and analysis. R package version 4.1.0. https://crian.r-project.org/web/packages/spsurvey/citation.html

Ramsey, A., Omdal, D., Dozic, A., Kohler, G., Hof, J., and M. Kimbrel. 2018. Coastal Washington Swiss Needle Cast Aerial and Ground Survey. Washington Department of Natural Resources. https://www.dnr.wa.gov/publications/rp_2018_swiss_needle_cast_report.pdf

Robertson, B.L., Brown, J.A., McDonald, T. and Jaksons, P. 2013. BAS: Balanced acceptance sampling of natural resources. Biometrics, 69(3) 776 - 784. https://doi.org/10.1111/biom.12059

Shaw, D.C., Ritóková, G., Lan, Y., Mainwarning, D.B., Russo, A., Comeleo, R., Navarro, S., Norlander, D., and Smith, B. Persistence of the Swiss needle cast outbreak in Oregon coastal Douglas-fir and new insights from research and monitoring. Journal of Forestry, 1 – 15. https://doi.org/10.1093/jofore/fvab011

Ritóková, G., Shaw, D.C., and Mainwaring, D. 2022. Silvicultural decision guide for Swiss needle cast in coastal Oregon and Washington. Oregon State University Extension Service. EM 9352. https://extension.oregonstate.edu/pub/em-9352

Swiss Needle Cast Co-op BC Update December 2022

David Rusch, Ministry of Forests, Lands and Natural Resource Operations, British Columbia

British Columbia (BC) has a total of 42 Oregon-style Swiss needle cast (SNC) permanent sample plots (PSPs) in three biogeoclimatic variants. Fourteen of the plots have weather stations. Twelve of the plots had their 5-year re-assessment in 2021, 23 are being re-measured this winter/spring, and the remaining 7 will be re-assessed in 2024.

There was no relationship between foliar nitrogen and pseudothecial counts when the plots were set up but there was a curious positive correlation between foliar potassium levels and SNC disease severity. As in Oregon, SNC severity appears to be correlated with warmer winter temperatures and wetter springs.

Anecdotal observations suggest that needle retention in lower branches is much greater near the bole of SNC affected trees than at the outer ends of the branches. This hypothesis will be tested this spring by measuring needle retention and pseudothecia from near the bole and at the end of the branches sampled from the lower crown.

Molecular ecology has identified 2 lineages in BC. Lineage 1 has both a coast and interior type. Lineage 2 is restricted to Vancouver Island and Metro Vancouver. Lineage 1c was the predominant lineage found in BC plots.

Unlike Oregon, SNC is not restricted to a well-defined geographic area and we have not been conducting annual aerial spring surveys for SNC. Even in areas with high SNC, severity between plots is highly variable. This is likely due to the complex topography in BC. To better define SNC impact and identify areas of high hazard we are asking licensees to voluntarily collect needle retention data as part of their regeneration and free growing surveys. A free growing declaration means that the licensee has met their regeneration obligations on a particular piece of crown land (public land). Most licensees collect ground survey data to support their free growing declaration. Our Silviculture Performance assessment specialist, Taisa Brown, has produced YouTube videos explaining how to collect the data. Hopefully this data can be used to address future stocking standards for SNC affected areas on the coast. We hope to pilot some spring helicopter survey flights this spring in the Chilliwack area.

Fungal Ecology 57-58 (2022) 101155

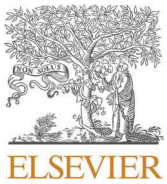

Contents lists available at ScienceDirect

Fungal Ecology

journal homepage: www.elsevier.com/locate/funeco

Crown closure affects endophytic leaf mycobiome compositional dynamics over time in *Pseudotsuga menziesii* var. *menziesii*

Kyle A. Gervers [a,*], Daniel C. Thomas [b], Bitty A. Roy [c], Joseph W. Spatafora [a], Posy E. Busby [a]

[a] Department of Botany and Plant Pathology, Oregon State University, Corvallis, OR, 97333, USA
[b] Department of Ecological Microbiology, Bayreuth Center of Ecology and Environmental Research (BayCEER), University of Bayreuth, Bayreuth, 95440, Germany
[c] Institute of Ecology and Evolution, University of Oregon, Eugene, OR, 97403, USA

ARTICLE INFO

Corresponding Editor: James White

Keywords:
Nothophaeocryptopus
Rhabdocline
Fungi
Endosphere
Old-growth
Community ecology
ITS
Metabarcoding
Airborne LiDAR

ABSTRACT

Old-growth *Pseudotsuga menziesii* var. *menziesii* forests produce complex environmental and spatial gradients along which biota assemble. Given this, it has been proposed that changes in the crown microenvironment are associated with different community assembly outcomes for needle fungi. Using high-throughput sequencing, the endophytic mycobiomes of needles were characterized for increasing ages of needles sampled along the boles of eight coastal Douglas-fir trees. Leveraging airborne light detection and ranging (LiDAR) data to create three-dimensional "point cloud" representations of tree crowns revealed that crown closure accounted for more fungal compositional variation than height in crown, and fungal richness and diversity were positively correlated with increasing crown closure. Supplementing the point clouds of each climbed tree with clouds from >5,000 randomly selected trees in the study area showed that fungal communities from closed portions of the crown were increasingly structured with needle age. These findings highlight the importance of the crown microenvironment in the development of foliar fungal communities for a foundation tree species.

1. Introduction

Endophytic fungi live a significant part of their life cycles within their hosts without producing symptoms of disease (Saikkonen et al., 1998). Those that infect plant leaves are generally horizontally transferred between host plants, comprise a diverse taxonomic and phylogenetic assemblage of fungi, and can modulate foliar disease severity (Busby et al., 2016), stomatal conductance (Arnold and Engelbrecht, 2007), and nutrient uptake (Christian et al., 2019). Given the functional importance of foliar fungal communities for regulating plant responses to biotic and abiotic stresses, elucidating the factors controlling their composition will have important implications for both basic and applied plant sciences.

Communities of foliar endophytic fungi vary along environmental gradients at landscape (Zimmerman and Vitousek, 2012) and regional (Barge et al., 2019) scales, yet there are few studies examining patterns of fungal community variation along the vertical axis of individual host plants (Osono and Mori, 2004; Harrison et al., 2016; Izuno et al., 2016; Oono et al., 2017). While this omission may be inconsequential for annuals and plants of modest stature, the crowns of tall, old-growth conifer species like *Pseudotsuga menziesii* var. *menziesii* support vertically stratified ecological communities in which compositions change with height in crown (McCune, 1993; Sillett and Rambo, 2000). And although *P. menziesii* crowns were among the first rigorously sampled for endophytic needle fungi (Sherwood and Carroll, 1974), further characterization of these endophyte communities with modern sequencing techniques is needed.

Tree crowns span multiple microclimatic gradients. UV-B and photosynthetically active radiation are abruptly attenuated by foliage in the mid-crown (Parker, 1997), while the upper crown is only intermittently wet, with generally warmer and less stable air temperatures than the lower portions of the crown that are buffered by vegetation (Heffernan, 2017). Further, unshaded foliage can become nearly 7 °C warmer than surrounding air temperatures, while leaf temperatures of shaded foliage are relatively stable (Doughty and Goulden, 2008). These and other microclimatic factors can also affect fungal colonization potential in other contexts (Carisse et al., 2000; Unterseher and Tal, 2006; Norros et al., 2015), and may also influence foliar mycobiome composition by acting as environmental filters dependent on the degree of canopy openness (Gilbert et al., 2007). Additionally, foliage at different heights in the crown possesses different morphological, physiological, and spectral properties (Ishii et al., 2002; Gebauer et al., 2015;

* Corresponding author.
E-mail address: gerversk@oregonstate.edu (K.A. Gervers).

https://doi.org/10.1016/j.funeco.2022.101155
Received 20 September 2021; Received in revised form 24 March 2022; Accepted 26 March 2022
Available online 28 April 2022

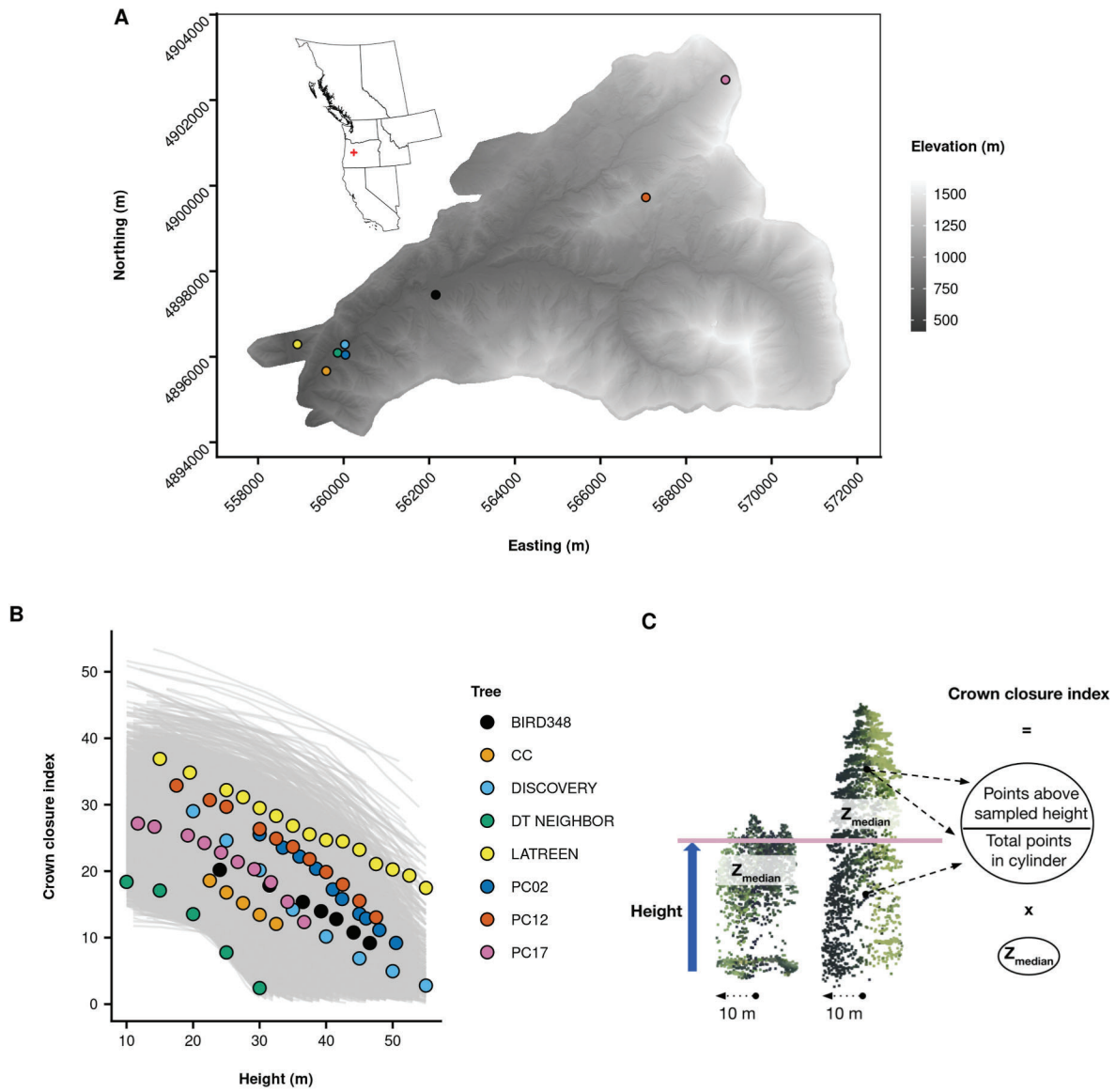

Fig. 1. Locations of the H.J. Andrews Experimental Forest (HJA) and the climbed and sampled trees (A). The inset and the red cross indicate the center position of HJA within the North American Pacific Northwest. The positions of sampled trees have been jittered (±150 m) to avoid overlap. The map is based on a digital terrain model from Spies, 2016. Relationship between height in crown and crown closure (B). Grey lines show data from point clouds associated with 5828 trees randomly sampled across HJA (each with randomly sampled crown heights), while colored lines and points represent point clouds associated with trees that were climbed and sampled as part of this study. Point cloud cylinders are centered on the treetop of a focal tree, but include all point returns within a 10 m radius (C). Although the same vertical height can be sampled in two different trees, these heights can be associated with different crown closure indices.

Schweiger et al., 2020), potentially allowing host-mediated, within-crown biotic filtering of needle communities. Because *P. menziesii* canopy foliage can be long-lived, community assembly outcomes for the canopy mycobiome at a point in time may have lasting impacts on future community structure and assembly as foliage is exposed to infection over time (Bernstein and Carroll, 1977; Arnold and Herre, 2003; Osono, 2008).

The potential for light detection and ranging (LiDAR) point cloud data to account for variation in the diversity and composition of terrestrial fungal communities (Peura et al., 2016; Thers et al., 2017; Valdez et al., 2021) and to characterize the habitat preferences of crown-dwelling organisms (Barnes et al., 2016) has recently been demonstrated. These and other approaches rely on LiDAR technologies, which associate several emitted and detected laser pulse echoes ("returns") with accurately recorded positions. Further processing yields three-dimensional "point clouds'', with each point in space representing a position where the laser pulse reflects off vegetation or other surfaces. Researchers can then obtain accurate estimates of canopy height, cover, and structure to inform their analyses of communities (Lefsky et al., 2002). LiDAR-derived metrics also correlate with specific aspects of the microclimate such as near-surface air temperatures in old-growth *P. menziesii* forests (George et al., 2015; Frey et al., 2016; Davis et al., 2019). Thus, combining mycobiome data with a co-localized measurement of the crown microenvironment may help to elucidate how endophyte communities vary along tree stems and among trees. Here, point cloud data derived from airborne LiDAR and high-throughput amplicon sequencing data were leveraged to test the hypothesis that the composition and diversity of fungal needle endophyte communities are correlated with crown exposure. In addition to examining the height above ground as a compositionally relevant factor, our definition of exposure considered an airborne LiDAR-derived measure of crown closure, which quantifies the amount of intervening foliage (measured as "points" in a point cloud) between the sky and a specified height in the tree. Altogether, positions in the crown that are further from the

ground and less obscured by foliage are more exposed; positions closer to the ground and more obscured by foliage (more closed) are less exposed. We further explored the relevance of exposure as a concept and hypothesized that more- or less-exposed crowns undergo different shifts in community structure with each age class of needle, potentially reflecting differences in needle endophyte community assembly. We report that only closure uniquely contributed to an ecologically informed metric of exposure, accounting for variation in community composition and diversity, and exposure groups showed differing patterns in community structure over the needle ages sampled.

2. Methods

2.1. Sampling and surface sterilization

Six trees (BIRD348, CC, LATREEN, PC02, PC12, and PC17) at the H. J. Andrews Experimental Forest (HJA, Fig. 1) were sampled in late winter 2016–2017, and two other trees (DISCOVERY and DT NEIGHBOR) were sampled in winter 2017–2018. HJA is located on the west side of the Cascade Range of central Oregon; its 6400 ha range from 410 to 1630 m in elevation, and canopies can exceed 93 m in height. Using single-rope climbing techniques (Video S1), where possible, accessible branches from opposing aspects were sampled every 1–5 m in each tree, and the height of each sample collection above ground level was noted. Collection of branches began with the first available branch closest to the ground, and continued as high as could be safely climbed. Due to safety concerns, climbing did not reach the tops of tree crowns. Branches were transported in coolers with ice blocks and then later refrigerated at 4 °C until they could be processed (within 72 h). Needles that experienced one (A1), two (A2), three (A3), and four (A4) growing seasons were sampled from each branch and represented four unique needle age classes. To target endophytic fungi, needles were surface sterilized via immersion in 70% ethanol for 1 min, 4 min in 5% sodium hypochlorite, 1 min again in 70% ethanol, followed by a sterile distilled water rinse before being frozen at −80 °C (modified from Thomas et al., 2016). Needles from different aspects at a given height on each tree were pooled prior to 72 h of lyophilization. Each sample consisted of a unique tree-by-height-by-age combination (71 heights x 4 ages = 284 samples).

Supplementary data related to this article can be found at https://doi.org/10.1016/j.funeco.2022.101155.

2.2. DNA extraction, Illumina MiSeq sequencing, and sequence processing

DNA was extracted using OPS Diagnostics' 96 Well Synergy™ Plant Homogenization plates (Lebanon, New Jersey, USA). Each well received five needles of a single age class, sourced from each sampled height; empty wells were processed per the kit instructions and served as extraction controls. To reduce PCR inhibition issues, DNA extractions were cleaned with 1.2X volumes of Mag-Bind® TotalPure NGS magnetic beads (Omega Bio-Tek, Norcross, Georgia, USA). The ITS2 region was amplified in a primary PCR using the 5.8S-Fun and ITS4-Fun fungal-specific primers (Taylor et al., 2016) Each primer consisted of sequences that amplified the ITS2 region, followed by 3–6 bp length heterogeneity spacers, and subsequently terminated with an Illumina adapter sequence. 25 μl PCRs were carried out with MyTaq™ HS Red Mix (Meridian Bioscience, Inc., Cincinnati, Ohio, USA), 0.4 μM of each primer, 5 μl of template, and applying the following cycling parameters: 3 min denaturation at 95 °C, 28 cycles of 95 °C (30 s), 58 °C (30 s), 72 °C (30 s), followed by a 2 min extension at 72 °C. Using a secondary PCR, sample barcodes and Illumina flow cell adapters were then incorporated into these PCR products after amplification was visually confirmed via agarose gel electrophoresis. 25 μl PCRs were carried out with MyTaq™ HS Red Mix, 0.5 μM of each barcode primer, 1 μl of template, and with the following cycling parameters: 3 min at 95 °C, eight cycles of 95 °C (30 s), 55 °C (30 s), 72 °C (30 s), followed by a 2 min extension at 72 °C. This PCR product was purified and normalized (to 2.5–3.0 ng μl^{-1}) using Charm Biotech's Just-a-Plate™ 96 Well Purification and Normalization plates (Cape Girardeau, Missouri, USA) and submitted the library to the Center for Genome Research and Biocomputing (Oregon State University, Corvallis, Oregon) for 2 × 300 paired end sequencing on the Illumina MiSeq platform (Reagent Kit v3, San Diego, California, USA).

Reads were demultiplexed with Pheniqs (Galanti et al., 2017) and adapters were trimmed using Cutadapt (Martin, 2011) and SeqPurge (Sturm et al., 2016). Reads were then denoised, filtered of chimeras, and merged using the DADA2 R package (Callahan et al., 2016), producing amplicon sequence variants (ASVs) using the pseudo-pooling method. ITS2 sequences were extracted with ITSx (Bengtsson-Palme et al., 2013) and were aligned to the 2020-02-04 UNITE eukaryote release (singletons included, Abarenkov et al., 2020a) with VSEARCH (Rognes et al., 2016). If at least half of each ASV's global alignments (at > 0.5 identity) were fungal, the ASV was retained as a putative fungal sequence. The LULU R package, implementing the LULU algorithm, was used to collapse potentially infragenomic or artifactual ASVs into OTUs (Frøslev et al., 2017), with minimum match = 97% similarity, and minimum relative occurrence = 95%. Although not all ASVs were affected by this approach, putative taxa will be referred to as OTUs. After this step, OTUs for which >1% of non-control reads were found in the extraction and PCR controls were identified as contaminants and removed. Taxonomy was then assigned to the remaining subset of OTUs using the fungal version of the 2020-02-04 UNITE release (without singletons, Abarenkov et al., 2020b) and the RDP classifier (Wang et al., 2007), implemented with DADA2. This release was supplemented with full ITS sequences belonging to fungal taxa known to associate with *P. menziesii* or other conifers, but not included in the UNITE release. The full ITS sequence of *P. menziesii* was also included in the release, allowing for host amplification to be identified and removed. The PERFect R package was used to remove spurious OTUs by identifying those OTUs which made insignificant contributions to the total covariance of the dataset (Smirnova et al., 2019); the permutation method with default significance thresholds (retaining OTUS with $P < 0.1$, with P values calculated using 1000 permutations) was applied. Altogether, LULU conditional OTU curation and PERFect filtering were employed as a means to retain as much sequence resolution as possible while also attempting to minimize the effects of infragenomic taxon splitting and artifactual sequence generation.

2.3. Airborne LiDAR data-processing

Crown closure values associated with each sample height were obtained by processing light detection and ranging point cloud data that had been collected for a larger survey of the McKenzie River study area. Between June 07, 2016 and June 21, 2016, Quantum Spatial (Portland, Oregon, now NV5 Geospatial, Hollywood, Florida, USA), commissioned by the Oregon LiDAR Consortium, obtained discrete-return airborne laser scans of the HJA area from a Leica ALS80 (Leica Geosystems, St. Gallen, Switzerland) mounted on a Cessna Grand Caravan (Textron Aviation Inc., Wichita, Kansas, USA), flying 1500 m above ground level. Across the entire 2016 McKenzie River survey area, an average pulse density of 12.64 m^{-2} (SD = 4.867, min = 6.70 pulses m^{-2}, max = 65.66 pulses m^{-2}) was verified by the Oregon Department of Geology and Mineral Industries. Using 1,723 ground survey points, it was also found that the aerial survey had a horizontal accuracy of 0.37 m root mean square error (RMSE) and a vertical accuracy of 0.053 m RMSE. Point cloud data from this survey (OCM Partners, 2020) were downloaded from the NOAA Data Access Viewer as a projection to UTM Zone 10 (horizontal datum = NAD83 (2011), vertical datum = NAVD88, geoid = GEOID18), with meters as horizontal and vertical units.

Point clouds were processed with the lidR package (Roussel et al., 2020). Point clouds were purged of point returns with GPS time errors and intensity values of zero. For each tree, cylindrical volumes with radius 10 m (and centered on tree positions) were clipped from these

point clouds. This was the minimum radius that contained the horizontal breadth of each crown for each sampled tree. Prior to clipping, tree positions were refined, starting with GPS coordinates on record for each tree. The expertise of the HJA forest director (Dr. Mark Schulze) was used to verify final tree positions, which were centered on each treetop. For each cylinder containing the point cloud of each tree, the bare earth elevation under each tree was estimated via k-nearest neighbor inverse-distance weighting (k-nearest neighbor points = 10) using all available ground points. This bare earth elevation was added to the heights at which needle material was sampled in each tree. From here, a crown closure index was defined for each sampled tree height as the number of point returns above the sampled height, divided by the total number of point returns in each cylinder (Lovell et al., 2003). These closure values were then multiplied by the median height of elevation-normalized, non-ground point returns (Z_{med}, Fig. 1C) to account for the fact that a point cloud cylinder with a greater amount of tall vegetation will generally yield more, intervening point returns than a cylinder containing shorter vegetation (assuming equal scan coverage).

2.4. Analysis

To determine how needle community composition varied across trees, needle ages, and crown properties, features for each sample were relativized by sample sequencing depth (i.e., converted to relative abundance), and a generalized log transformation was applied to dampen the compositional influence of highly abundant OTUs. Bray-Curtis dissimilarity matrices were generated for use in downstream analyses. All subsequent analyses and ordinations were performed using functions from the vegan R package (Oksanen et al., 2020) unless stated otherwise. Dissimilarities associated with the full dataset were ordinated with non-metric multidimensional scalings (NMDS), using a two-dimensional solution. NMDS significance was evaluated by performing a Monte Carlo test (with 999 permutations) on the results using R scripts (calling vegan functions) modified from those originally created by Dr. Kevin McGarigal (pers. comm.). Four samples which prevented the NMDS ordination from converging were purged from the first needle age class. In trimming each needle age subset down to only the samples that shared a tree height with every other subset prior to analysis, samples were removed from the other three needle age classes if one needle age class was missing. This resulted in the retention of 64 samples for each needle age class subset (256 samples total). Permutation analyses of variance (PERMANOVA; Anderson, 2001) were performed with the *adonis2* function on the full dataset to determine whether needle compositions differed by tree and needle age, and the homogeneity of variances among levels of each factor was tested using the *betadisper* (implementing PERMDISP2; Anderson, 2006) and *permutest* functions to assess whether differences in composition were influenced by differences in group dispersion. For these tests, 999 random permutations were used to generate null pseudo-F ratio distributions, designating source tree ("tree") as a permutation stratum. Analyses were then followed by a PERMANOVA on the full dataset testing the effects of height and closure after accounting for needle age class, employing 999 permutations to generate P values and with "tree" as permutation stratum. Distance-based redundancy analyses (dbRDA) were constrained on crown variables, and PERMANOVAs were performed on each needle age subset to determine whether compositional variation accounted for by both crown variables changed with each needle age class.

Crown terms (i.e., among height and closure) accounting for unique compositional variation in the marginal test on the full dataset were retained to generate exposure groups. To ensure that group assignment procedure was not influenced by the small sampling of trees in our dataset, the point clouds of 5828 randomly sampled trees across HJA were also characterized by calculating closure at 10 random heights in each tree, using the method described above (Fig. 1B). Random sampling was restricted to trees attaining the minimum treetop height (35 m) and Z_{med} (22.67 m) values observed among the climbed trees in our dataset, and random height sampling was also restricted to the range observed for climbed trees (lowest height = 10 m, greatest height = 55 m). Closure values calculated at each sampled height were clustered into two groups using the Hartigan-Wong k-means clustering algorithm (Hartigan and Wong, 1979) with the maximum number of iterations and the number of random starts both set to 999. Samples from heights associated with the lower mean cluster were designated as belonging to the "open" exposure group, and samples associated with the higher mean cluster were designated as belonging to the "closed" exposure group. This was followed by indicator species analysis on the full dataset (Dufrene and Legendre, 1998; as implemented with the labdsv package by Roberts, 2019), which was used to identify taxa that occurred more frequently and with greater relative abundance than expected by chance in either open or closed exposure groups. Only OTUs occurring in at least 10% of samples were subjected to indicator species analysis. P-values were adjusted to control for the false discovery rate of indicator taxa using a Benjamini-Hochberg correction (Benjamini and Hochberg, 1995).

To determine whether alpha diversity varied with tree, needle age, and closure, and height richness (Hill number $q = 0$) and the exponent of Shannon entropy ($q = 1$) were estimated for each sample using the iNEXT package (Hsieh et al., 2016). Both metrics were estimated at a depth of 1000 reads, and variation in richness and $\log_2$-transformed Shannon entropy (i.e, the Shannon index of diversity) was tested among source tree and needle age (and their interaction) using analysis of variance (ANOVA) *F*-tests (Fox and Weisberg 2019). Assumptions of normality and homoscedasticity were investigated. In the event of putative heteroscedasticity, a White standard error adjustment was applied in an attempt to correct for its influence in the ANOVA (Long and Ervin, 2000). Results of F-tests were investigated further with Tukey honest significant differences *post-hoc* tests (alpha = 0.05). Alpha diversity means were bootstrapped and confidence intervals were generated with the *bca* function of the coxed R package (Kropko and Harden, 2020). Linear mixed-effect models were created using the nlme package (Pinheiro et al., 2021) to test the correlations of alpha diversity metrics with closure and height, setting source tree as a random effect. Reduced models containing either height or closure were compared to each other, a full model containing both crown variables, and a base model that only contained the tree random effect according to their corrected Akaike information criterion (AICc) and Bayesian information criterion (BIC) values using the AICcmodavg R package (Mazerolle, 2020). Reduced model P-values were obtained by performing a likelihood-ratio test comparing the reduced model to the base model. Models included needle age class as a fixed effect term if the term was significant in earlier ANOVAs. Pseudo-R^2 values of fixed effects were calculated using the piecewiseSEM package (Lefcheck, 2016).

Open and closed exposure groups were examined for changes in community structure over time by performing Mantel tests at each transition between needle age classes (A1 to A2, A2 to A3, A3 to A4). Rows and columns associated with samples belonging to either the open or closed exposure groups were extracted from the Bray-Curtis distance matrix associated with each needle age class and used as input matrices for Mantel tests, each using 999 permutations, setting source tree as a permutation stratum. Spearman ranked Mantel statistics were also bootstrapped with 999 permutations. With each permutation, tree heights shared by the needle age classes being compared were randomly sampled with replacement and the Bray-Curtis dissimilarity matrix was generated among the corresponding samples belonging to each needle age class. As above, samples belonging to either the open or closed exposure groups were extracted and the ranked Spearman correlation between matrices was found. Means were calculated from these bootstrapped correlation coefficients, and confidence intervals were generated as above. To compare the relative abundances of dominant OTUs across needle age transitions, paired Wilcoxon signed rank tests were

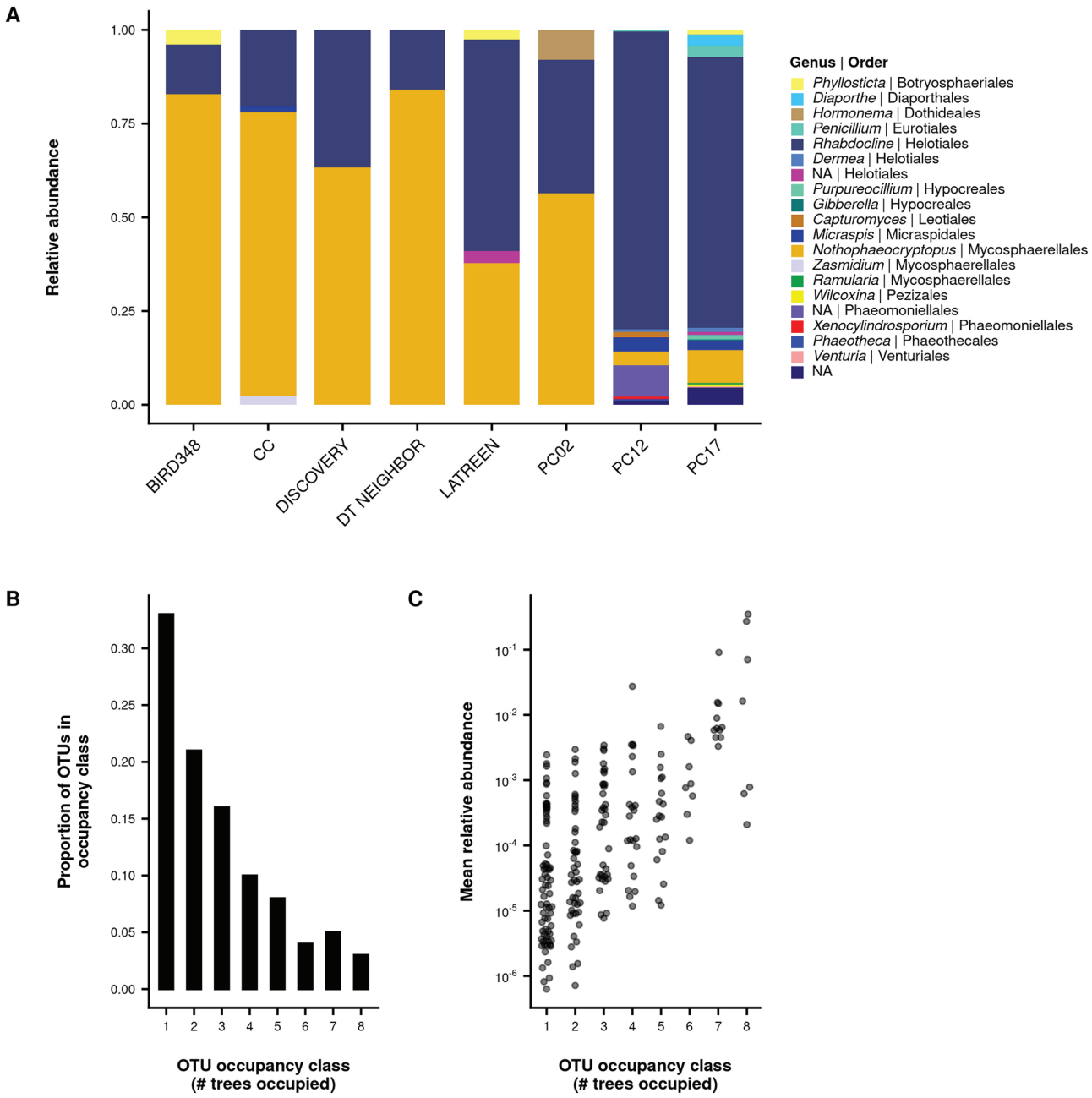

Fig. 2. Taxonomic assignments of OTUs present in the top 95% of reads, pooled at the tree-level (A). OTUs are colored by genus. OTU abundance distribution across the eight trees sampled in this study (B). Occupancy-abundance curve, plotting the mean relative abundance of each OTU against the number of trees it was found to occupy (C). The y-axis of (C) was log10-transformed. Each point represents a different OTU.

performed in R. When the null hypothesis was rejected for a pair of age classes (alpha = 0.05), a two-sample Wilcoxon ranked sum test was performed comparing OTU relative abundances between open and closed exposure groups for the older needle age class. Exact P values (as opposed to normally approximated P values) were calculated when possible.

2.5. Reproducibility

All statistical analyses were conducted in the R v4.0.3 statistical computing environment (R Core Team 2020). The functions associated with the tidyverse R package (Wickham et al., 2019) featured heavily in many scripts and facilitated the manipulation of data structures. Handling of metabarcoding data was accomplished with the phyloseq package (McMurdie and Holmes, 2013). Novel code and metadata associated with bioinformatics, point cloud processing, statistical analyses, and figures have been publicly archived (https://doi.org/10.5281/zenodo.6360767). Demultiplexed sequencing data are deposited in the NCBI Sequence Read Archive (BioProject ID PRJNA748821, BioSample accession SAMN20345134). LiDAR point cloud data are available for download from the NOAA data portal (https://www.fisheries.noaa.gov/inport/item/49949).

3. Results

3.1. Overview

Before the removal of contaminants and non-fungal sequences, ITS

Table 1
PERMANOVA results displaying the amount of compositional variation accounted for by needle age and tree, and the marginal variation of height and crown closure. P values are the results of permutation tests of pseudo F-ratios using 999 iterations, setting "tree" as a stratum.

	Df	R^2	F	P
Age class and tree				
Tree	7	0.266	14.568	0.001
Age	3	0.059	7.537	0.001
tree:age	21	0.090	1.636	0.001
Residual	224	0.585		
Total	255	1.000		
Age class and crown variables				
age:height	4	0.023	1.654	0.124
age:closure	4	0.053	3.753	0.001
Residual	244	0.859		
Total	255			

extraction, chimera removal, and LULU clustering, 1786 ASVs were identified across 284 non-control samples. After ITS extraction, there were 1316 ASVs and 1292 ASVs after chimera filtering. 138 ASVs were attributed to *Pseudotsuga* ITS sequences, totalling 561,671 reads. 1115 putatively fungal ASVs were retained after the VSEARCH filtering process. After 97% LULU clustering and contaminant removal, 899 OTUs were delineated, represented by 6,123,130 sequences over 282 samples. This was reduced to 218 OTUs, 5,001,904 sequences, and 256 samples after PERFect OTU filtering, contaminant removal, and the removal of samples that did form a full complement of needle age classes. OTU accumulation curves, generated with functions from the BiodiversityR package (Kindt and Coe 2005), indicated that each tree was adequately sampled (Fig. S1).

3.2. Composition

OTU.1, identified as *Nothophaeocryptopus gaeumannii* (Mycosphaerellales, Dothideomycetes), was the most dominant OTU in the dataset, followed by OTUs identified as *Rhabdocline parkeri* (OTU.2, OTU.3, and OTU.6; Helotiales, Leotiomycetes) (Fig. 2A). 54% of the OTUs retained occurred on two or fewer trees, while only 3% of OTUs occurred on every tree (Fig. 2B). Only eight of 218 OTUs (3.67%) achieved average relative abundances greater than 1%, with *Penicillium expansum* (OTU.65) representing the lower end of this subset (1.5%, Fig. 2C). Analyzing the full dataset revealed that source tree ($F = 14.568$, $P = 0.001$, $R^2 = 0.266$) and needle age class ($F = 7.537$, $P = 0.001$, $R^2 = 0.059$) accounted for a large portion of variation in community composition (Table 1; Fig. S2). However, these differences were influenced by unequal variance among levels within each factor ($7.643 < F < 11.575$, $P = 0.001$, Table S1). Marginal testing revealed that only crown closure accounted for unique components of variation ($F = 3.753$, $P = 0.001$, $R^2 = 0.053$; Table 1). This proportion increased when untransformed relative abundance data were used ($F = 6.294$, $P = 0.004$, $R^2 = 0.085$). When performing PERMANOVAs on each needle age subset individually, crown closure accounted for the most compositional variation in needle age classes A2 ($F = 5.849$, $P = 0.001$, $R^2 = 0.084$) and A3 ($F = 4.637$, $P = 0.002$, $R^2 = 0.068$; Table S2, Fig. 3B and Fig. 3C).

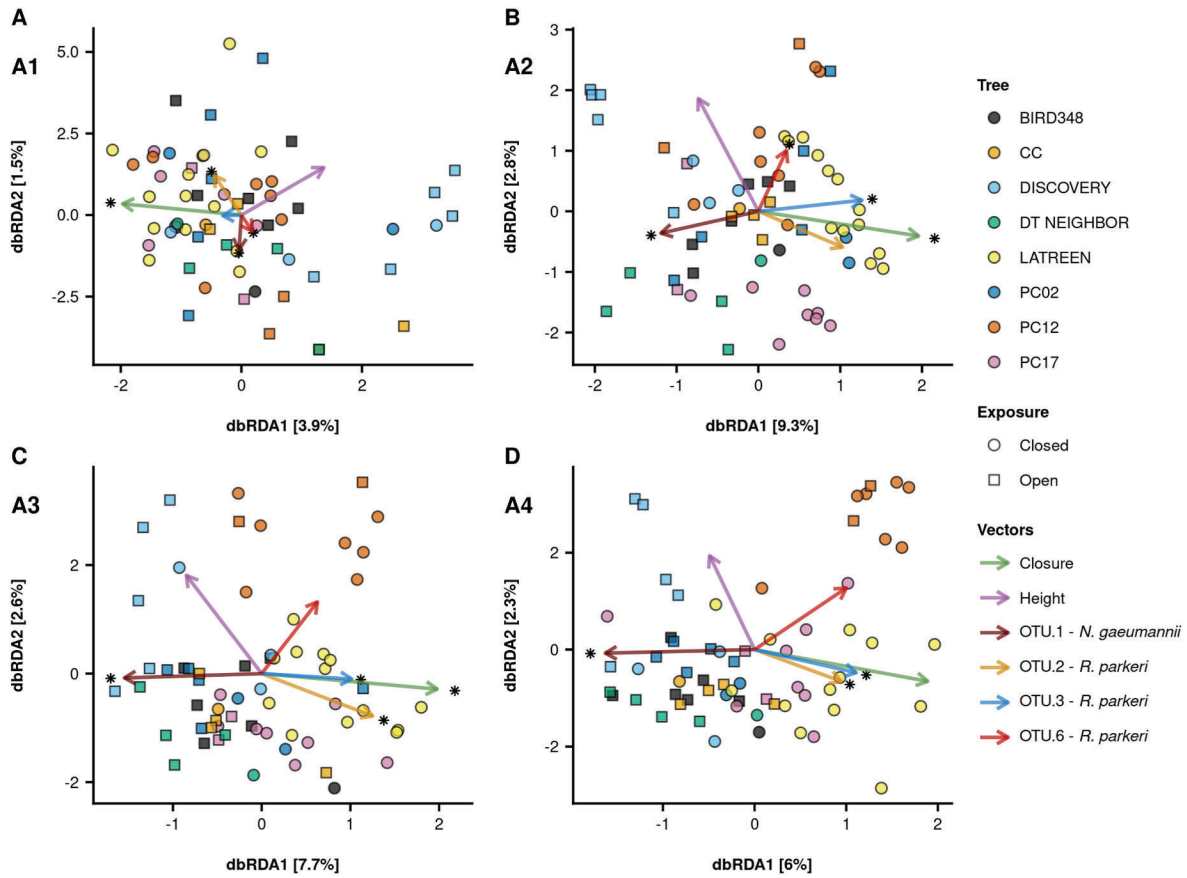

Fig. 3. Distance-based redundancy analyses (dbRDA) of Bray-Curtis dissimilarities for each needle age subset, constrained on height and crown closure. OTU vectors demonstrate correlations between ordination axes and untransformed OTU relative abundances, as assessed with the *envfit* function from the vegan R package, while crown variable vectors are extracted directly from the dbRDA biplot scores. Asterisks are associated with significant vectors (alpha = 0.05), longer vectors signify stronger correlations, but vector length should only be compared within crown variable and OTU vectors. Vector significance was assessed with 999 permutations, treating "tree" as a permutation stratum; tests involving crown variables were marginal pseudo-F tests.

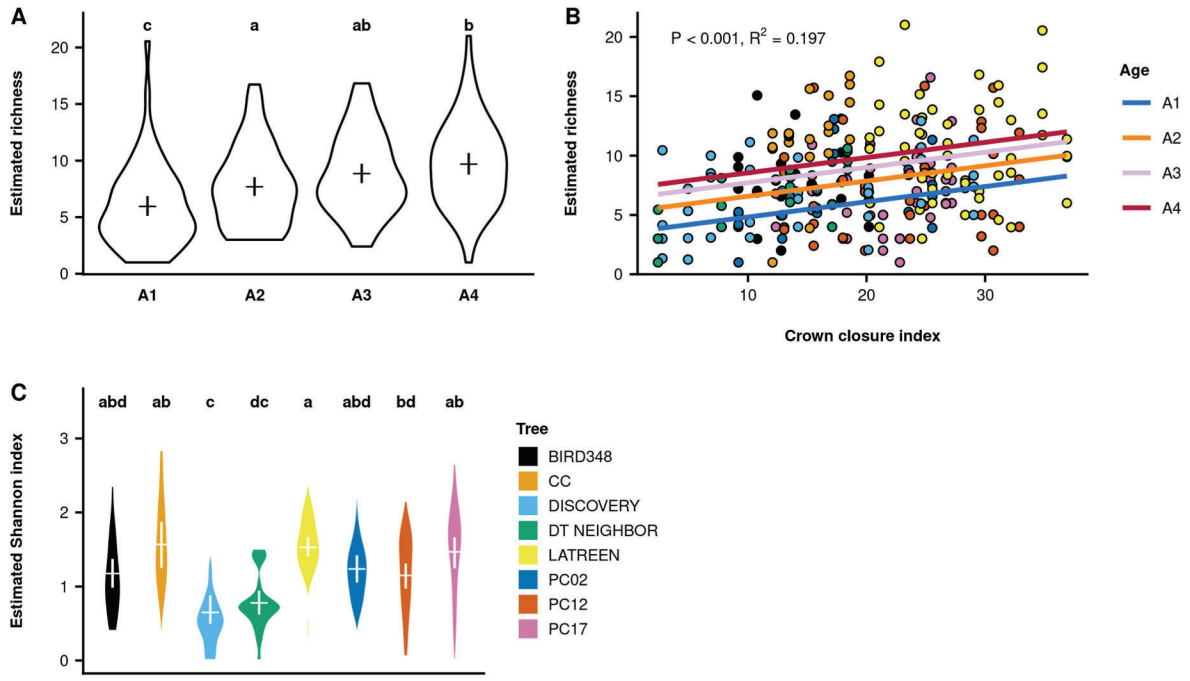

Fig. 4. Estimates of OTU richness or the Shannon index of diversity associated with needle age (A), crown closure index (B), and tree (C). Estimates were obtained for each sample via interpolation or extrapolation to a depth of 1000 reads. Violin plots illustrate the distribution of richness and Shannon index diversity estimates for each grouping. Letters for (A) and (C) indicate significant difference groups from Tukey HSD *post-hoc* comparisons (alpha = 0.05) among levels of each factor after performing ANOVA F-tests. Horizontal lines delineate the bootstrapped means of estimates, while vertical lines correspond to bootstrapped 95% confidence intervals (n = 999).

When this same analysis was performed with untransformed relative abundance data, closure only accounted for a significant component of variation in needle age class A3 ($F = 9.679$, $P = 0.003$, $R^2 = 0.131$). Given these results, only crown closure was used to define exposure groups. Exposure group assignment resulted in relatively similar numbers of open (n = 28) and closed (n = 36) exposures. Across all trees and needle age classes, OTU.1 (estimated as *N. gaeumanni*) was found to strongly associate with needles in open exposures ($P = 0.006$, IV = 0.629) and OTU.2 (*Rhabdocline parkeri*) was the strongest indicator taxon for closed exposures ($P = 0.009$, IV = 0.488). Another *Rhabocline parkeri* OTU (OTU.3) was also identified as an indicator taxon for closed exposures ($P = 0.022$, IV = 0.482). The roster of closed exposure indicator taxa exceeded the roster of open exposure indicators (Table S3).

3.3. Diversity

OTU richness varied across trees ($F = 11.264$, $P < 0.001$) and needle ages ($F = 16.343$, $P < 0.001$), increasing with needle age class (Fig. 4A) and with increasing crown closure ($\Delta AICc_{min} = 1.97$, AICc weight = 0.67, $\Delta BIC_{min} = 4.31$, BIC weight = 0.84, $P < 0.001$, $R^2 = 0.197$; Fig. 4B). Additionally, the Shannon index of diversity varied among trees ($F = 32.209$, $P < 0.001$; Fig. 4C). The Shannon index of diversity was also found to increase with increasing closure ($\Delta AICc_{min} = 1.06$, AICc weight = 0.50, $\Delta BIC_{min} = 1.06$, BIC weight = 0.60, $P < 0.001$, $R^2 = 0.079$; Fig. S3).

3.4. Structure

Fungal community composition from heights in the open and closed exposure groups were differentially structured over needle age class transitions (Fig. 5). For closed exposures, community structure became increasingly correlated over the A1-A4 transitions. No significant structural correlation was detected at the A1 to A2 transition ($P = 0.762$), nor for the A2 to A3 transition ($P = 0.204$) but community structures were strongly correlated with each other at the A3 to A4 ($P = 0.034$, Spearman correlation $\rho = 0.782$). Conversely, the community structures of open exposures were not correlated at any transition stage ($P \geq 0.220$). The relative abundance of *N. gaeumannii* (OTU.1) in all exposures only increased at the A2 to A3 transition (Wilcoxon signed rank test, $V = 208$, $P < 0.001$). OTU.1 relative abundances in closed exposures, however, remained lower than relative abundances in open exposures at A3 (Wilcoxon rank sum test, $W = 815.5$, $P < 0.001$) with slightly elevated proportions in A3 and A4 (Fig. 6A). Conversely, *R. parkeri* OTUs (OTU.2, OTU.3, and OTU.6) across all exposures increased in relative abundance from A1 to A2 ($V = 406$, $P < 0.001$), but larger relative abundances were achieved in closed exposures at A2 ($W = 238$, $P < 0.001$, Fig. 6B). These *R. parkeri* OTUs decreased in relative abundance at the A2 to A3 transition ($V = 1649$, $P < 0.001$), but closed exposures had higher relative abundances than open exposures ($W = 206$, $P < 0.001$) at A3.

4. Discussion

This study is the first of its kind to combine airborne LiDAR-derived metrics with fine-scale, within-crown foliage sampling of known needle age classes, and high-throughput amplicon sequencing. Additionally, forest-level LiDAR data were exploited to more objectively classify the crowns of climbed trees in the dataset. Altogether, these approaches showed that the diversity, composition, and structure of the endophytic needle mycobiome are correlated with the surrounding crown microenvironment in a way that depends on the age classes of needles. This study demonstrates the unique utility that remote sensing technologies like LiDAR can provide to studies of "hard-to-reach" ecological communities, while also allowing researchers to frame the sometimes limited environmental variation among their sampled sites in the context of variation observed at larger scales. Further, the high throughput amplicon sequencing approach taken here resulted in identifications of the same dominant taxa described in earlier, established work. Namely, *Nothophaecryptopus gaeumannii* (Stone et al., 2008), *Rhabdocline parkeri* (Sherwood-Pike et al., 1986), and *Phyllosticta*

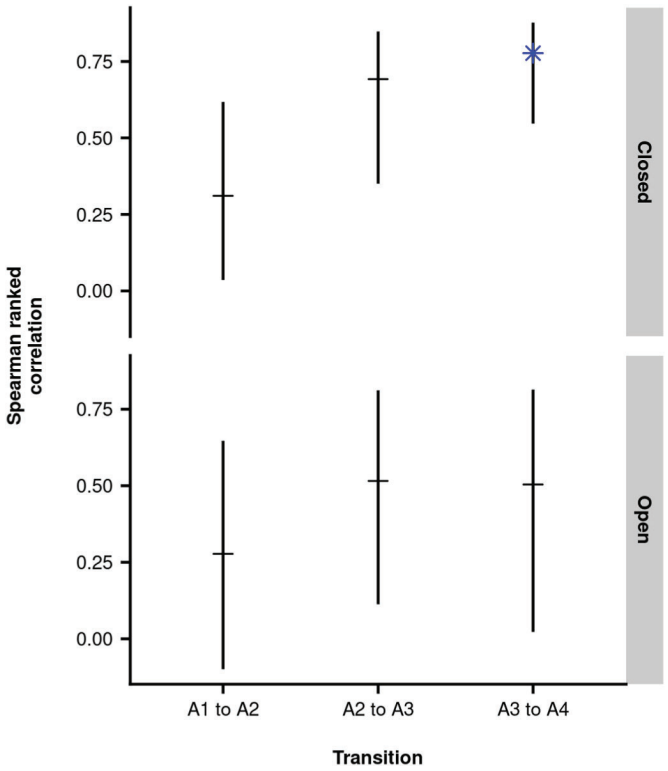

Fig. 5. Spearman Mantel correlations between increasing needle age classes for samples in open and closed exposure groups. Horizontal lines show the mean bootstrapped correlation statistics (n = 999), and vertical lines show the bootstrapped 95% confidence intervals. Higher correlation statistics indicate greater similarities in community structure between two needle age classes. Results of sample estimate Mantel tests with $P < 0.05$ are indicated by blue asterisks. P values were the result of 999 permutations, treating "tree" as permutation stratum.

spp. (Petrini et al., 1991) have been described as key members of the *Pseudotsuga menziesii* needle endophyte community. Taxa previously reported on the *P. menziesii* phylloplane or spermosphere (or associated with other conifers) were also frequently detected. These included *Zasmidium pseudotsugae* (Barr, 2009), *Hormonema macrosporum* (Bergmann and Busby, 2021), *Diaporthe* spp. (Gomes et al., 2013), *Micraspis strobilina* (Quijada et al., 2020), Phaeomoniellaceae sp. (Chen et al., 2015, Fig. 2).

4.1. Crown closure, interacting with needle age, accounted for more community variation than height

Source tree accounted for the greatest amount of compositional variation among samples (Table 1, Fig. S2), likely due to the large number of OTUs specific to only one or a few trees (Fig. 2). These results are similar to those of Harrison et al., (2016) and Oono et al., (2017), where, despite spatial ranges differing between the three studies by an order of magnitude (~10 km for the current study vs ~100 km for Oono et al. vs ~700 km for Harrison et al.), source tree or site also accounted for a large portion of variation in the composition of the foliar endophytic mycobiome of conifers. Further, these and other (Izuno et al., 2016), earlier studies find compositional differences between sampled crown positions. Analogous to crown position, height measured in the present study was unable to account for unique compositional variation (Table 1), perhaps suggesting that previously reported vertical stratification effects are actually unmeasured crown closure effects, given that crown closure decreases monotonically with increasing height in crown. This is supported by culture-based and visual survey studies which showed that certain foliar fungal taxa appeared to demonstrate preferences for either qualitatively defined shaded or exposed foliage (Osono and Mori, 2004; Gilbert et al., 2007; Unterseher et al., 2007; Scholtysik et al., 2013), but this effect is not consistently observed (Taudière et al., 2018). However, other work examining terrestrial macrofungal communities has established correlations between airborne LiDAR-derived measurements of canopy cover, maximum canopy height aboveground, and compositional turnover (Thers et al., 2017). In any case, quantifying exposure beyond canopy position or height should facilitate comparisons between studies of crown-associated foliar fungi (Arnold and Herre, 2003).

Analyzing each needle age class separately showed that compositional signal attributable to crown closure was detected at all needle ages, but peaked at A2 and A3 (Table S2, Fig. 3). The closure signal was stronger overall, but constrained to one needle age class when metabarcoding data were analyzed according to relative abundances that were not log-transformed. This result is indicative of the extent to which endophytic fungal communities were dominated by a few common taxa, a condition also reported by Harrison et al., (2016). Regardless of whether rarer or more common taxa were given more weight, closure-mediated compositional signal continued to collapse after needle age class A3 (Fig. 3). Thus, this shift in community composition for older needle age classes marks when smaller-scale, intra-crown community dynamics might give way to larger-scale or non-closure-mediated assembly dynamics. Needle age class has also been found to account for compositional variation of foliar fungal communities in both metabarcoding (Würth et al., 2019) and culture-based studies (Osono, 2008), and this is likely due to higher incidences of infection observed for older needle age classes (Sherwood and Carroll, 1974; Bernstein and Carroll, 1977; Petrini and Carroll, 1981) resulting from longer exposure to inoculum sources (Arnold and Herre, 2003). However, differences in needle physiology and morphology also accrue with increasing needle age class (Porte and Loustau, 1998; Bernier et al., 2001; Apple et al., 2002; Ishii et al., 2002; Yan et al., 2012; Eimil-Fraga et al., 2015), potentially accounting for its influence on endophyte community composition.

The relevance of crown closure is also supported by the finding that OTU richness and diversity increased with increasing closure (Fig. 4B, Fig. S3), with the model selection process explicitly excluding height. Again, these findings are similar to those reported from foliar fungal surveys and airborne LiDAR-supported macrofungal studies (Osono and Mori, 2004; Gilbert et al., 2007; Unterseher et al., 2007; Scholtysik et al., 2013; Thers et al., 2017), but evidence from metabarcoding studies is mixed and complicated by the inconsistent use of canopy position or light exposure groups between studies (Harrison et al., 2016; Izuno et al., 2016; Oono et al., 2017; Taudière et al., 2018). If compared with findings that composition and richness vary along larger-scale temperature and precipitation gradients (Giauque and Hawkes, 2016; Bowman and Arnold, 2021; Oita et al., 2021), the results observed in the current study might suggest the more immediate action of microclimate-mediated environmental filtering mechanisms that operate at smaller scales. However, this interpretation relies on the strength of the relationship between within-crown LiDAR and microclimatic metrics, which has yet to be sufficiently demonstrated. Further, physiological and morphological needle traits vary within the crowns of conifers in response to these same microclimatic gradients (Ishii et al., 2002, 2008; Gebauer et al., 2015; Schweiger et al., 2020), and this variation may have the potential to act with even more immediacy in structuring conifer endophyte communities. In fact, correlations of crown closure with composition and diversity can still suggest a role for closure-mediated dispersal limitation in structuring these communities (Gilbert and Reynolds, 2005), modifying the effect of closure-mediated environmental filtering.

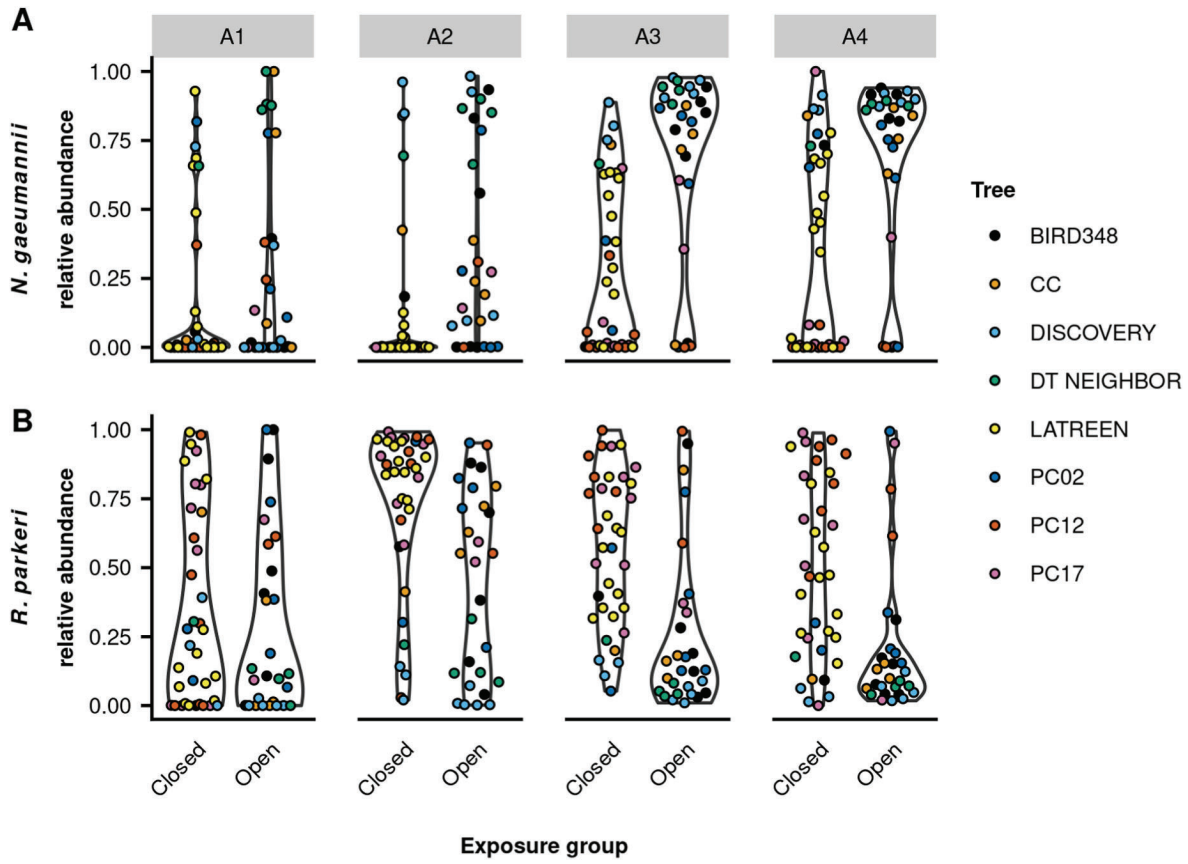

Fig. 6. Relative abundances of OTU.1 (identified to *Nothophaeocryptopus gaeumannii*) (A) and OTU.2, OTU.3, and OTU.6 (identified to *Rhabdocline parkeri*) (B) in each exposure group and needle age class.

4.2. Community structure diverges via interactions between needle age and needle exposure

Further exploration of needle age class and exposure group showed that inter-age differences in community structure differed between open and closed exposure groups. Although no structural correlations were detected at the A1-A2 and A2-A3 transitions for both exposure groups, strongly correlated structure was detected for closed exposures at the A3-A4 transition, indicating that turnover proceeded in a way that preserved some of the structure associated with the previous needle age class (Fig. 5). Conversely, open exposures never demonstrated significant structural correlations, signifying dynamic shifts in one or many compositional elements between needle age classes. Although the relative abundance of open exposure indicator OTU.1 (identified as *Nothophaeocryptopus gaeumannii;* Table S3) increased at the A2 to A3 transition, this increase was less pronounced for needles sampled from closed exposures (Figs. 3 and 6A), suggestive of altered community assembly dynamics relative to needles from open exposures. However, without sampling even older needle age classes, it is not apparent that (1) endophyte communities in needles from closed exposures would ever fully converge on a composition defined by *N. gaeumannii* dominance, (2) that the community structure of needles from open exposures ever stabilizes, or (3) that closed exposures retain age-class-to-age-class community structure.

Overall, observations from this study align with what is known about the infection cycle of *N. gaeumannii* and the general pathology of the Swiss needle cast (SNC) disease it can cause in *P. menziesii*. Conidium production has never been observed. Instead, needles are initially infected solely via ascospores (Stone et al., 2008) dispersed by rain. Ascospore release generally coincides with *P. menziesii* bud burst, and older needles appear to resist ascospore infection to some degree, leading pathologists to conclude that infection primarily occurs on newly emerged foliage during the spring and summer. After entering via stomata, *N. gaeumannii* proceeds to extensively colonize intercellular spaces over the lifetime of the needle, perhaps assisted by periodic epiphytic growth and stomatal reentry. Thus, continued colonization after early infection likely accounted for the majority of the observed increases in *N. gaeumannii* relative abundance at each needle age class transition (Fig. 6). The extent of this advantage was apparent given that the increase in OTU richness from A1 to A4 (Fig. 4A) was not met with an increase in the Shannon index of diversity over these needle age classes (Table S4). This suggests that while other taxa are able to at least infect a needle over its lifetime, they are generally unable to colonize the needle as effectively as *N. gaeumannii* over this period. The greater relative abundance and incidence of *N. gaeumannii* OTU.1 in open exposures is corroborated by experimental findings that shade-treated *P. menziesii* seedlings showed reduced SNC severity relative to the full-sun treatments (Manter et al., 2005). This measure of severity was also correlated with higher winter temperatures measured over the course of the experiment. Results from this earlier experiment are also in accordance with the common observation that SNC disease severity is negatively correlated with depth in crown in natural and managed stands of *P. menziesii* (Hansen et al., 2000; Lan et al., 2019, 2022; Ritokova et al., 2020). A greater abundance of *N. gaeumannii* in warm, open exposures could reflect morphological and/or physiological adaptations to this niche. For example, previous work has reported that cultures of *N. gaeumannii* can deposit red pigments into the growth medium, suggesting that *N. gaeumannii*, like *Cercospora* spp. also in the Mycosphaerellaceae, may produce cercosporin or cercosporin-like perylenequinones (Winton et al., 2007). Cercosporin, which is red in its active, oxidized state, was originally isolated from *Cercospora kikuchii* and since been shown to disrupt plant cell membranes via the

photoactivation of singlet oxygen (Daub and Ehrenshaft, 2000). Similar to SNC patterns, the incidence and progression of several diseases caused by perylenequinone-producing fungi (*Cercospora* spp., *Alternaria alternata*) are also positively associated with increased light exposure (Daub et al., 2013). Further investigation of the most recent assembly of the *N. gaeumannii* genome (BioProject PRJNA212511, BioSample SAMN02254965) with the antiSMASH BGC prediction program (fungiSMASH default parameters, Blin et al., 2021) revealed the presence of a putative cercosporin BGC resembling one found in *Cercospora beticola* with 31% similarity (Table S5). Additionally, a T1PKS melanin BGC was identified, showing 100% similarity with a cluster found in *Bipolaris oryzae*. These findings, taken alongside increasing relative abundance of *N. gaeumannii* with decreasing crown closure, suggest that *N. gaeumannii* may be adapted to a niche characterized by warm temperatures and/or pronounced light exposure.

In contrast to *N. gaeumannii*, dominant *Rhabdocline parkeri* OTUs (OTU.2, OTU.3) were identified as taxa associated with closed exposures (Table S3), which is also in accordance with the known biology of this endophyte. Conidia of *R. parkeri* infect needles of *P. menziesii* and remain within a single epidermal cell until the needle approaches senescence. Rain-dispersed conidia produced on abscised needles can infect living needles of all needle age classes during the wet winter months (Sherwood-Pike et al., 1986). Needles are soon overtaken by generalist saprotroph communities once abscised needles reach terrestrial leaf litter (Stone, 1987), but *R. parkeri* has been shown to dominate the endosphere of abscised needles shaken directly from ten year-old *P. menziesii* crowns (Gonen, 2020). These abscised needles lodged in the crown then serve as inoculum sources for new infections in the crown. To account for the results of our indicator species analysis, it is hypothesized that the crowns above closed exposures intercept and/or retain more abscised needles on branches compared to portions above open exposures. *P. menziesii* canopy soils are derived from bark and decomposing needles deposited on branches (Pike et al., 1975), and these soils might then serve as reservoirs for *R. parkeri* and potentially other endophytic fungi (Looby et al., 2020). The capacity for a tree crown to retain needle litter reservoirs close to living foliage might also be adaptive if fungi sourced from this litter can reduce pest or pathogen damage, as has been described for *R. parkeri* (Carroll, 1988). This reservoir effect could also account for the finding that OTU richness and diversity increased with increasing crown closure (Fig. 4B; Fig. S3). However, closed exposures could also be associated with more moist, thermostable, and otherwise accommodating microhabitats that are favorable to infection by *R. parkeri* and/or fungi in general, potentially accounting for or contributing to the indicator status of *R. parkeri* OTUs and the greater taxonomic diversity associated with closed exposures (Unterseher and Tal, 2006).

Declaration of competing interest

The authors declare no conflicts of interest.

Acknowledgements

Data were provided by the HJ Andrews Experimental Forest and Long Term Ecological Research (LTER) program, administered cooperatively by the USDA Forest Service Pacific Northwest Research Station, Oregon State University, and the Willamette National Forest. This material is based upon work supported by the National Science Foundation under LTER7 DEB-1440409 (2014–2020).

The authors would also like to acknowledge Dr. Mark Schulze, Dr. Adam Sibley, Robert Miron, and Sarah Ward for organizing and executing needle collection. Additionally, the authors thank the H.J. Andrews Forest Canopy Group for their interest and input throughout the execution and analysis of the study. Lastly, the authors also wish to recognize the significant contributions of Dr. George Carroll, Dr. Lawrence Pike, Dr. Martha Sherwood, and Dr. Jeffrey Stone to the study of *P. menziesii* crowns and needle fungi, which greatly facilitated interpretation of the results obtained here.

Appendix A. Supplementary data

Supplementary data to this article can be found online at https://doi.org/10.1016/j.funeco.2022.101155.

References

Abarenkov, K., Zirk, A., Piirmann, T., Pöhönen, R., Ivanov, F., Nilsson, R.H., Kõljalg, U., 2020a. UNITE general FASTA release for eukaryotes 2. Version 04.02.2020. UNITE Community. https://doi.org/10.15156/BIO/786371.

Abarenkov, K., Zirk, A., Piirmann, T., Pöhönen, R., Ivanov, F., Nilsson, R.H., Kõljalg, U., 2020b. UNITE general FASTA release for Fungi. Version 04.02.2020. UNITE Community. https://doi.org/10.15156/BIO/786368.

Anderson, M.J., 2001. A new method for non-parametric multivariate analysis of variance: non-parametric MANOVA for ecology. Austral Ecol 26, 32–46. https://doi.org/10.1111/j.1442-9993.2001.01070 x.

Anderson, M.J., 2006. Distance-based tests for homogeneity of multivariate dispersions. Biometrics 62, 245–253. https://doi.org/10.1111/j.1541-0420.2005.00440.x.

Apple, M., Tiekotter, K., Snow, M., Young, J., Soeldner, A., Phillips, D., Tingey, D., Bond, B.J., 2002. Needle anatomy changes with increasing tree age in Douglas-fir. Tree Physiol 22, 129–136. https://doi.org/10.1093/treephys/22.2-3.129.

Arnold, A.E., Engelbrecht, B.M.J., 2007. Fungal endophytes nearly double minimum leaf conductance in seedlings of a neotropical tree species. J. Trop. Ecol. 23, 369–372. https://doi.org/10.1017/S0266467407004038.

Arnold, A.E., Herre, E.A., 2003. Canopy cover and leaf age affect colonization by tropical fungal endophytes: ecological pattern and process in *Theobroma cacao* (Malvaceae). Mycologia 95, 388–398. https://doi.org/10.1080/15572536.2004.11833083.

Barge, E.G., Leopold, D.R., Peay, K.G., Newcombe, G., Busby, P.E., 2019. Differentiating spatial from environmental effects on foliar fungal communities of Populus trichocarpa. J. Biogeogr 46, 2001–2011. https://doi.org/10.1111/jbi.13641.

Barnes, K.W., Islam, K., Auer, S.A., 2016. Integrating LIDAR-derived canopy structure into cerulean warbler habitat models. J. Wildl. Manag. 80, 101–116. https://doi.org/10.1002/jwmg.995.

Barr, M.E., 2009. A nomenclator of loculoascomycetous fungi from the Pacific Northwest. North Am. Fungi 4, 1–94. https://doi.org/10.2509/naf2009.004.001.

Bengtsson-Palme, J., Ryberg, M., Hartmann, M., Branco, S., Wang, Z., Godhe, A., Wit, P. D., Sánchez-García, M., Ebersberger, I., de Sousa, F., Amend, A., Jumpponen, A., Unterseher, M., Kristiansson, E., Abarenkov, K., Bertrand, Y.J.K., Sanli, K., Eriksson, K.M., Vik, U., Veldre, V., Nilsson, R.H., 2013. Improved software detection and extraction of ITS1 and ITS2 from ribosomal ITS sequences of fungi and other eukaryotes for analysis of environmental sequencing data. Methods Ecol. Evol. 4, 914–919. https://doi.org/10.1111/2041-210X.12073.

Benjamini, Y., Hochberg, Y., 1995. Controlling the false discovery rate: a practical and powerful approach to multiple testing. J. R. Stat. Soc. Ser. B Methodol. 57, 289–300. https://doi.org/10.1111/j.2517-6161.1995.tb02031.x.

Bergmann, G.E., Busby, P.E., 2021. The core seed mycobiome of *Pseudotsuga menziesii* var. *menziesii* across provenances of the Pacific Northwest, USA. Mycologia, pp. 1–12. https://doi.org/10.1080/00275514.2021.1952830.

Bernier, P.Y., Raulier, F., Stenberg, P., Ung, C.-H., 2001. Importance of needle age and shoot structure on canopy net photosynthesis of balsam fir (*Abies balsamea*): a spatially inexplicit modeling analysis. Tree Physiol 21, 815–830. https://doi.org/10.1093/treephys/21.12-13.815.

Bernstein, M.E., Carroll, G.C., 1977. Internal fungi in old-growth Douglas fir foliage. Can. J. Bot. 55, 644–653. https://doi.org/10.1139/b77-079.

Blin, K., Shaw, S., Kloosterman, A.M., Charlop-Powers, Z., van Weezel, G.P., Medema, M. H., Weber, T., 2021. antiSMASH 6.0: improving cluster detection and comparison capabilities. Nucleic Acids Res 49, W29–W35. https://doi.org/10.1093/nar/gkab335.

Bowman, E.A., Arnold, A.E., 2021. Drivers and implications of distance decay differ for ectomycorrhizal and foliar endophytic fungi across an anciently fragmented landscape. ISME J 1–18. https://doi.org/10.1038/s41396-021-01006-9.

Busby, P.E., Peay, K.G., Newcombe, G., 2016. Common foliar fungi of *Populus trichocarpa* modify *Melampsora* rust disease severity. New Phytol 209, 1681–1692. https://doi.org/10.1111/nph.13742.

Callahan, B.J., McMurdie, P.J., Rosen, M.J., Han, A.W., Johnson, A.J.A., Holmes, S.P., 2016. DADA2: high-resolution sample inference from Illumina amplicon data. Nat. Methods 13, 581–583. https://doi.org/10.1038/nmeth.3869.

Carisse, O., Bourgeois, G., Duthie, J.A., 2000. Influence of temperature and leaf wetness duration on infection of strawberry leaves by *Mycosphaerella fragariae*. Phytopathology 90, 1120–1125. https://doi.org/10.1094/PHYTO.2000.90.10.1120.

Carroll, G., 1988. Fungal endophytes in stems and leaves: from latent pathogen to mutualistic symbiont. Ecology 69, 2–9. https://doi.org/10.2307/1943154.

Chen, K.-H., Miadlikowska, J., Molnár, K., Arnold, A.E., U'Ren, J.M., Gaya, E., Gueidan, C., Lutzoni, F., 2015. Phylogenetic analyses of eurotiomycetous endophytes reveal their close affinities to Chaetothyriales, Eurotiales, and a new order – Phaeomoniellales. Mol. Phylogenet. Evol. 85, 117–130. https://doi.org/10.1016/j.ympev.2015.01.008.

Christian, N., Herre, E.A., Clay, K., 2019. Foliar endophytic fungi alter patterns of nitrogen uptake and distribution in *Theobroma cacao*. New Phytol 222, 1573–1583. https://doi.org/10.1111/nph.15693.

Daub, M.E., Ehrenshaft, M., 2000. The photoactivated *Cercospora* toxin cercosporin: contributions to plant disease and fundamental biology. Annu. Rev. Phytopathol. 38, 461–490. https://doi.org/10.1146/annurev.phyto.38.1.461.

Daub, M.E., Herrero, S., Chung, K.-R., 2013. Reactive oxygen species in plant pathogenesis: the role of perylenequinone photosensitizers. Antioxidants & Redox Signaling 19, 970–989. https://www.liebertpub.com/doi/abs/10.1089/ars.2012.5080.

Davis, F.W., Synes, N.W., Fricker, G.A., McCullough, I.M., Serra-Diaz, J.M., Franklin, J., Flint, A.L., 2019. LiDAR-derived topography and forest structure predict fine-scale variation in daily surface temperatures in oak savanna and conifer forest landscapes. Agric. For. Meteorol. 269–270, 192–202. https://doi.org/10.1016/j.agrformet.2019.02.015.

Doughty, C.E., Goulden, M.L., 2008. Are tropical forests near a high temperature threshold? J. Geophys. Res. 113, G00B07. https://doi.org/10.1029/2007JG000632.

Eimil-Fraga, C., Sánchez-Rodríguez, F., Álvarez-Rodríguez, E., Rodríguez-Soalleiro, R., 2015. Relationships between needle traits, needle age and site and stand parameters in *Pinus pinaster*. Trees 29, 1103–1113. https://doi.org/10.1007/s00468-015-1190-7.

Fox, J., Weisberg, S., 2019. In: An R Companion to Applied Regression, third ed. https://doi.org/10.1126/sciadv.1501392 Thousand Oaks, California, USA.

Frey, S.J.K., Hadley, A.S., Johnson, S.L., Schulze, M., Jones, J.A., Betts, M.G., 2016. Spatial models reveal the microclimatic buffering capacity of old-growth forests. Sci. Adv. 2, e1501392 https://doi.org/10.1126/sciadv.1501392.

Frøslev, T.G., Kjøller, R., Bruun, H.H., Ejrnæs, R., Brunbjerg, A.K., Pietroni, C., Hansen, A. J., 2017. Algorithm for post-clustering curation of DNA amplicon data yields reliable biodiversity estimates. Nat. Commun. 8, 1188. https://doi.org/10.1038/s41467-017-01312-x.

Galanti, L., Shasha, D., C. Gunsalus, K., 2017. Pheniqs: fast and flexible quality-aware sequence demultiplexing. bioRxiv. https://doi.org/10.1101/128512.

Gebauer, R., Čermák, J., Plichta, R., Špinlerová, Z., Urban, J., Volařík, D., Ceulemans, R., 2015. Within-canopy variation in needle morphology and anatomy of vascular tissues in a sparse Scots pine forest. Trees 29, 1447–1457. https://doi.org/10.1007/s00468-015-1224-1.

George, A.D., Thompson, F.R., Faaborg, J., 2015. Using LiDAR and remote microclimate loggers to downscale near-surface air temperatures for site-level studies. Remote Sens. Lett. 6, 924–932. https://doi.org/10.1080/2150704X.2015.1088671.

Giauque, H., Hawkes, C.V., 2016. Historical and current climate drive spatial and temporal patterns in fungal endophyte diversity. Fungal Ecol 20, 108–114. https://doi.org/10.1016/j.funeco.2015.12.005.

Gilbert, G.S., Reynolds, D.R., 2005. Nocturnal fungi: airborne spores in the canopy and understory of a tropical rain forest. Biotropica 37, 462–464. https://doi.org/10.1111/j.1744-7429.2005.00061.x.

Gilbert, G.S., Reynolds, D.R., Bethancourt, A., 2007. The patchiness of epifoliar fungi in tropical forests: host range, host abundance, and environment. Ecology 88, 575–581. https://doi.org/10.1890/05-1170.

Gomes, R.R., Glienke, C., Videira, S.I.R., Lombard, L., Groenewald, J.Z., Crous, P.W., 2013. *Diaporthe*: a genus of endophytic, saprobic and plant pathogenic fungi. Persoonia Mol. Phylogeny Evol. Fungi 31, 1–41. https://doi.org/10.3767/003158513X666844.

Gonen, L., 2020. Community Ecology of Foliar Fungi and Oomycetes of *Pseudotsuga menziesii* on the Pacific Northwest Coast. Master's thesis. Oregon State University, Corvallis, Oregon, USA.

Hansen, E.M., Stone, J.K., Capitano, B.R., Rosso, P., Sutton, W., Winton, L., Kanaskie, A., McWilliams, M.G., 2000. Incidence and impact of Swiss needle cast in forest plantations of Douglas-fir in coastal Oregon. Plant Dis 84, 773–778. https://doi.org/10.1094/PDIS.2000.84.7.773.

Harrison, J.G., Forister, M.L., Parchman, T.L., Koch, G.W., 2016. Vertical stratification of the foliar fungal community in the world's tallest trees. Am. J. Bot. 103, 2087–2095. https://doi.org/10.3732/ajb.1600277.

Hartigan, J.A., Wong, M.A., 1979. Algorithm AS 136: a k-means clustering algorithm. Appl. Stat. 28, 100. https://doi.org/10.2307/2346830.

Heffernan, E., 2017. Canopy Microclimates and Epiphytes: Examining Dynamic Patterns and Influences. Master's thesis. Oregon State University, Corvallis, Oregon, USA.

Hsieh, T.C., Ma, K.H., Chao, A., 2016. iNEXT: an R package for rarefaction and extrapolation of species diversity (Hill numbers). Methods Ecol. Evol. 7, 1451–1456. https://doi.org/10.1111/2041-210X.12613.

Ishii, H., Ford, E.D., Boscolo, M.E., Manriquez, A.C., Wilson, M.E., Hinckley, T.M., 2002. Variation in specific needle area of old-growth Douglas-fir in relation to needle age, within-crown position and epicormic shoot production. Tree Physiol 22, 31–40. https://doi.org/10.1093/treephys/22.1.31.

Ishii, H.T., Jennings, G.M., Sillett, S.C., Koch, G.W., 2008. Hydrostatic constraints on morphological exploitation of light in tall Sequoia sempervirens trees. Oecologia 156, 751–763. https://doi.org/10.1007/s00442-008-1032-z.

Izuno, A., Kanzaki, M., Artchawakom, T., Wachrinrat, C., Isagi, Y., 2016. Vertical structure of phyllosphere fungal communities in a tropical forest in Thailand uncovered by high-throughput sequencing. PLOS ONE 11, e0166669. https://doi.org/10.1371/journal.pone.0166669.

Kindt, R., Coe, R., 2005. Tree Diversity Analysis. A Manual and Software for Common Statistical Methods for Ecological and Biodiversity Studies. World Agroforestry Centre.

Kropko, J., Harden, J.J., 2020. coxed: duration-based quantities of interest for the Cox proportional hazards model. R package version 0.3.3. https://doi.org/10.1002/ece3.1589.

Lan, Y.-H., Shaw, D.C., Beedlow, P.A., Lee, E.H., Waschmann, R.S., 2019. Severity of Swiss needle cast in young and mature Douglas-fir forests in western Oregon. USA. For. Ecol. Manag. 442, 79–95. https://doi.org/10.1016/j.foreco.2019.03.063.

Lan, Y.-H., Shaw, D.C., Lee, E.H., Beedlow, P.A., 2022. Distribution of a foliage disease fungus within canopies of mature Douglas-fir in Western Oregon. Front. For. Glob. Change 5, 743039. https://doi.org/10.3389/ffgc.2022.743039.

Lefcheck, J.S., 2016. piecewiseSEM: piecewise structural equation modelling in R for ecology, evolution, and systematics. Methods Ecol. Evol. 7, 573–579. https://doi.org/10.1111/2041-210X.12512.

Lefsky, M.A., Cohen, W.B., Parker, G.G., Harding, D.J., 2002. Lidar remote sensing for ecosystem studies: lidar, an emerging remote sensing technology that directly measures the three-dimensional distribution of plant canopies, can accurately estimate vegetation structural attributes and should be of particular interest to forest, landscape, and global ecologists. BioScience 52, 19–30. https://doi.org/10.1641/0006-3568(2002)052[0019:LRSFES]2.0.CO;2.

Long, J.S., Ervin, L.H., 2000. Using heteroscedasticity consistent standard errors in the Linear Regression Model. Am. Stat. 54, 217–224.

Looby, C.I., Hollenbeck, E.C., Treseder, K.K., 2020. Fungi in the canopy: how soil fungi and extracellular enzymes differ between canopy and ground soils. Ecosystems 23, 768–782. https://doi.org/10.1007/s10021-019-00439-w.

Lovell, J.L., Jupp, D.L.B., Culvenor, D.S., Coops, N.C., 2003. Using airborne and ground-based ranging lidar to measure canopy structure in Australian forests. Can. J. Remote Sens. 29, 607–622.

Manter, D.K., Reeser, P.W., Stone, J.K., 2005. A climate-based model for predicting geographic variation in Swiss needle cast severity in the Oregon Coast Range. Phytopathology 95, 1256–1265. https://doi.org/10.1094/PHYTO-95-1256.

Martin, M., 2011. Cutadapt removes adapter sequences from high-throughput sequencing reads. EMBnet.journal 17, 10–12. https://doi.org/10.14806/ej.17.1.200.

Mazerolle, M.J., 2020. AICcmodavg: model selection and multimodel inference based on (Q)AIC(c). R package version 2.3-1. https://cran.r-project.org/package=AICcmodavg.

McCune, B., 1993. Gradients in epiphyte biomass in three *Pseudotsuga-Tsuga* forests of different ages in western Oregon and Washington. The Bryologist 96, 405–411. https://doi.org/10.2307/3243870.

McMurdie, P.J., Holmes, S., 2013. phyloseq: an R package for reproducible interactive analysis and graphics of microbiome census data. PLoS ONE 8, e61217. https://doi.org/10.1371/journal.pone.0061217.

Norros, V., Karhu, E., Nordén, J., Vähätalo, A.V., Ovaskainen, O., 2015. Spore sensitivity to sunlight and freezing can restrict dispersal in wood-decay fungi. Ecol. Evol. 5, 3312–3326. https://doi.org/10.1002/ece3.1589.

Oita, S., Ibáñez, A., Lutzoni, F., Miadlikowska, J., Geml, J., Lewis, L.A., Hom, E.F.Y., Carbone, I., U'Ren, J.M., Arnold, A.E., 2021. Climate and seasonality drive the richness and composition of tropical fungal endophytes at a landscape scale. Commun. Biol. 4, 1–11. https://doi.org/10.1038/s42003-021-01826-7.

Oksanen, J., Blanchet, F.G., Friendly, M., Kindt, R., Legendre, P., McGlinn, D., Minchin, P.R., O'Hara, R.B., Simpson, G.L., Solymos, P., Stevens, M.H.H., Szoecs, E., Wagner, H., 2020. vegan: community ecology package. R package version 2.5-7. https://doi.org/10.2307/3242161.

Oono, R., Rasmussen, A., Lefèvre, E., 2017. Distance decay relationships in foliar fungal endophytes are driven by rare taxa: distance decay in fungal endophytes. Environ. Microbiol. 19, 2794–2805. https://doi.org/10.1111/1462-2920.13799.

Osono, T., 2008. Endophytic and epiphytic phyllosphere fungi of *Camellia japonica* : seasonal and leaf age-dependent variations. Mycologia 100, 387–391. https://doi.org/10.3852/07-110R1.

Osono, T., Mori, A., 2004. Distribution of phyllosphere fungi within the canopy of giant dogwood. Mycoscience 45, 161–168. https://doi.org/10.1007/S10267-003-0167-3.

Parker, G., 1997. Canopy structure and light environment of an old-growth Douglas-fir/western hemlock forest. Northwest Sci 71, 261–270.

Partners, O.C.M., 2020. 2016 Oregon department of Geology and mineral industries (DOGAMI) Oregon lidar: McKenzie river. https://www.fisheries.noaa.gov/inport/item/49949.

Petrini, O., Carroll, G., 1981. Endophytic fungi in foliage of some Cupressaceae in Oregon. Can. J. Bot. 59, 629–636. https://doi.org/10.1139/b81-089.

Petrini, L.E., Petrini, O., Leuchtmann, A., Carroll, G.C., 1991. Conifer inhabiting species of *Phyllosticta*. Sydowia 148–169.

Peura, M., Silveyra Gonzalez, R., Müller, J., Heurich, M., Vierling, L.A., Mönkkönen, M., Bässler, C., 2016. Mapping a 'cryptic kingdom': performance of lidar derived environmental variables in modelling the occurrence of forest fungi. Remote Sens. Environ. 186, 428–438. https://doi.org/10.1016/j.rse.2016.09.003.

Pike, L.H., Denison, W.C., Tracy, D.M., Sherwood, M.A., Rhoades, F.M., 1975. Floristic survey of epiphytic lichens and bryophytes growing on old-growth conifers in western Oregon. The Bryologist 78, 389–402. https://doi.org/10.2307/3242161.

Pinheiro, J., Bates, D., DebRoy, S., Sarkar, D., R Core Team, 2021. nlme: linear and nonlinear mixed effects models. R package version 3.1-152. https://CRAN.R-project.org/package=nlme.

Porte, A., Loustau, D., 1998. Variability of the photosynthetic characteristics of mature needles within the crown of a 25-year-old *Pinus pinaster*. Tree Physiol 18, 223–232. https://doi.org/10.1093/treephys/18.4.223.

Quijada, L., Tanney, J.B., Popov, E., Johnston, P.R., Pfister, D.H., 2020. Cones, needles and wood: *Micraspis* (Micraspidaceae, Micraspidales fam. et ord. nov.) speciation segregates by host plant tissues. Fungal Syst. Evol. 5, 99–111. https://doi.org/10.3114/fuse.2020.05.05.

R Core Team, 2020. R: A Language and Environment for Statistical Computing. R Foundation for Statistical Computing, Vienna, Austria. https://doi.org/10.1093/biostatistics/kxy020.

Ritokova, G., Mainwaring, D.B., Shaw, D.C., Lan, Y.-H., 2020. Douglas-fir foliage retention dynamics across a gradient of Swiss needle cast in coastal Oregon and Washington. Can. J. For. Res. https://doi.org/10.1139/cjfr-2020-0318 cjfr-2020-0318.

Roberts, David W., 2019. labdsv: Ordination and Multivariate Analysis for Ecology. R package version 2.0-1. https://CRAN.R-project.org/package=labdsv.
Rognes, T., Flouri, T., Nichols, B., Quince, C., Mahé, F., 2016. VSEARCH: a versatile open source tool for metagenomics. PeerJ 4, e2584. https://doi.org/10.7717/peerj.2584.
Roussel, J.-R., Auty, D., Coops, N.C., Tompalski, P., Goodbody, T.R.H., Meador, A.S., Bourdon, J.-F., de Boissieu, F., Achim, A., 2020. lidR: an R package for analysis of Airborne Laser Scanning (ALS) data. Remote Sens. Environ. 251, 112061. https://doi.org/10.1016/j.rse.2020.112061.
Saikkonen, K., Faeth, S.H., Helander, M., Sullivan, T.J., 1998. Fungal endophytes: a continuum of interactions with host plants. Annu. Rev. Ecol. Syst. 29, 319–343. https://doi.org/10.1146/annurev.ecolsys.29.1.319.
Scholtysik, A., Unterseher, M., Otto, P., Wirth, C., 2013. Spatio-temporal dynamics of endophyte diversity in the canopy of European ash (*Fraxinus excelsior*). Mycol. Prog. 12, 291–304. https://doi.org/10.1007/s11557-012-0835-9.
Schweiger, A.K., Lussier Desbiens, A., Charron, G., La Vigne, H., Laliberté, E., 2020. Foliar sampling with an unmanned aerial system (UAS) reveals spectral and functional trait differences within tree crowns. Can. J. For. Res. 50, 966–974. https://doi.org/10.1139/cjfr-2019-0452.
Sherwood, M., Carroll, G., 1974. Fungal succession on needles and young twigs of old-growth Douglas fir. Mycologia 66, 499–506. https://doi.org/10.1080/00275514.1974.12019631.
Sherwood-Pike, M., Stone, J.K., Carroll, G.C., 1986. *Rhabdocline parkeri* , a ubiquitous foliar endophyte of Douglas-fir. Can. J. Bot. 64, 1849–1855. https://doi.org/10.1139/b86-245.
Sillett, S.C., Rambo, T.R., 2000. Vertical distribution of dominant epiphytes in Douglas-fir forests of the central Oregon Cascades. Northwest Sci 74, 44–49.
Smirnova, E., Huzurbazar, S., Jafari, F., 2019. PERFect: PERmutation Filtering test for microbiome data. Biostatistics 20, 615–631. https://doi.org/10.1093/biostatistics/kxy020.
Spies, T., 2016. LiDAR Data (August 2008) for the Andrews Experimental Forest and Willamette National Forest Study Areas. Long-Term Ecological Research. Forest Science Data Bank, Corvallis, Oregon, USA. https://doi.org/10.6073/pasta/c47128d6c63dff39ee48604ecc6fabfc. Database.
Stone, J.K., 1987. Initiation and development of latent infections by *Rhabdocline parkeri* on Douglas-fir. Can. J. Bot. 65, 2614–2621. https://doi.org/10.1139/b87-352.
Stone, J.K., Capitano, B.R., Kerrigan, J.L., 2008. The histopathology of *Phaeocryptopus gaeumannii* on Douglas-fir needles. Mycologia 100, 431–444. https://doi.org/10.3852/07-170R1.
Sturm, M., Schroeder, C., Bauer, P., 2016. SeqPurge: highly-sensitive adapter trimming for paired-end NGS data. BMC Bioinformatics 17, 208. https://doi.org/10.1186/s12859-016-1069-7.
Taudière, A., Bellanger, J.-M., Carcaillet, C., Hugot, L., Kjellberg, F., Lecanda, A., Lesne, A., Moreau, P.-A., Scharmann, K., Leidel, S., Richard, F., 2018. Diversity of foliar endophytic ascomycetes in the endemic Corsican pine forests. Fungal Ecol 36, 128–140. https://doi.org/10.1016/j.funeco.2018.07.008.
Taylor, D.L., Walters, W.A., Lennon, N.J., Bochicchio, J., Krohn, A., Caporaso, J.G., Pennanen, T., 2016. Accurate estimation of fungal diversity and abundance through improved lineage-specific primers optimized for Illumina amplicon sequencing. Appl. Environ. Microbiol. 82, 7217–7226. https://doi.org/10.1128/AEM.02576-16.
Thers, H., Brunbjerg, A.K., Læssøe, T., Ejrnæs, R., Bøcher, P.K., Svenning, J.-C., 2017. Lidar-derived variables as a proxy for fungal species richness and composition in temperate Northern Europe. Remote Sens. Environ. 200, 102–113. https://doi.org/10.1016/j.rse.2017.08.011.
Thomas, D.C., Vandegrift, R., Ludden, A., Carroll, G.C., Roy, B.A., 2016. Spatial ecology of the fungal genus *Xylaria* in a tropical cloud forest. Biotropica 48, 381–393. https://doi.org/10.1111/btp.12273.
Unterseher, M., Tal, O., 2006. Influence of small scale conditions on the diversity of wood decay fungi in a temperate, mixed deciduous forest canopy. Mycol. Res. 110, 169–178. https://doi.org/10.1016/j.mycres.2005.08.002.
Unterseher, M., Reiher, A., Finstermeier, K., Otto, P., Morawetz, W., 2007. Species richness and distribution patterns of leaf-inhabiting endophytic fungi in a temperate forest canopy. Mycol. Prog. 6, 201–212. https://doi.org/10.1007/s11557-007-0541-1.
Valdez, J.W., Brunbjerg, A.K., Fløjgaard, C., Dalby, L., Clausen, K.K., Pärtel, M., Pfeifer, N., Hollaus, M., Wimmer, M.H., Ejrnæs, R., Moeslund, J.E., 2021. Relationships between macro-fungal dark diversity and habitat parameters using LiDAR. Fungal Ecol 51, 101054. https://doi.org/10.1016/j.funeco.2021.101054.
Wang, Q., Garrity, G.M., Tiedje, J.M., Cole, J.R., 2007. Naïve Bayesian classifier for rapid assignment of rRNA sequences into the new bacterial taxonomy. Appl. Environ. Microbiol. 73, 5261–5267. https://doi.org/10.1128/AEM.00062-07.
Wickham, H., Averick, M., Bryan, J., Chang, W., D'Agostino McGowan, L., François, R., Grolemund, G., Hayes, A., Henry, L., Hester, J., Kuhn, M., Pedersen, T.L., Miller, E., Milton Bache, S., Müller, K., Ooms, J., Robinson, D., Seidel, D.P., Spinu, V., Takahashi, K., Vaughan, D., Wilke, C., Woo, K., Yutani, H., 2019. Welcome to the tidyverse. J. Open Source Softw. 4, 1686.
Winton, L.M., Stone, J.K., Hansen, E.M., Shoemaker, R.A., 2007. The systematic position of *Phaeocryptopus gaeumannii*. Mycologia 99, 240–252. https://doi.org/10.1080/15572536.2007.11832584.
Würth, D.G., Dahl, M.B., Trouillier, M., Wilmking, M., Unterseher, M., Scholler, M., Sørensen, S., Mortensen, M., Schnittler, M., 2019. The needle mycobiome of *Picea glauca* – a dynamic system reflecting surrounding environment and tree phenological traits. Fungal Ecol 41, 177–186. https://doi.org/10.1016/j.funeco.2019.05.006.
Yan, C.-F., Han, S.-J., Zhou, Y.-M., Wang, C.-G., Dai, G.-H., Xiao, W.-F., Li, M.-H., 2012. Needle-age related variability in nitrogen, mobile carbohydrates, and δ13C within *Pinus koraiensis* tree crowns. PLoS ONE 7, e35076. https://doi.org/10.1371/journal.pone.0035076.
Zimmerman, N.B., Vitousek, P.M., 2012. Fungal endophyte communities reflect environmental structuring across a Hawaiian landscape. Proc. Natl. Acad. Sci. 109, 13022–13027. https://doi.org/10.1073/pnas.1209872109.

frontiers in Forests and Global Change

ORIGINAL RESEARCH
published: 25 February 2022
doi: 10.3389/ffgc.2021.756678

Genetic Lineage Distribution Modeling to Predict Epidemics of a Conifer Disease

Naomie Y. H. Herpin-Saunier[1,2], Kishan R. Sambaraju[1,2], Xue Yin[3], Nicolas Feau[3,4], Stefan Zeglen[5], Gabriela Ritokova[6], Daniel Omdal[7], Chantal Côté[2] and Richard C. Hamelin[1,3]*

[1] Department of Wood Sciences and Forestry, Laval University, Quebec, QC, Canada, [2] Laurentian Forestry Centre, Natural Resources Canada, Canadian Forest Service, Quebec, QC, Canada, [3] Department of Forest and Conservation Sciences, The University of British Columbia, Vancouver, BC, Canada, [4] Pacific Forestry Centre, Canadian Forest Service, Natural Resources Canada, Victoria, BC, Canada, [5] British Columbia Ministry of Forests, Lands, Natural Resource Operations and Rural Development, Nanaimo, BC, Canada, [6] Oregon Department of Forestry, Oregon State Hospital, Salem, OR, United States, [7] Department of Natural Resources, Washington State Government, Olympia, WA, United States

OPEN ACCESS

Edited by:
Ari Mikko Hietala, Norwegian Institute of Bioeconomy Research (NIBIO), Norway

Reviewed by:
Juha Honkaniemi, Natural Resources Institute Finland (Luke), Finland
Jeffrey Stone, Oregon State University, United States

***Correspondence:**
Naomie Y. H. Herpin-Saunier
naomie.herpin-saunier.1@ulaval.ca

Specialty section:
This article was submitted to Pests, Pathogens and Invasions, a section of the journal Frontiers in Forests and Global Change

Received: *10 August 2021*
Accepted: *23 December 2021*
Published: *25 February 2022*

Citation:
Herpin-Saunier NYH, Sambaraju KR, Yin X, Feau N, Zeglen S, Ritokova G, Omdal D, Côté C and Hamelin RC (2022) Genetic Lineage Distribution Modeling to Predict Epidemics of a Conifer Disease. Front. For. Glob. Change 4:756678. doi: 10.3389/ffgc.2021.756678

A growing body of evidence suggests that climate change is altering the epidemiology of many forest diseases. *Nothophaeocryptopus gaeumannii* (Rhode) Petrak, an ascomycete native to the Pacific Northwest and the causal agent of the Swiss needle cast (SNC) disease of Douglas-fir [*Pseudotsuga menziesii* (Mirbel) Franco], is no exception. In the past few decades, changing climatic conditions have coincided with periodic epidemics of SNC in coastal forests and plantations from Southwestern British Columbia (B.C.) to Southwestern Oregon, wherein an increase in the colonization of needles by *N. gaeumanii* causes carbon starvation, premature needle shedding and a decline in growth. Two major sympatric genetic lineages of *N. gaeumannii* have been identified in the coastal Pacific Northwest. Past research on these lineages suggests they have different environmental tolerance ranges and may be responsible for some variability in disease severity. In this study, we examined the complex dynamics between biologically pertinent short- and long-term climatic and environmental factors, phylogenetic lineages of *N. gaeumannii* and the severity patterns of the SNC disease. Firstly, using an ensemble species distribution modeling approach using genetic lineage presences as model inputs, we predicted the probability of occurrence of each lineage throughout the native range of Douglas-fir in the present as well as in 2050 under the "business as usual" (RCP8.5) emissions scenario. Subsequently, we combined these model outputs with short-term climatic and topographic variables and colonization index measurements from monitoring networks across the SNC epidemic area to infer the impacts of climate change on the SNC epidemic. Our results suggest that the current environmental tolerance range of lineage 1 exceeds that of lineage 2, and we expect lineage 1 to expand inland in Washington and Oregon, while we expect lineage 2 will remain relatively constrained to its current range with some slight increases in suitability,

particularly in coastal Washington and Oregon. We also found that disease colonization index is associated with the climatic suitability of lineage 1, and that the suitability of the different lineages could impact the vertical patterns of colonization within the crown. We conclude that unabated climate change could cause the SNC epidemic to intensify.

Keywords: climate change, epidemiology, Douglas-fir, Swiss needle cast, pathogen genetics

INTRODUCTION

Anthropogenic climate change threatens the health and resilience of forest trees and their ecosystems through a variety of direct and indirect effects (Shaw and Osborne, 2011; Sturrock et al., 2011; Desprez-Loustau et al., 2016). Conifers are believed to be particularly vulnerable to a warming climate (McDowell et al., 2016). Among these effects is the rising risk from biotic disturbance agents such as forest diseases (Drew Harvell et al., 2002; Sturrock et al., 2011). Fungal disease agents, due to their relatively short lifespans, are able to evolve adaptive traits more rapidly in response to environmental changes than their perennial hosts. Consequently, unprecedented epidemics can occur when favorable environmental conditions persist and exacerbate the effects of climate change on forest health, potentially resulting in severe ecological and economic impacts (Desprez-Loustau et al., 2016; Hessenauer et al., 2021).

One noteworthy example is *Nothophaeocryptopus gaeumannii* (Rhode) Petrak, an endophytic fungal associate of Douglas-fir [*Pseudotsuga menziesii* (Mirbel) Franco], an ecologically, economically and culturally important conifer native to the Pacific Northwest Coast in the United States and Canada. Though *N. gaeumannii* was previously only considered pathogenic in Douglas-fir's planted range, it has emerged as a threat in the tree's native range in western North America in recent decades (Hansen et al., 2000). The fungus is the causal agent of Swiss needle cast (SNC), a disease that results in premature defoliation of Douglas-fir, jeopardizing its health and productivity (Gaumann, 1928; Boyce, 1940; Hood and Kershaw, 1975; Maguire et al., 2002; Lavender and Hermann, 2014). Like most forest foliar pathogens, the presence and abundance of *N. gaeumannii* is linked to short and long-term climate patterns (Manter et al., 2003, 2005; Stone et al., 2007; Mildrexler et al., 2019). As outbreaks of SNC have become unprecedentedly frequent and severe, there have been considerable efforts to understand the factors driving its distribution and severity patterns (Shaw et al., 2021).

The emergence of SNC is inextricably tied to the reproductive cycle of *N. gaeumannii*, which in turn depends on local environmental conditions and the life cycle of its host. The fungus produces sexual fruiting bodies called pseudothecia that erupt through the stomata of Douglas-fir needles. With the right environmental conditions, these structures can increase in abundance and subsequently inhibit gas exchange and cause needle chlorosis and premature senescence, ultimately reducing vertical and radial growth by over 50% in the most severely affected stands (Manter et al., 2000; Maguire et al., 2011). The specific conditions leading to proliferation of *N. gaeumannii* are understood to be in large part linked to temperature and moisture fluctuations at relevant times in the life cycle of the fungus (Stone et al., 2008a). Mild fall and winter temperatures, concurrent with epiphytic and endophytic hyphae growth in Douglas-fir needles, are conducive to fungal development (Manter et al., 2005; Bennett and Stone, 2019). Wet conditions in the spring and summer, coincident with Douglas-fir bud burst and *N. gaeumannii* spore dispersal, increase spore-needle adherence and rainsplash dispersal, favoring *N. gaeumannii* abundance. Additionally, topographical features such as elevation, slope aspect and shading that moderate microclimate have also been identified as important predictors of disease severity (Rosso and Hansen, 2003; Manter et al., 2005; Lee et al., 2017). While the extent and severity of epidemics has varied over the last decades, coastal forests of Oregon and Washington states largely planted with young Douglas-fir have been the epicenter of SNC outbreaks. Hence, silvicultural factors such as tree age and species diversity, along with the Pacific Northwest coastal characteristics such as fog and oceanic climate are considered conducive to increased severity (Ritóková et al., 2016, 2021; Shaw et al., 2021).

Recent explorations into the phylogeography of *N. gaeumannii* in the Pacific Northwest suggest that the current crisis is not solely attributable to climatic changes (Winton et al., 2006; Bennett and Stone, 2016, 2019). The population structure and genetics of *N. gaeumannii* have also been investigated as a source of variability in disease severity. Two major non-interbreeding phylogenetic lineages of *N. gaeumannii* (named lineages 1 and 2) have been identified in the Pacific Northwest, and though they are sympatric, their spatial distributions suggest that they may be adapted to different environmental conditions and climates (Bennett and Stone, 2016, 2019). Whereas lineage 1 has been detected across the native range of Douglas-fir as well as in exotic plantations from Europe to New Zealand, lineage 2 has been detected almost exclusively in coastal areas west of the Coast mountains of Washington and Oregon in addition to a small number of sites in New Zealand (Bennett and Stone, 2016; Bennett et al., 2019). Prior observations have indicated that regions where both lineages are detected are generally more severely infected (Winton et al., 2006; Bennett and Stone, 2016), but thus far, the role of the lineages in disease patterns remains unclear (Bennett and Stone, 2019).

In this paper, we report the use of genetic lineage distribution modeling (LDM) to explore the epidemiology of SNC at different scales. Presence-only species distribution models (SDM), which predict the probability of occurrence of a species based on georeferenced presence points, true absence or pseudo-absence points and environmental predictors, are becoming essential tools in conservation biology and disease epidemiology, including for assessing the ecological and epidemiological implications of climate change

(Thuiller et al., 2005; Purse and Golding, 2015; Liu et al., 2020). In the context of a changing climate and increasingly accessible genomic tools, the integration of evolutionary information such as genetic clusters into SDMs can provide more accurate and informative predictions (Hoffmann and Sgrò, 2011; Gotelli and Stanton-Geddes, 2015; Desprez-Loustau et al., 2016; Nadeau and Urban, 2019). We believe that incorporating lineage-level distribution modeling with fine-scale severity data at monitoring sites may answer some important questions about the genetic and climatic characteristics underlying SNC epidemiology. The main questions we sought to address are: (i) What is the relationship between the climatic determinants of SNC and the distribution of lineages 1 and 2?; (ii) How will the potential distributions of the lineages change from the current climate to a future time period (2035–2065) under the "business as usual" climate scenario (RCP8.5)?; and (iii) can lineage climatic suitability be used to predict the average SNC severity at a site and to explain differences in within-tree severity patterns?

MATERIALS AND METHODS

Lineage Distribution Modeling Input Data

The study area chosen for the training and testing of our LDMs is the Marine West Coast Forests EPA Level I ecoregion, which covers the area of monitoring and provides a relatively ecologically homogeneous area for pseudo-absence selection (**Figure 1A**). The area of interest onto which we extrapolated our predictions is the entire Douglas-fir native range, which encompasses both the coastal (*P. menziesii* var. *menziesii*) and interior (*P. menziesii* var. *glauca*) varieties of Douglas-fir (Little, 1971) (**Figure 1A**).

Presence and absence points for the two phylogenetic lineages of *N. gaeumannii* in the PNW (**Supplementary Data Sheet S1**) were obtained from two sources: (i) lineage proportion data published by Bennett and Stone (2019) obtained using multilocus genotypes of a collection of isolates and (ii) lineage presence detection from samples of pseudothecia via real-time PCR using the methods described in **Supplementary Protocol S1**. The lineage identification from pseudothecia via real-time PCR used an established false positive signal to determine true presence with 99.5% accuracy if the targeted lineage constituted at least 5% of the pseudothecia in the sample using a statistical approach based on Geng et al. (1983). Therefore, to establish an equivalency in presence detection between these two sources of points, a lineage was considered absent in Bennett and Stone's (2019) collection of isolates wherever the proportion of the lineage was below 5%. The compilation of points from these two sources produced a dataset of 62 presence points and 9 absence points of lineage 1 (**Figure 1B**), and 42 presence points and 29 absence points of lineage 2 (**Figure 1C**). In order to reduce the spatial clustering of the data, the points were rarefied to a 5 km resolution using the SDMtoolbox 2.0 python package (Brown et al., 2017).

Nine pseudo-absence datasets were generated using several pseudo-absence selection methods and numbers of pseudo-absences to collectively maximize performance for all the selected algorithms while reducing the bias from each individual pseudo-absence generation method. These were (i) surface range envelope with the quantile value set at 0.025, (ii) a minimum buffer of 20 km between an absence and the nearest presence, and (iii) randomly selected points masked by an exhaustive collection of *N. gaeumannii* presence points from past published research and aerial surveys in Oregon, Washington and British Columbia (**Supplementary Data Sheet S2**). For each of the pseudo-absence methods, three datasets were generated containing different numbers of points. These were (i) the same number of pseudo-absence points as presence points (ii) one hundred pseudo-absence points, and (iii) one thousand pseudo-absence points. In total, this led to nine pseudo-absence datasets. The prevalence was set at 0.5, weighting the total presences and total absences and pseudo-absences equally. These methods are based on our interpretation of the results and

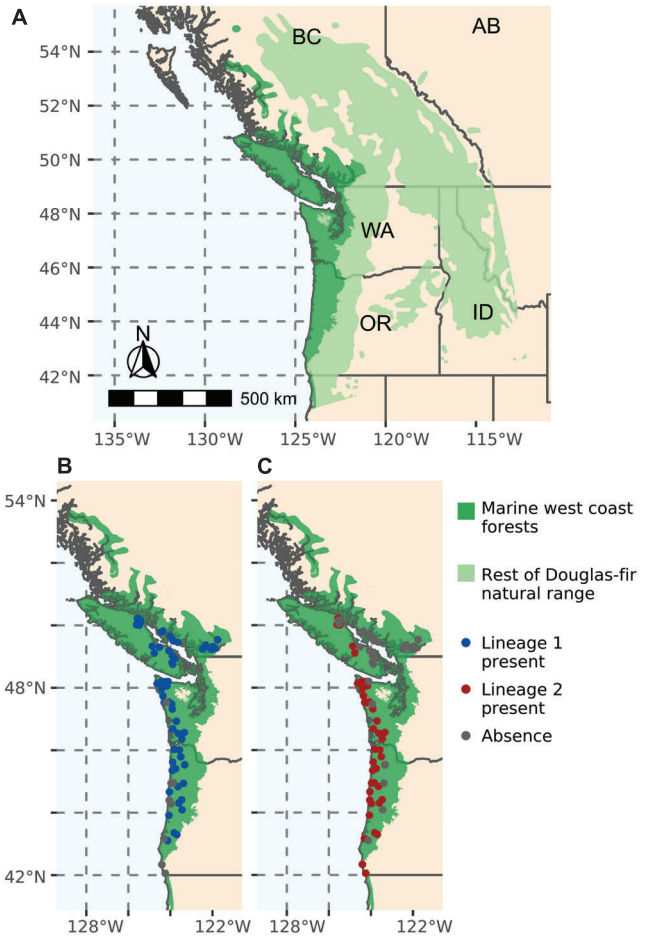

FIGURE 1 | (A) Douglas-fir native range in the Pacific Northwest (Little, 1971). The darker green shaded area is the Marine West Coast Forest EPA Level I Ecoregion, which is the study area used to train and test our lineage distribution modelings (LDMs). The lighter green shaded area is the rest of the Douglas-fir native range, the Area of Interest onto which we extrapolate our LDM predictions. **(B)** 62 presence and 9 absence points of lineage 1 of *Nothophaeocryptopus gaeumannii* across 71 sampled locations. **(C)** 42 presence and 29 absence points of lineage 2 of *N. gaeumannii* across 71 sampled locations.

recommendations of Barbet-Massin et al. (2012) and Liu et al. (2019).

Environmental Variables Selected for Lineage Distribution Modeling

The environmental variables incorporated in this analysis were average degree days above 5°C (DD5), Summer Heat Moisture Index (SHM) and annual Relative Humidity (RH) between 1980 and 2010 (henceforth the "current" climate), as well as distance from the nearest coastline (km).[1] DD5, SHM and RH were selected from a set of 28 bioclimatic variables produced by ClimateNA for different time periods (Wang et al., 2016). The variables were narrowed down based on their contribution to aforementioned temperature and wetness conditions conducive to *N. gaeumannii* proliferation, and then filtered based on their multicollinearity; only variables with a VIF below 0.5 were maintained. A short description of each variable and its rationale for inclusion in the LDM analysis is described in **Table 1**.

Rasters for future climate conditions were downloaded from ClimateNA for the period 2035-2065 (midpoint = 2050) under an ensemble of 13 Atmosphere-Ocean General Circulation Models (ACCESS-ESM1-5, BCC-CSM2-MR, CNRM-ESM2-1, CanESM5, EC-Earth3, GFDL-ESM4, GISS-E2-1-G, INM-CM5-0, IPSL-CM6A-LR, MIROC6, MPI-ESM1-2-HR, MRI-ESM2-0 and UKESM1-0-LL) of the Representative Concentration Pathway 8.5 climate change scenario (henceforth the "RCP8.5 2050 scenario"). This scenario, also known as the "business as usual" scenario, is intended to indicate the worst case scenario of climate change in the absence of mitigation policies, reflecting an increase in radiative forcing of 8.5 Watts/m^2 by the end of twenty-first century relative to pre-industrial levels (Moss et al., 2010).

[1]https://oceancolor.gsfc.nasa.gov/docs/distfromcoast/

To provide an overview of how the values of the climate variables are forecast to change under the RCP8.5 2050 scenario, we extracted values from the climate variable rasters at the 71 lineage sampling locations and graphed box plots and probability densities comparing their current and future values.

Lineage Distribution Modeling Analysis

We used the SDM framework of the biomod2 R package (Thuiller et al., 2009). Four algorithms, Generalized Linear Models (GLM), Multiple Adaptive Regression Splines (MARS), Breiman and Cutler's Random Forests (RF) and Maximum Entropy (MAXENT) were used to construct an ensemble model for each lineage. This set of algorithms was selected to maximize both predictive performance and interpretability while minimizing bias by combining traditional regression methods with more flexible and computationally intensive machine learning algorithms. Three cross validation runs with a training:testing data split of 80:20 were computed for each pseudo-absence dataset. A total of 108 models were developed (nine pseudo-absence sets x four algorithms x three cross-validation runs) to predict the potential distributions of lineage 1 and lineage 2 in the study area.

Models were evaluated by examining the True Skill Statistic (TSS) scores, which are calculated by taking the sum of the True Positive Rate (sensitivity) and True Negative Rate (specificity) minus 1, for each combination of the algorithm, pseudo-absence set, and cross-validation run. To examine the relationship between *N. gaeumanii* lineage occurrence and the explanatory variables used in this analysis, variable importance values were computed as explained in Thuiller et al. (2009). In our study, this was calculated using three permutations (i.e., random rearrangements of data) of each variable and via comparison of the correlations between the predictions from the

TABLE 1 | Description, reason for inclusion and source of variables used in LDM.

Variable	Description	Reason for inclusion	Source
Annual degree days above 5°C (DD5)	The sum of the total number of accumulated degrees between 5°C and the mean daily temperature of each day in the year.	Mild winter conditions favour *N. gaeumannii* epiphytic and endophytic growth (Manter et al., 2005; Stone et al., 2008a; Bennett and Stone, 2019). Ascospore dispersal requires temperatures of 5°C to 28°C and growth is inhibited above 30°C, therefore mild summer temperatures are also favourable to *N. gaeumannii* (Michaels and Chastagner, 1984; Capitano, 1999; Rosso and Hansen, 2003). DD5 is also an important predictor of Douglas-fir productivity (Weiskittel et al., 2012).	ClimateNA/ Adaptwest
% Annual Relative Humidity (RH)	Proportion of absolute humidity in an air parcel out of the maximum humidity at that temperature.	Relative humidity favours ascospore germination (Wicklow and Zak, 1979; Beyer et al., 2005) and has been found to be a trigger of SNC epidemics (Watts et al., 2014).	ClimateNA/ Adaptwest
Summer Heat Moisture Index (SHM)	Ratio of the mean temperature of the warmest month to the mean May-September precipitation divided by 1000. Hot, dry summers have high SHM, while cool, wet years have low SHM.	Mild and wet spring and summer conditions are known to favour reproductive success and growth of *N. gaeumannii* (Michaels and Chastagner, 1984; Capitano, 1999; Rosso and Hansen, 2003; Mildrexler et al., 2016, 2019)	ClimateNA/ Adaptwest
Distance (km) to coast (dist)	Distance to the nearest coastline.	Distance from the coast is a proxy for a variety of environmental conditions strongly related to Swiss needle cast symptom presence and severity and is an important indicator of the relative proportion of Lineage 2 (Lee et al., 2017; Bennett and Stone, 2019; Mildrexler et al., 2019).	National Oceanic and Atmospheric Administration (NOAA)

re-arranged data versus the unshuffled data. Influential variables will have higher variable importance values (range: 0–1). Finally, to understand the relationships between the variables and the occurrence probability of the lineages, we graphed response plots for each variable developed based on the GLM models with a TSS score of 0.7 or above.

Ensemble modeling, where predictions from several different modeling techniques are combined, is applied to reduce bias and improve performance of SDMs (Araújo et al., 2005; Marmion et al., 2009). The predictions from the different modeling techniques were "ensembled" based on the average probabilities from high performing models (TSS > 0.7 for lineage 1 and TSS > 0.75 for lineage 2). Predictions from the ensembles were then projected to the entire range of Douglas-fir in the Pacific Northwest for current (1980–2010) and future conditions (2035–2065) under the RCP8.5 2050 scenario. Interpreting the probabilities of occurrence from this analysis as a measure of climatic suitability, we sought to explore associations between these outputs and disease severity.

Severity Modeling

Fine-scale severity data from across the epidemic zone sampled between 2015 and 2019 were acquired from researchers of monitoring networks in Washington, Oregon and B.C. The response variable used to signify *N. gaeumannii* abundance and therefore disease severity is the Colonization Index (CI), a heuristic approximation of the probability percentage that a given stoma is occluded by *N. gaeumannii* pseudothecia. This was assessed on 2-year old needles from the top, middle and bottom crown sections of trees. The number of trees and crown sections sampled per site varied in the different networks; only the upper crown was sampled in Washington, and mostly 5 trees were assessed in B.C. and 10 trees in Washington and Oregon. The CI (%) was obtained by multiplying the incidence (proportion of needles exhibiting occluded stomata) by the severity (proportion of pseudothecia occluded on the base, middle and tip of needles) on a subset of needles. The number of needles in these subsets also varied between the networks, with ten to 50 needles used for incidence assessment, and five to ten needles used for severity assessment.

To investigate the influence of lineage suitability on site-level average CI while controlling for sampling heterogeneity, local topography and short-term climate patterns, we utilized a binomial logistic regression with a logit link, incorporating only sites where data from all three crown sections were available (131 sites in total from Oregon and B.C.) (**Supplementary Data Sheet S3**). To account for sampling heterogeneity across the monitoring sites, we implemented a weighting system of observations with weights assigned as a function of the amount of sampling done at the site. To account for the effect of fine-scale topography and the degree of shading on a site, we chose to include hillshade pixel depth into the analysis, which is an indication of the level of shading at the site; high pixel depth signifies lighter color and hence a more illuminated site, while low pixel depth means a darker color and therefore a more shaded site. This variable was obtained by applying the hillshade function in QGIS 3.10.9 to a digital elevation model from ClimateNA with the azimuth set at 315° (NW). Additionally, the natural log of the average precipitation as snow in January (PAS01) from the two years preceding needle sampling was used to control for short-term winter conditions.

Model selection and inference in this study drew on an information theoretic approach proposed by Burnham and Anderson (2002) and implemented in the AICcmodavg package in R (Mazerolle, 2017). We built a global model along with a set of plausible nested candidate models (**Table 2**). Variables were scaled and centered on the mean prior to modeling. We assessed the evidence for each model based on the second-order Akaike Information Criterion for small sample sizes (AICc); the evidence ratios obtained are an indication of the number of times a given model is more parsimonious than a lower-ranked model (Burnham and Anderson, 2002; Mazerolle, 2017). Since more than one model carried a consequential proportion of the AICc weight, we employed multi-model averaging to compute model-averaged parameters and measures of uncertainty for the explanatory variables, with shrinkage applied based on the AICc weight of the different candidate models as suggested by Calin-Jageman and Cumming (2019). In accordance with Mazerolle (2017), model fit was evaluated based on the global model, which was designed as follows:

$$log(\frac{u_i(y\ =\ 1)}{u_i(y\ =\ 0)})\ =\ \beta_0\ +\ \beta_1 X_{1i}\ +\ \beta_2 X_{2i}\ +\ \beta_3 X_{3i}\ +\ \beta_4 X_{4i}$$

$$\frac{u_i(y\ =\ 1)}{u_i(y\ =\ 0)}\ =\ e^{\beta_0\ +\ \beta_1 X_{1i}\ +\ \beta_2 X_{2i}\ +\ \beta_3 X_{3i}\ +\ \beta_4 X_{4i}}$$

where $\frac{u_i(y=1)}{u_i(y=0)}$ is the odds ratio that a given stomata on a given needle is occluded *versus* unoccluded by pseudothecia at the i^{th} site. The weight of each observation is an estimation of the number of needles measured for pseudothecia occlusion at the site, calculated by taking the total of the product of the number of needles measured for prevalence and severity at the site. For instance, at a site where all three crown sections of ten trees are sampled, and at every crown section ten needles are used for severity estimation and 50 needles for prevalence estimation,

TABLE 2 | (A) Akaike's Information Criterion adjusted for small sample sizes (AICc) weight and AICc score of the highest ranked (AICc weight above 0) generalized linear models associating colonization index (CI) values with lineage suitability, climate and topography and **(B)** estimates of the mean and standard deviations of the response (CI probability) and explanatory variables [ln(PAS01), hillshade, L1 suitability, L2 suitability].

(A) Candidate model	AICc	AICc Weight
L1 suitability, ln(PAS01), hillshade	–260.52	0.74
L1 suitability, L2 suitability, ln(PAS01), Hillshade	–258.39	0.25
ln(PAS01), hillshade	–251.44	0.01

(B) Variable	Mean value ± SD	Model-averaged estimate ± SE
L1 suitability	0.56 ± 0.22	0.03 ± 0.01
L2 suitability	0.50 ± 0.32	0 ± 0
ln(PAS01)	2.26 ± 0.79	–0.03 ± 0.01
Hillshade	179.5 ± 10.70	0.02 ± 0.01
CI (probability)	0.16 ± 0.10	

the weight is equal to 3 × 10 × (10 × 50) = 15000. The weights range from 2,450 to 18,150. The intercept, β_0 is the value of the CI when the other variables are held at 0 (i.e., at their mean values). $\beta_1$is the coefficient for the effect of PAS01 on CI, $X_{1i}$is the millimeters of PAS01 at the i^{th} site. $\beta_2$is the coefficient for the effect of hillshade on CI, $X_{2i}$is the hillshade pixel depth at the i^{th} site. $\beta_3$is the coefficient for the effect of lineage 1 probability of occurrence on CI, $X_{3i}$is the probability of occurrence of lineage 1 at the i^{th} site. $\beta_4$is the coefficient for the effect of lineage 2 probability of occurrence on CI, $X_{4i}$is the probability of occurrence of lineage 2 at the i^{th} site. The probability of occurrence values for lineage 1 (X_{3i}) and lineage 2 (X_{4i}) for each site were extracted from the ensemble model-based lineage potential distribution maps for the current (1980-2010) time period.

Finally, we explored correlations between the two lineage suitability outcomes and average CI in the different crown sections using correlation plots and Pearson's correlation tests based on data from all the SNC monitoring networks (a total of 211 sites in Oregon, Washington and B.C.).

RESULTS

Environmental Variables Shaping Lineage Climatic Suitability

DD5 and SHM are the two most important predictors among the explanatory variables for both lineage 1 and lineage 2, though the importance of DD5 appears to be higher for lineage 1, while SHM is more important for lineage 2 (**Figure 2A**). Distance to coast and RH are also much more important predictors for presence of lineage 2 than for lineage 1 (**Figure 2A**). According to the averaged predictions of the best performing GLMs, the optimal conditions for presence differ significantly between the lineages. Lineage 1 has a much broader range of suitability for distances further from the coast and for hotter and drier summers than lineage 2 (**Figure 2B**). The tolerance range of lineage 1 for both low and high annual average RH values exceeds that of lineage 2 (**Figure 2B**). In contrast, lineage 2 has a slightly broader tolerance in terms of higher DD5 (a greater accumulation of daily degrees experienced above 5°C) (**Figure 2B**).

Evaluation scores for lineage 1 were generally lower than for lineage 2, which may be a reflection of its broader environmental tolerance throughout the study area (**Figure 3**). According to their TSS scores, the regression methods discriminated between presences and absences better for lineage 2 than for lineage 1 (L1 GLM = 0.72, L1 MARS = 0.7, L2 GLM = 0.6, L2 MARS = 0.64), while random forests performed similarly for both (L1 RF = 0.66, L2 RF = 0.65). Maxent had the weakest discrimination capacity for both lineages (L1 MAXENT.Phillips = 0.5, L2 MAXENT.Phillips = 0.61) (**Figure 3**). However, the TSS scores, which range from -1 (no points classified correctly) to 1 (all points classified correctly) were 0.74 and 0.78 for lineages 1 and 2 ensemble models, respectively (**Figure 3**). Such TSS values indicate "good" to "very good" model predictions (Préau et al., 2019).

Impact of Climate Change on the Distribution of the *Nothophaeocryptopus gaeumannii* Lineages

At the lineage presence points included in the LDMs, the climate variables are forecast to change between "current" climate conditions and those in the 2050 RCP8.5 scenario. The most remarkable change is DD5, which will increase across its entire range of values, with its mean increasing from 1996 to 2700 degree days (**Figure 4A**). The mean SHM will increase from 53 to 73, indicating hotter and drier summers overall (**Figure 4B**). The range of RH will remain relatively unchanged, with the mean decreasing from 71 to 69% (**Figure 4C**).

These changes are reflected in the patterns of probability of occurrence forecast for the two lineages, which can be interpreted as a measure of climatic suitability. Under the current climate, the coastal zone west of the Cascade and Coast ranges extending from the Lower Mainland of B.C. to central Oregon is highly suitable for both lineages. However, the areas of very high suitability for lineage 1 extend further inland into the B.C. Fraser valley and northeast out to the eastern coast of Vancouver Island, as well as inland to the western slopes of the Oregon Cascades (**Figure 5A**). Lineage 1 also has relatively higher suitability values throughout the interior Douglas-fir range than lineage 2, particularly in the interior (**Figures 5A** vs. **C**). In contrast, the areas of high suitability for lineage 2 under current conditions are constrained to a narrow strip of land along the coast of the study area along with a pocket on the eastern coast of Vancouver Island. However, its range of high suitability values extends further South than that of lineage 1, to the Southern limit of our study area (**Figure 5C**).

Under the climatic conditions forecast by the RCP8.5 2050 scenario, changes in the climatic suitability of lineage 1 are predicted to increase by a probability of up to 0.1 in large swathes of the Douglas-fir range (**Figure 5B**). The highest increase in suitability is predicted east of the coast in Washington and Oregon; for example, the Willamette Valley and Western slopes of the Oregon and Washington Cascades should become significantly more suitable areas for lineage 1 (**Figure 5B**). There are some areas where the suitability of lineage 1 is forecast to decrease; Vancouver Island, the Olympic Peninsula and Puget Sound (**Figure 5B**).

Under the RCP8.5 scenario, lineage 2 is likely to remain similarly geographically limited, with areas in the interior of the Douglas-fir range becoming generally even less suitable to Lineage 2 (**Figure 5D**). Some increases in suitability are forecast in Southeastern Vancouver Island and the Puget Sound (**Figure 5D**).

Lineage Suitability and Colonization Index

Out of our set of plausible candidate models for predicting CI, two models carried the highest proportion of the AICc weight. These were (i) the one including ln(PAS01), hillshade and lineage 1 suitability and the global model, carrying 74% and 25%, respectively (**Table 2**). Using model-averaging, we are able to obtain parameter estimates and their uncertainties as measured by standard error for each of our explanatory

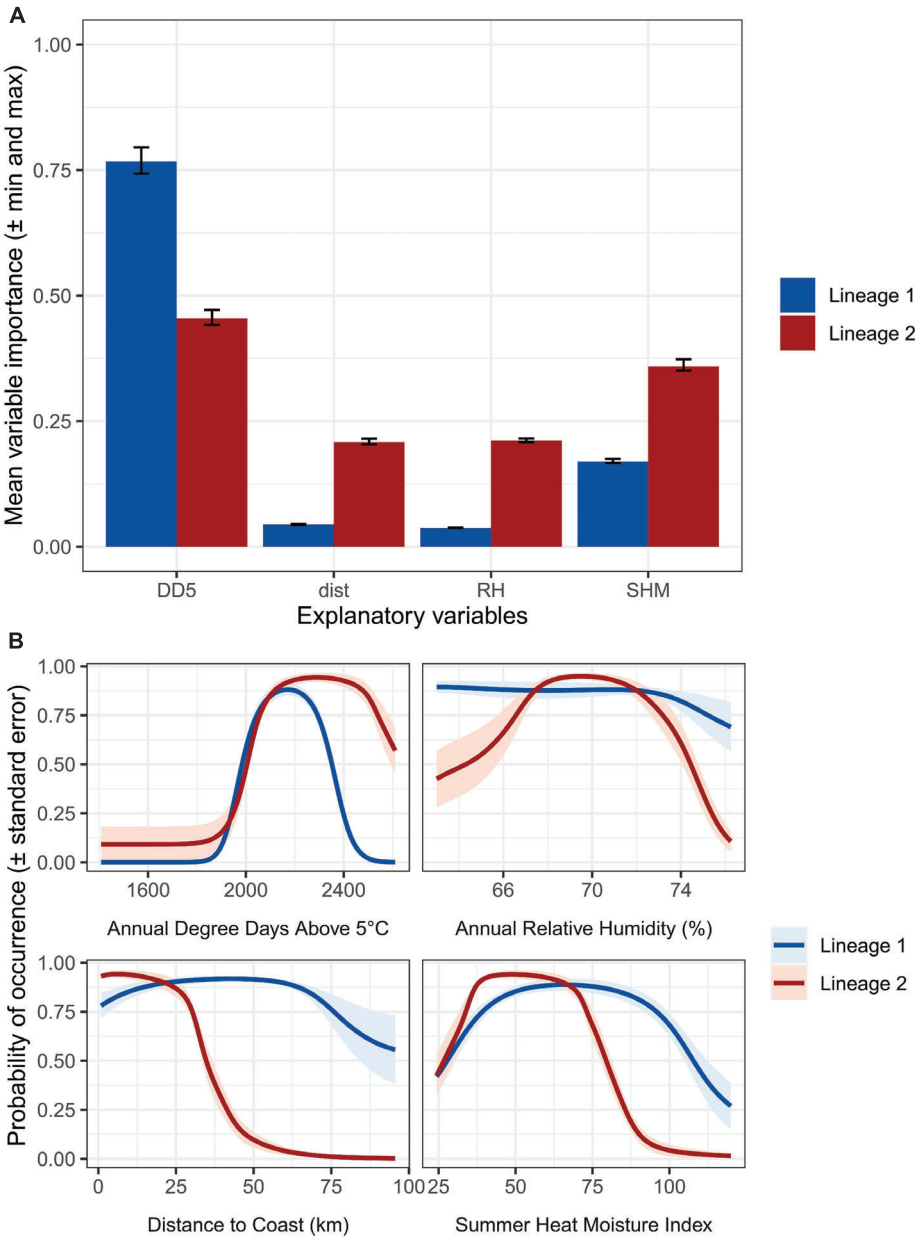

FIGURE 2 | (A) Importance of explanatory variables for lineage (blue bars) 1 and lineage 2 (red bars) of *Nothophaeocryptopus gaeumannii* for the ensemble models. Error bars indicate the maximum and minimum importance values calculated by permuting each variable three times and comparing the correlation between predictions when the variable is randomized *versus* not randomized. **(B)** Response plots of explanatory variables for the generalized linear models included in the ensembles of lineage 1 (blue lines and light blue shading) and lineage 2 (red lines and light red shading). Lines indicate the mean probability of occurrence prediction of the models. Shading indicates the standard error of the mean probability of occurrence estimates of the models.

variables. These are 0.03 (±0.01) for lineage 1, 0.0 for lineage 2, –0.03 (±0.01) for ln(PAS01), and 0.01 (±0.01) for hillshade (**Table 2**). This means that when ln(PAS01) and hillshade are held constant, the odds of a stomata being occluded by a pseudothecium are multiplied by 1.03 ($e^{0.03}$) with a 1 unit increase in lineage 1 suitability. In effect, this indicates a positive association between lineage 1 climatic suitability and CI, even when short-term winter conditions and local topography are taken into account. This association is supported by the evidence ratios between the models; the candidate model including lineage 1 suitability along with the log of PAS01 and hillshade was 93.966 times more parsimonious than the one including only the log of PAS01 and hillshade. We found no such association with lineage 2 climatic suitability. In terms of the effects of short-term winter climate patterns and topography, ln(PAS01) of the previous two years has a negative association with CI, while hillshade pixel value has a positive association with CI, implying that higher CI should

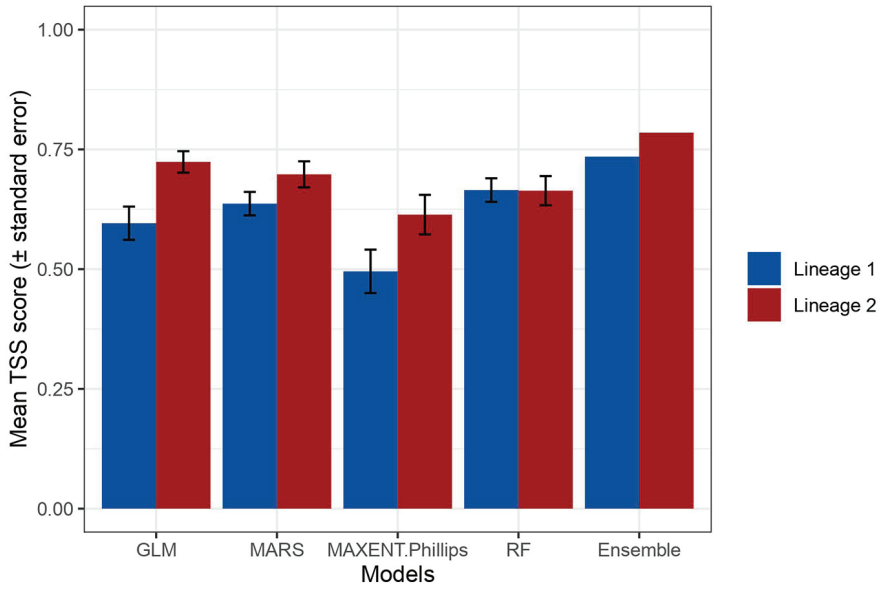

FIGURE 3 | Mean True Skill Statistic (TSS) scores of the individual and ensemble models for lineage 1 (blue bars) and lineage 2 (red bars) of *Nothophaeocryptopus gaeumannii*. Error bars represent the standard error around the mean TSS score. TSS scores range from -1 (none of the presences or absences classified correctly) to 1 (all presences and absences classified correctly).

be found where there is lower precipitation in January and on less shaded sites.

The logistic regression model fit of our global model was excellent, with a Hosmer Lemeshow test p-value of 0.99 and no concerning patterns in the residuals once a log-transformation was applied to PAS01 (**Supplementary Figure S1**).

Lineage Suitability and Within-Tree Vertical Infection Patterns

Significant positive correlations were observed between lineage 1 climatic suitability and CI in the middle (r = 0.17, P = 0.04) and lower (r = 0.29, P = 0.0004) crown sections (**Figure 6A**). A weak positive correlation was observed between lineage 2 climatic suitability and the upper crown section CI (r = 0.14, P = 0.05). Lineage 2 climatic suitability and the CI values in the lower crown section were negatively correlated (r = –0.39, $P < 0.0001$) (**Figure 6B**).

DISCUSSION

Climatic Niches of Two Genetic Lineages of Swiss Needle Cast

Our results indicate that the two genetic lineages described for *N. gaeumannii* have overlapping environmental distributions but different environmental tolerance ranges. Indeed, while there are areas where one lineage completely supplants the other, they are also often present in the same site, sometimes in very close proximity; in fact, both lineages have been identified on a single needle (Bennett and Stone, 2019). Our research adds support to a number of previous findings relating to *N. gaeumannii* and its lineages, while providing further insight into the niche optima of the lineages in terms of a few key variables.

Overall, both lineages 1 and 2 (and therefore the whole *N. gaeumannii* species in the Pacific Northwest) prefer coastal climate and warm temperatures, and favor mild and wet conditions, as opposed to hot and dry conditions, in the spring and summer, suggesting that geographic areas under these conditions should be more susceptible to SNC epidemics. This agrees with the conclusions of a wide range of other studies into the climatic determinants of SNC distribution and severity (Manter et al., 2005; Lee et al., 2017; Shaw et al., 2021).

The difference in niche in terms of DD5 corresponds with the dominance of lineage 2 and absence of lineage 1 at survey sites in southernmost Oregon sites. Similarly, the much broader tolerance for higher SHM and continentality of lineage 1 manifests in its complete supplantation of lineage 2 in hotter and drier conditions farther from the coast, a phenomenon also remarked by Bennett and Stone (2019). These differences in tolerance may be explained by the population structure of the lineages. *N. gaeumannii* is a homothallic species which appears to reproduce predominantly via selfing with occasional outcrossing events (Bennett and Stone, 2019). According to multilocus genotypes analyzed by Bennett and Stone (2016, 2019) lineage 1 has a higher genotypic diversity, genotypic richness and genetic diversity than lineage 2, which is considered relatively clonal. The diversity of genotypes in lineage 1 and the different phenotypes they can produce could be an explanation for its broad environmental tolerance. Conversely, the lack of genotypic diversity in lineage 2 may explain its limited environmental range. The phenotypes produced by these different genetic clusters may also hold insights into relationships between severity and lineage climatic suitability evoked by our CI modeling.

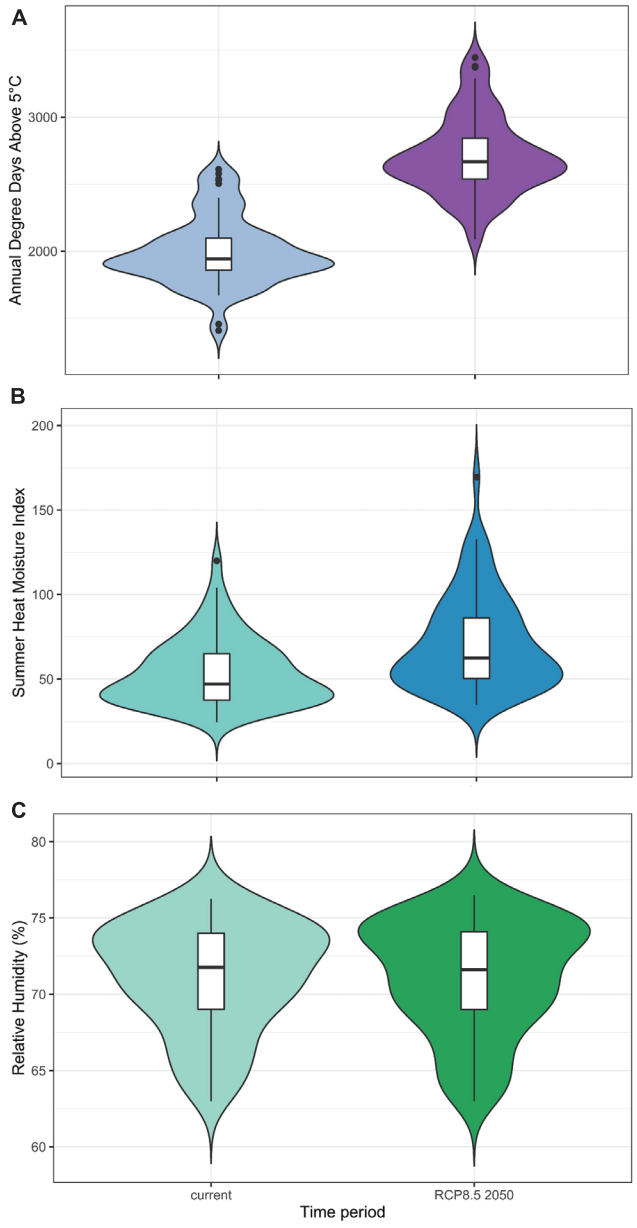

FIGURE 4 | Boxplots of median, interquartile range and outliers, with probability distributions of **(A)** degree days above 5°C, **(B)** summer heat moisture index and **(C)** relative humidity (%) at the 71 sampling sites used in the LDMs. The left side violin plot represents the current (1980–2010) distribution of values, while the right side violin plot represents distribution of values in 2035–2065 under the RCP8.5 emissions scenario (RCP8.5 2050).

Differences in Pathogenicity Between Lineage 1 and Lineage 2

The results of our severity modeling demonstrates the utility of LDMs for predicting forest disease severity, while also highlighting the importance of using both short-term winter climate along with topography data in improving prediction of colonization levels of *N. gaeumannii* when using down-scaled climate data.

While precipitation as snow was a strong predictor of CI, the inclusion of hillshade in models helped to explain the values of outliers such as several highly infected sites in the Chilliwack area of B.C. and the Tillamook area of Oregon, as well as relatively uninfected sites in the Florence and Coos Bay areas of Oregon that were not explained by PAS01 or lineage suitability. This is in agreement with previous research that noted the importance of shading, aspect and elevation in SNC epidemics (Rosso and Hansen, 2003; Lee et al., 2017). Our results also suggest that the distribution and suitability of the lineages may assist in predicting disease severity along with short-term climate.

Differences in pathogenicity between genetic lineages is not uncommon in forest pathogens. Some of the most notable examples include the lineages of *Phytophthora ramorum* Werres, De Cock, and Man in't Veld (Elliott et al., 2011) and *Ophiostoma ulmi* (Buisman) Melin and Nannf. (Hessenauer et al., 2020). In the case of SNC for which infection severity is dependent on abundance of pseudothecia, differences in pathogenicity between lineages should arise as the result of competitive advantages such as improved dispersal ability, higher growth rate, or an adaptation to the local environment. Initially, the clonal population structure of lineage 2 and the concentration of the most severe outbreaks in areas of Washington and Oregon where this lineage was abundant led to the proposition that this lineage had a competitive advantage over lineage 1 and is part of the etiology of the PNW's SNC epidemic (Winton et al., 2006; Bennett et al., 2019). Yet, lineage 2 is conspicuously absent from the B.C. Lower Mainland's most severely infected stands, while several sites in Southern Oregon almost exclusively populated with lineage 2 have little to no symptoms of SNC according to aerial surveys (Bennett and Stone, 2019). Indeed, though they do not allow us to infer causality, our results indicate a slight association between climatic suitability of lineage 1 and the site average levels of colonization by *N. gaeumannii*, even after accounting for short-term climatic and topographic effects. In contrast, our model averaging revealed no such association with lineage 2 climatic suitability. According to ecological niche theory, the climatic suitability values generated by our LDMs should approximate the local abundance of each lineage (Maguire, 1973; Guisan et al., 2017). As CI is a reflection of pathogen abundance, its association with lineage 1 suitability and lack thereof with lineage 2 suitability may be interpreted as evidence for a competitive advantage in favor of lineage 1. Our findings are supported by preliminary results from phenotyping experiments, which showed that isolates of lineage 1 most common on the coast have a higher phenotypic plasticity and grow faster than those of lineage 2 in three different temperature conditions and three drought conditions (Yin et al., 2020). Our findings also concur with those from Bennett and Stone (2019), who tested the hypothesis of higher pathogenicity of lineage 2, but found no association between the relative proportion of lineage 2 and SNC symptoms when distance from the coast was held constant.

The significant association between CI and lineage suitability, as well as the high evidence ratios of models that incorporated lineage 1 suitability over those that didn't, provides evidence that LDMs can be useful in estimating the severity patterns of the epidemic. This not only helps us to make inferences

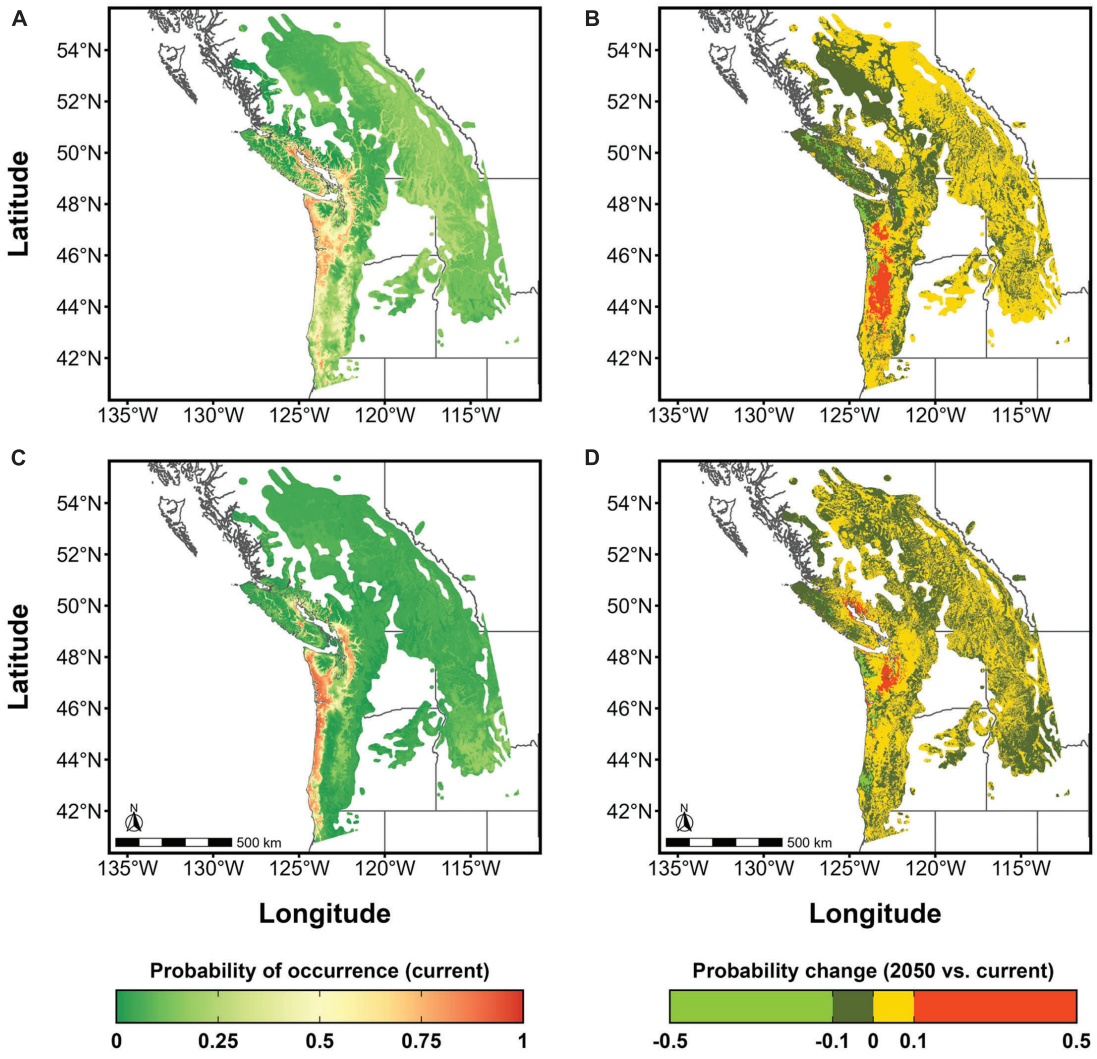

FIGURE 5 | Maps of climatic suitability of lineages 1 and 2 of *Nothophaeocryptopus gaeumannii* in the Pacific Northwest Douglas-fir range **(A)** Lineage 1 climatic suitability map under current (1980–2010) climate; **(B)** Change in lineage 1 climatic suitability under the RCP8.5 2050 climate; **(C)** Lineage 2 climatic suitability map under current (1980–2010) climate; **(D)** Change in lineage 2 climatic suitability under the RCP8.5 2050 climate.

to greater spatial scales, but also to much smaller scales such as within the tree. Differences in the relationships between CI and lineage suitability in the upper, middle and lower crown sections reveal some intriguing possibilities such as within-tree niche partitioning between the lineages, and may help to explain the differing patterns of vertical colonization in the monitoring networks. The occupation of the same host by different species or reproductively isolated lineages as is the case with *N. gaeumannii* poses a problem in ecology as it violates the competitive exclusion principle (Hardin, 1960). However, a possible answer to this conundrum has been found in fine-scale spatial or temporal niche partitioning between cryptic species or non-interbreeding subpopulations. Evidence of this in forest pathogens includes the complex of fungal species causing oak powdery mildew in Europe and fungal symbionts of the mountain pine beetle in western North-America (Feau et al., 2012; Hamelin et al., 2016; Ojeda Alayon et al., 2017). The correlation between lineage 1 suitability and lower and middle crown section CI and the weak correlation between lineage 2 suitability and the upper crown section CI suggests that the lineages may prefer different crown sections - lineage 1 the lower and middle sections, and lineage 2 the upper section. This would be consistent with the different colonization levels found in B.C., where lineage 1 is most prominent and the lower sections are most severely infected, as opposed to Oregon where the upper section of the crown is most infected in highly diseased sites and lineage 2 is more common (Shaw et al., 2014; Bennett and Stone, 2019).

It is important to note that although CI is the primary mechanistic sign of SNC, it is not always correlated with the ultimately damaging symptom of premature defoliation (Manter et al., 2003; Montwé et al., 2021). The host dynamics of this disease remain obscure; indeed, studies on silvicultural practices (Filip et al., 2000; El-Hajj et al., 2004; Lan et al., 2019a), as well as host age (Lan et al., 2019b), tree provenance and family

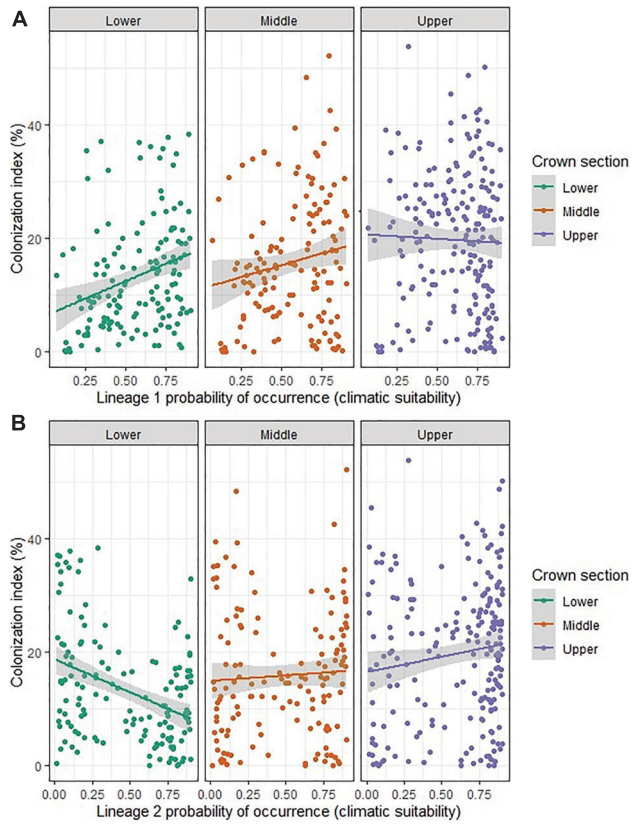

FIGURE 6 | Correlation plots between *Nothophaeocryptopus gaeumannii* lineage suitability and colonization index (CI) in different crown sections **(A)** Relationship between lineage 1 suitability and CI in the upper, middle and lower sections of the tree; **(B)** Relationship between lineage 2 suitability and CI in the upper, middle and lower sections of the tree.

(Johnson, 2002; Montwé et al., 2021) have reported different and even contradictory results on relationships of these factors with symptom severity and disease tolerance and resistance. Crucially, the interacting effect of climate change on both the host and pathogen is an important knowledge gap which should be addressed in further research. In addition, the importance of different climate variables on disease severity seems to vary spatially, according to differences in site biogeoclimatic characteristics (Stone et al., 2008a; Lee et al., 2013). Hitherto, distance from the coast has been widely used in SNC modeling as a proxy for this variability in site characteristics as it applies well to the relatively linear coastline of Oregon where the disease has been most studied, but the parameter is not as useful in Washington and Southwestern B.C, which have more complex coastlines. Modeling work such as ours on the full extent of the epidemic requires replacement of this proxy variable with more widely applicable variables such as ecosystem classification zones. The lack of compatibility between ecosystem classification systems across the national boundaries of the Pacific Northwest is a barrier to this effort. While many important challenges for understanding and managing the SNC epidemic remain, the combined use of genetic information along with climate data at different timescales and topographic data provides some useful insight that could aid forest management decision-making in the context of climate change.

Implications for Climate Change

The results of our study suggest that it is not lineage 2 but rather lineage 1 that may be the driver of disease severity currently in the coastal Pacific Northwest. Though it can be problematic to extrapolate results beyond the spatial and temporal scope of an observational dataset, we do so under the fundamental assumption that species conserve their niches (Peterson et al., 1999; Liu et al., 2020). This allows us to make some informed predictions about the trajectory of the SNC epidemic to the rest of the Douglas-fir range under the RCP8.5 2050 scenario. The increase in lineage 1 suitability observed in our predictions in this scenario indicate that the frequency of SNC epidemics may increase in coming years, particularly extending into the Willamette valley and Western slopes of the Cascades, which until now have been spared of the disease's impact (Ritóková et al., 2016; Shaw et al., 2021). The expansion to new suitable locations reflects the current tolerance of lineage 1 for a wide range of climate conditions. Considering the relatively high genetic diversity of this lineage, it is consistent with the general idea that a more diverse subpopulation of a fungus will have more chance to adapt successfully to a changing environment than a clonal subpopulation (Drenth et al., 2019). When taken together with our severity modeling results, the outputs of our lineage 1 LDMs can be interpreted as indicators of future disease severity, assuming that warmer climates will also lead to an increase in the frequency of optimal short-term winter conditions such as low PAS01. As such, the increase in the overall suitability values across much of the Douglas-fir range in the RCP8.5 2050 scenario suggests that the severity of epidemics can be expected to intensify throughout much of the lineage 1 distribution if greenhouse gas emissions continue unabated in the coming decades.

In contrast, the extent and suitability levels of lineage 2 are predicted to remain relatively similar according to our LDMs, with increases in probability over 0.1 in Northern Washington and Northeastern Vancouver Island. We believe this may be due to increases in suitability resulting from favorable DD5 being offset by rising SHM to which lineage 2 has a very limited tolerance (**Figure 4**). However, it is important to mention a number of caveats to this result. Firstly, clonal populations such as that of lineage 2 tend to expand spatially as they do not need to compete against other genotypes and are usually indicative of a highly successful individual, but they are more vulnerable to collapse due to their lack of adaptability; this population structure is epidemiologically important but difficult to factor into modeling. It is also noteworthy that various studies in the epidemic zone show a historical trend toward increasing spring and summer precipitation in the epidemic zone (Stone et al., 2008b; Mildrexler et al., 2019; Montwé et al., 2021), as opposed to the drying trend forecast in our RCP8.5 scenario. This and fluctuations in short-term weather patterns introduce additional uncertainties in our future

predictions under the RCP8.5 emission scenario, which call for caution in interpreting our maps. Future risk assessments will immensely benefit from rangewide determinations of SNC genetic lineages and accurate estimations of climate and host dynamics in this region.

CONCLUSION

Climate-driven SDMs have traditionally been used to assess habitat suitability for a given species including forest pathogens (Pandit et al., 2020; Pedlar et al., 2020). We are unaware of studies in forest pathology that have used genetic clusters as inputs into SDM, and outputs of these models for assessing the severity of forest pests or diseases. Our study addresses this knowledge gap by including results from predictive maps of the climatic suitability of the two *N. gaeumannii* lineages (lineage 1 and 2) into severity modeling. By considering the whole epidemic area this study provides the most geographically extensive investigation of the short and long-term climate dynamics of SNC. We believe that future research should focus on the phenotyping of the *N. gaeumannii* lineages, including the coastal and interior variants of lineage 1, as well as other evolutionary differences between the lineages, such as dispersal ability. This could be used to fine-tune our SDMs using mechanistic models which are known to perform better with native pathogens in their realized niches. Our results indicate that there is a sound theoretical and empirical underpinning for using LDMs as tools to not only predict the current and future climatic suitability of the SNC lineages, but also to attempt to identify high disease severity risk areas under current and future climate conditions.

DATA AVAILABILITY STATEMENT

The original contributions presented in the study are included in the article/**Supplementary Material**, further inquiries can be directed to the corresponding author.

AUTHOR CONTRIBUTIONS

NH-S conceptualized the research with help from KRS and RCH, did labwork for lineage qPCR identification, completed the data analysis, and wrote the manuscript. KRS contributed to conceptualization, co-supervision, and writing (review and editing). XY contributed by developing the methods used for lineage identification by qPCR in this research and by helping NH-S with labwork and data collection. NF contributed by supervising the development of the methods used for lineage identification by qPCR and writing (review and editing). SZ contributed to sample and data acquisition. DO and GR contributed to sample acquisition. CC contributed to data acquisition. RCH contributed to conceptualization. All authors contributed to the article and approved the submitted version.

FUNDING

This research was financially supported by the CoAdapTree Project (241REF), with funding from Genome Canada, Genome British Columbia, Genome Alberta, and Genome Québec (a full list of sponsors is available at https://coadaptree.forestry.ubc.ca/sponsors/). The Pest Risk Management Programme of Natural Resources Canada also provided funding for this project.

ACKNOWLEDGMENTS

We would like to thank the many researchers and assistants who helped provide us with samples and severity data from the different monitoring networks. From the B.C. monitoring network, Lucy Stad, Ann Wong, Jack Sweeten, B A Blackwell and Associates and Kerley and Associates Forestry Consulting. From the Oregon and Washington network, the members of the Swiss Needle Cast Cooperative, particularly Doug Mainwaring and Andrew Bluhm, plus John Browning and Anna Leon. From the Washington monitoring network, Rachel Brooks. We also owe a debt of gratitude to the student lab assistants involved in the quantification of disease severity, including Berni Van der Meer, Alanna Love and Yifan Yuan. Finally, we would like to thank Isabelle Giguère for her essential logistical work in receiving samples from the different networks and providing lab training and overall support throughout the completion of this project.

SUPPLEMENTARY MATERIAL

The Supplementary Material for this article can be found online at: https://www.frontiersin.org/articles/10.3389/ffgc.2021.756678/full#supplementary-material

Supplementary Figure S1 | Assumptions of logistic regression tested on our global model. **(A)** Parametric bootstrap of the deviance simulated on 5000 binomial models. **(B)** Kolmogorov-Smirnov tests for model adjustment and comparisons of standardized residuals with ranked model predictions to test for outliers and model fit, based on 250 simulations of binomial models. **(C)** Various plots to check for residual heterogeneity (residuals vs fitted), normality (QQ-plot), and outliers (Scale-location, residuals vs leverage), as well as to check for patterns in residuals for the different predictors.

Supplementary Data Sheet S1 | Data sheet of SNC presence points collected by Chantal Coté and Naomie Herpin-Saunier. Chantal Coté compiled a collection of points from published articles and online repositories of species occurrences (e.g. GBIF), while Naomie generated additional points by converting shapefiles of areas showing SNC symptoms from aerial surveys by the Swiss Needle Cast Cooperative, Washington Department of Natural Resources and British Columbia Ministry of Forests, Lands, Natural Resource Operations and Rural Development into points. All of these points were combined and rarefied to a 5 km distance between points. These were used as a mask for pseudo-absence data selection in the building of the SDM datasets.

Supplementary Data Sheet S2 | Data sheet of lineages 1 and 2 presence and absence points.

Supplementary Data Sheet S3 | Data sheet of colonization index measurements at Swiss needle cast monitoring sites used for severity modelling.

Supplementary Protocol S1 | Real-time PCR protocol used for lineage presence detection at monitoring sites using multiple pseudothecia per site.

REFERENCES

Araújo, M. B., Whittaker, R. J., Ladle, R. J., and Erhard, M. (2005). Reducing uncertainty in projections of extinction risk from climate change. *Glob. Ecol. Biogeogr.* 14, 529–538.

Barbet-Massin, M., Jiguet, F., Albert, C. H., and Thuiller, W. (2012). Selecting pseudo-absences for species distribution models: how, where and how many? *Methods Ecol. Evol.* 3, 327–338.

Bennett, P. I., Hood, I. A., and Stone, J. K. (2019). The genetic structure of populations of the Douglas-Fir Swiss needle cast fungus *Nothophaeocryptopus gaeumannii* in New Zealand. *Phytopathology* 109, 446–455. doi: 10.1094/PHYTO-06-18-0195-R

Bennett, P. I., and Stone, J. K. (2016). Assessments of population structure, diversity, and phylogeography of the Swiss needle cast fungus (*Phaeocryptopus gaeumannii*) in the U.S. *Pacif. Northwest. For. Trees Livelihoods* 7:14.

Bennett, P. I., and Stone, J. K. (2019). Environmental variables associated with *Nothophaeocryptopus gaeumannii* population structure and Swiss needle cast severity in Western Oregon and Washington. *Ecol. Evol.* 9, 11379–11394. doi: 10.1002/ece3.5639

Beyer, M., Verreet, J.-A., and Ragab, W. S. M. (2005). Effect of relative humidity on germination of ascospores and macroconidia of *Gibberella zeae* and deoxynivalenol production. *Int. J. Food Microbiol.* 98, 233–240. doi: 10.1016/j.ijfoodmicro.2004.07.005

Boyce, J. S. (1940). A needle cast of douglas-fir associated with *Adelopus gaeumannii*. *Phytopathol* 30, 649–659.

Brown, J. L., Bennett, J. R., and French, C. M. (2017). SDMtoolbox 2.0: the next generation Python-based GIS toolkit for landscape genetic, biogeographic and species distribution model analyses. *PeerJ* 5:e4095. doi: 10.7717/peerj.4095

Burnham, K. P., and Anderson, D. R. (Eds.) (2002). *Model Selection and Multimodel Inference: A Practical Information–Theoretic Approach*. New York, NY: Springer.

Calin-Jageman, R. J., and Cumming, G. (2019). The New statistics for better science: ask how much, how uncertain, and what else is known. *Am. Stat.* 73(Supp 1), 271–280. doi: 10.1080/00031305.2018.1518266

Capitano, B. R. (1999). *The Infection and Colonization of Douglas-fir Needles by the Swiss Needle Cast Pathogen, Phaeocryptopus gaeumannii* (Rhode) Petrak (MS Thesis). Corvallis, OR: Oregon State University.

Desprez-Loustau, M.-L., Aguayo, J., Dutech, C., Hayden, K. J., Husson, C., Jakushkin, B., et al. (2016). An evolutionary ecology perspective to address forest pathology challenges of today and tomorrow. *Ann. For. Sci.* 73, 45–67. doi: 10.1007/s13595-015-0487-4

Drenth, A., McTaggart, A. R., and Wingfield, B. D. (2019). Fungal clones win the battle, but recombination wins the war. *IMA Fungus* 10:18.

Drew Harvell, C., Mitchell, C. E., Ward, J. R., Altizer, S., Dobson, A. P., Ostfeld, R. S., et al. (2002). Climate warming and disease risks for terrestrial and marine Biota. *Science* 296, 2158–2162. doi: 10.1126/science.1063699

El-Hajj, Z., Kavanagh, K., Rose, C., and Kanaan-Atallah, Z. (2004). Nitrogen and carbon dynamics of a foliar biotrophic fungal parasite in fertilized Douglas-fir. *New Phytol.* 163, 139–147. doi: 10.1111/j.1469-8137.2004.01102.x

Elliott, M., Sumampong, G., Varga, A., Shamoun, S. F., James, D., Masri, S., et al. (2011). Phenotypic differences among three clonal lineages of *Phytophthora ramorum*. *For. Pathol.* 41, 7–14. doi: 10.1111/j.1439-0329.2009.00627.x

Feau, N., Lauron-Moreau, A., Piou, D., Marçais, B., Dutech, C., and Desprez-Loustau, M.-L. (2012). Niche partitioning of the genetic lineages of the oak powdery mildew complex. *Fungal Ecol.* 5, 154–162. doi: 10.1016/j.funeco.2011.12.003

Filip, G. M., Kanaskie, A., Kavanagh, K. L., Johnson, G., Johnson, R., and Maguire, D. A. (2000). *Silviculture and Swiss Needle Cast: Research and Recommendations.* Corvallis, OR: Forest Research Laboratory, Oregon State University.

Gaumann. (1928). Eine neue krankheit der douglastanne. *Zeitschrift Fur Pflanzenkrankheiten Pflanzenschutz* 38, 70–78.

Geng, S., Campbell, R. N., Carter, M., and Hills, F. J. (1983). Quality control programs for seedborne pathogens. *Plant Dis.* 67, 236–242. doi: 10.1094/pd-67-236

Gotelli, N. J., and Stanton-Geddes, J. (2015). Climate change, genetic markers and species distribution modelling. *J. Biogeogr.* 42, 1577–1585. doi: 10.1111/jbi.12562

Guisan, A., Thuiller, W., and Zimmermann, N. E. (2017). *Habitat Suitability and Distribution Models: With Applications in R*. Cambridge: Cambridge University Press.

Hamelin, F. M., Bisson, A., Desprez-Loustau, M.-L., Fabre, F., and Mailleret, L. (2016). Temporal niche differentiation of parasites sharing the same plant host: oak powdery mildew as a case study. *Ecosphere* 7:e01517.

Hansen, E. M., Stone, J. K., Capitano, B. R., Rosso, P., Sutton, W., Winton, L., et al. (2000). Incidence and impact of Swiss needle cast in forest plantations of Douglas-fir in Coastal Oregon. *Plant Dis.* 84, 773–778. doi: 10.1094/PDIS.2000.84.7.773

Hardin, G. (1960). The competitive exclusion principle. *Science* 131, 1292–1297.

Hessenauer, P., Feau, N., Gill, U., Schwessinger, B., Brar, G. S., and Hamelin, R. C. (2021). Evolution and adaptation of forest and crop pathogens in the *Anthropocene*. *Phytopathology* 111, 49–67. doi: 10.1094/PHYTO-08-20-0358-FI

Hessenauer, P., Fijarczyk, A., Martin, H., Prunier, J., Charron, G., Chapuis, J., et al. (2020). Hybridization and introgression drive genome evolution of Dutch elm disease pathogens. *Nat. Ecol. Evol.* 4, 626–638. doi: 10.1038/s41559-020-1133-6

Hoffmann, A. A., and Sgrò, C. M. (2011). Climate change and evolutionary adaptation. *Nature* 470, 479–485.

Hood, I. A., and Kershaw, J. D. (1975). *Distribution and Infection Period of Phaeocryptopus gaeumannii in New Zealand*. Available online at: https://www.scionresearch.com/__data/assets/pdf_file/0006/58848/NZJFS51975HOOD201_208.pdf (accessed October 30, 1974).

Johnson, G. R. (2002). Genetic variation in tolerance of Douglas-fir to Swiss needle cast as assessed by symptom expression. *Silvae Genet.* 51, 80–88.

Lan, Y.-H., Shaw, D. C., Ritóková, G., and Hatten, J. A. (2019a). Associations between Swiss needle cast severity and foliar nutrients in young-growth Douglas-fir in Coastal Western Oregon and Southwest Washington, USA. *For. Sci.* 65, 537–542. doi: 10.1093/forsci/fxz022

Lan, Y. H., Shaw, D. C., Beedlow, P. A., Lee, E. H., and Waschmann, R. S. (2019b). Severity of Swiss needle cast in young and mature Douglas-fir forests in western Oregon, USA. *For. Ecol. Manag.* 442, 79–95. doi: 10.1016/j.foreco.2019.03.063

Lavender, D. P., and Hermann, R. K. (2014). *The Genus Pseudotsuga*. Available online at: https://www.for.gov.bc.ca/ftp/rsi/external/!publish/Dry%20Fir%20Committee/Literature%20Review/Baseline%20Literature/Lavender_Hermann_2014_Douglasfir.pdf (accessed June 25, 2021).

Lee, E. H., Beedlow, P. A., Waschmann, R. S., Burdick, C. A., and Shaw, D. C. (2013). Tree-ring analysis of the fungal disease Swiss needle cast in western Oregon coastal forests. *Can. J. For. Res.* 43, 677–690. doi: 10.1139/cjfr-2013-0062

Lee, E. H., Beedlow, P. A., Waschmann, R. S., Tingey, D. T., Cline, S., Bollman, M., et al. (2017). Regional patterns of increasing Swiss needle cast impacts on Douglas-fir growth with warming temperatures. *Ecol. Evol.* 7, 11167–11196. doi: 10.1002/ece3.3573

Little, E. L. (1971). *Atlas of United States trees. Volume 1. Conifers and Important Hardwoods. Miscellaneous Publication 1146.* Washington, DC: U.S. Department of Agriculture, Forest Service, 320.

Liu, C., Newell, G., and White, M. (2019). The effect of sample size on the accuracy of species distribution models: considering both presences and pseudo-absences or background sites. *Ecography* 42, 535–548. doi: 10.1111/ecog.03188

Liu, C., Wolter, C., Xian, W., and Jeschke, J. M. (2020). Most invasive species largely conserve their climatic niche. *Proc. Natl. Acad. Sci. U.S.A.* 117, 23643–23651. doi: 10.1073/pnas.2004289117

Maguire, B. (1973). Niche response structure and the analytical potentials of its relationship to the habitat. *Am. Natural.* 107, 213–246.

Maguire, D. A., Kanaskie, A., and Voelker, W. (2002). Growth of young Douglas-fir plantations across a gradient in Swiss needle cast severity. *West. J. Appl. For.* 17, 86–95. doi: 10.1093/wjaf/17.2.86

Maguire, D. A., Mainwaring, D. B., and Kanaskie, A. (2011). Ten-year growth and mortality in young Douglas-fir stands experiencing a range in Swiss needle cast severity. *Can. J. For. Res.* 41, 2064–2076. doi: 10.1139/x11-114

Manter, D. K., Bond, B. J., Kavanagh, K. L., Rosso, P. H., and Filip, G. M. (2000). *Pseudothecia* of Swiss needle cast fungus, *Phaeocryptopus gaeumannii*, physically block stomata of Douglas fir, reducing CO2 assimilation. *New Phytol.* 148, 481–491. doi: 10.1046/j.1469-8137.2000.00779.x

Manter, D. K., Reeser, P. W., and Stone, J. K. (2005). A climate-based model for predicting geographic variation in swiss needle cast severity in the Oregon Coast range. *Phytopathology* 95, 1256–1265. doi: 10.1094/PHYTO-95-1256

Manter, D. K., Winton, L. M., Filip, G. M., and Stone, J. K. (2003). Assessment of Swiss needle cast disease: temporal and spatial investigations of fungal colonization and symptom severity. Phytopathologische Zeitschrift. *J. Phytopathol.* 151, 344–351. doi: 10.1046/j.1439-0434.2003.00730.x

Marmion, M., Parviainen, M., Luoto, M., Heikkinen, R. K., and Thuiller, W. (2009). Evaluation of consensus methods in predictive species distribution modelling. *Divers. Distrib.* 15, 59–69. doi: 10.1111/j.1472-4642.2008.00491.x

Mazerolle, M. J. (2017). *Package "AICcmodavg." R Package*. 281. Available online at: https://cran.uib.no/web/packages/AICcmodavg/AICcmodavg.pdf (accessed August 21, 2020).

McDowell, N. G., Williams, A. P., Xu, C., Pockman, W. T., Dickman, L. T., Sevanto, S., et al. (2016). Multi-scale predictions of massive conifer mortality due to chronic temperature rise. *Nat. Clim. Chang.* 6, 295–300. doi: 10.1038/nclimate2873

Michaels, E., and Chastagner, G. A. (1984). Seasonal availability of *Phaeocryptopus gaeumannii* ascospores and conditions that influence their release. *Plant Dis.* 68, 942–944. doi: 10.1094/pd-69-942

Mildrexler, D. J., Shaw, D. C., and Cohen, W. B. (2019). Short-term climate trends and the Swiss needle cast epidemic in Oregon's public and private coastal forestlands. *For. Ecol. Manag.* 432, 501–513. doi: 10.1016/j.foreco.2018.09.025

Mildrexler, D. J., Yang, Z., Cohen, W. B., and Bell, D. M. (2016). A forest vulnerability index based on drought and high temperatures. *Remote Sens. Environ.* 173, 314–325.

Montwé, D., Elder, B., Socha, P., Wyatt, J., Noshad, D., Feau, N., et al. (2021). Swiss needle cast tolerance in British Columbia's coastal Douglas-fir breeding population. *Forestry* 94, 193–203. doi: 10.1093/forestry/cpaa024

Moss, R. H., Edmonds, J. A., Hibbard, K. A., Manning, M. R., Rose, S. K., van Vuuren, D. P., et al. (2010). The next generation of scenarios for climate change research and assessment. *Nature* 463, 747–756. doi: 10.1038/nature08823

Nadeau, C. P., and Urban, M. C. (2019). Eco-evolution on the edge during climate change. *Ecography* 42, 1280–1297. doi: 10.1086/704780

Ojeda Alayon, D. I., Tsui, C. K. M., Feau, N., Capron, A., Dhillon, B., Zhang, Y., et al. (2017). Genetic and genomic evidence of niche partitioning and adaptive radiation in mountain pine beetle fungal symbionts. *Mol. Ecol.* 26, 2077–2091. doi: 10.1111/mec.14074

Pandit, K., Smith, J., Quesada, T., Villari, C., and Johnson, D. J. (2020). Association of recent incidence of foliar disease in pine species in the Southeastern United States with Tree and Climate Variables. *Forests* 11:1155. doi: 10.3390/f11111155

Pedlar, J. H., McKenney, D. W., Hope, E., Reed, S., and Sweeney, J. (2020). Assessing the climate suitability and potential economic impacts of Oak wilt in Canada. *Sci. Rep.* 10:19391. doi: 10.1038/s41598-020-75549-w

Peterson, A. T., Soberón, J., and Sánchez-Cordero, V. (1999). Conservatism of ecological niches in evolutionary time. *Science* 285, 1265–1267. doi: 10.1126/science.285.5431.1265

Préau, C., Isselin-Nondedeu, F., Sellier, Y., Bertrand, R., and Grandjean, F. (2019). Predicting suitable habitats of four range margin amphibians under climate and land-use changes in southwestern France. *Reg. Environ. Chang.* 19, 27–38. doi: 10.1007/s10113-018-1381-z

Purse, B. V., and Golding, N. (2015). Tracking the distribution and impacts of diseases with biological records and distribution modelling. *Biol. J. Linn. Soc.* 115, 664–677. doi: 10.1186/s12868-016-0283-6

Ritóková, G., Mainwaring, D. B., Shaw, D. C., and Lan, Y.-H. (2021). Douglas-fir foliage retention dynamics across a gradient of Swiss needle cast in coastal Oregon and Washington. *Can. J. For. Res.* 51, 573–582. doi: 10.1139/cjfr-2020-0318

Ritóková, G., Shaw, D. C., Filip, G., Kanaskie, A., and Norlander, D. (2016). Swiss needle cast in western oregon douglas-fir plantations: 20-year monitoring results. *For. Trees Livelihoods* 7:155.

Rosso, P. H., and Hansen, E. M. (2003). Predicting swiss needle cast disease distribution and severity in young douglas-fir plantations in coastal Oregon. *Phytopathology* 93, 790–798. doi: 10.1094/PHYTO.2003.93.7.790

Shaw, D. C., Ritóková, G., Lan, Y.-H., Mainwaring, D. B., Russo, A., Comeleo, R., et al. (2021). Persistence of the Swiss needle cast outbreak in Oregon Coastal Douglas-fir and new insights from research and monitoring. *J. For.* 119, 407–421.

Shaw, D. C., Woolley, T., and Kanaskie, A. (2014). Vertical foliage retention in Douglas-fFir across environmental gradients of the Western Oregon Coast range influenced by Swiss needle cast. *Northwest Sci.* 88, 23–32. doi: 10.3955/046.088.0105

Shaw, M. W., and Osborne, T. M. (2011). Geographic distribution of plant pathogens in response to climate change. *Plant Pathol.* 60, 31–43. doi: 10.1111/j.1365-3059.2010.02407.x

Stone, J. K., Capitano, B. R., and Kerrigan, J. L. (2008a). The histopathology of *Phaeocryptopus gaeumannii* on Douglas-fir needles. *Mycologia* 100, 431–444. doi: 10.3852/07-170r1

Stone, J. K., Coop, L. B., and Manter, D. K. (2008b). Predicting effects of climate change on Swiss needle cast disease severity in Pacific Northwest forests. *Can. J. Plant Pathol.* 30, 169–176.

Stone, J. K., Hood, I. A., Watt, M. S., and Kerrigan, J. L. (2007). Distribution of Swiss needle cast in New Zealand in relation to winter temperature. *Australas. Plant Pathol. APP* 36, 445–454.

Sturrock, R. N., Frankel, S. J., Brown, A. V., Hennon, P. E., Kliejunas, J. T., Lewis, K. J., et al. (2011). Climate change and forest diseases. *Plant Pathol.* 60, 133–149. doi: 10.1016/j.actatropica.2021.106123

Thuiller, W., Lafourcade, B., Engler, R., and Araújo, M. B. (2009). BIOMOD - a platform for ensemble forecasting of species distributions. *Ecography* 32, 369–373. doi: 10.1111/j.1600-0587.2008.05742.x

Thuiller, W., Lavorel, S., Araújo, M. B., Sykes, M. T., and Colin Prentice, I. (2005). Climate change threats to plant diversity in Europe. *Proc. Natl. Acad. Sci. U.S.A.* 102, 8245–8250. doi: 10.1073/pnas.0409902102

Wang, T., Hamann, A., Spittlehouse, D., and Carroll, C. (2016). Locally downscaled and spatially customizable climate data for historical and future periods for North America. *PLoS One* 11:e0156720. doi: 10.1371/journal.pone.0156720

Watts, A., Meinzer, F., and Saffell, B. J. (2014). *Fingerprints of a Forest Fungus: Swiss Needle Cast, Carbon Isotopes, Carbohydrates, and Growth in Douglas-fir. Science Findings 167*. Portland, OR: US Department of Agriculture, Forest Service, Pacific Northwest Research Station, 167.

Weiskittel, A. R., Crookston, N. L., and Rehfeldt, G. E. (2012). Projected future suitable habitat and productivity of Douglas-fir in western North America. *Schweiz. Z. For.* 163, 70–78.

Wicklow, D. T., and Zak, J. C. (1979). Ascospore germination of carbonicolous ascomycetes in fungistatic soils: an ecological interpretation. *Mycologia* 71, 238–242.

Wilhelmi, N. P., Shaw, D. C., Harrington, C. A., St. Clair, J. B., and Ganio, L. M. (2017). Climate of seed source affects susceptibility of coastal Douglas-fir to foliage diseases. *Ecosphere* 8:e02011.

Winton, L. M., Hansen, E. M., and Stone, J. K. (2006). Population structure suggests reproductively isolated lineages of *Phaeocryptopus gaeumannii*. *Mycologia* 98, 781–791. doi: 10.3852/mycologia.98.5.781

Yin, X., Feau, N., Tanney, J. B., and Hamelin, R. C. (2020). Mining herbarium samples to study adaptation to climate change in a tree pathogen. [Conference Presentation Abstract]. British Columbia regional meeting, 2020/Réunion régionale de la Colombie-Britannique, 2020. *Can. J. Plant Pathol.* 43, 332–338. doi: 10.1080/07060661.2021.1889804

Conflict of Interest: The authors declare that the research was conducted in the absence of any commercial or financial relationships that could be construed as a potential conflict of interest.

Publisher's Note: All claims expressed in this article are solely those of the authors and do not necessarily represent those of their affiliated organizations, or those of the publisher, the editors and the reviewers. Any product that may be evaluated in this article, or claim that may be made by its manufacturer, is not guaranteed or endorsed by the publisher.

List of Refereed Publications

Disease Distribution, Severity and Epidemiology

Agne, MC, Beedlow PA, Shaw DC, Woodruff DR, Lee EH, Cline S, Comeleo RL. 2018. Interactions of predominant insects and diseases with climate change in Douglas-fir forests of western Oregon and Washington, U.S.A.. Forest Ecology and Management. 409:317-332.

Hansen, E. M., Stone, J. K., Capitano, B. R., Rosso, P., Sutton, W., Winton, L., Kanaskie, A. and M. G. McWilliams. 2000. Incidence and impact of Swiss needle cast in forest plantations of Douglas-fir in coastal Oregon. Plant Disease. 84: 773-779.

Hennon, P.E., Frankel, S.J., Woods, A.J., Worrall, J.J., Ramsfield, T.D., Zambino, P.J., Shaw, D.C., Ritóková, G., Warwell, M.V., Norlander, D. and Mulvey, R.L., 2021. Applications of a conceptual framework to assess climate controls of forest tree diseases. Forest Pathology, 51(6), p.e12719.

Lan Y-H, Shaw D.C., Beedlow P.A., Lee E.H., Waschmann R.S.. 2019. Severity of Swiss needle cast in young and mature Douglas-fir forests in western Oregon, USA. Forest Ecology and Management. 442:79-95.

Manter, D. K., Reeser, P. W., and J. K. Stone. 2005. A climate-based model for predicting geographic variation in Swiss needle cast severity in the Oregon coast range. Phytopathology. 95: 1256-1265.

Ritóková, G, Shaw DC, Filip GM, Kanaskie A, Browning J, Norlander D. 2016. Swiss Needle Cast in Western Oregon Douglas-Fir Plantations: 20-Year Monitoring Results. Forests. 7(155)

Ritóková, G, Mainwaring, D.B., Shaw D.C., Lan, Y-H. 2020. Douglas-fir foliage retention dynamics across a gradient of Swiss needle cast in coastal Oregon and Washington. Canadian Journal of Forest Research. https://doi.org/10.1139/cjfr-2020-0318

Rosso, P. H. and E. M. Hansen. 2003. Predicting Swiss needle cast disease distribution and severity in young Douglas-fir plantations in coastal Oregon. Phytopathology. 93: 790-798.

Shaw D.C., Ritóková, G, Lan, Y-H, Mainwaring, D.B., Russo, A., Comeleo, R., Navaro, S., Norlander, D., Smith, B. 2021. Persistence of the Swiss Needle Cast Outbreak in Oregon Coastal Douglas-fir, and New Insights from Research and Monitoring. Journal of Forestry.

Stone, J. K., Hood, I. A., Watt, M. S. and J. L. Kerrigan. 2007. Distribution of Swiss needle cast in New Zealand in relation to winter temperature. Australasian Plant Pathology. 36: 445-454.

Stone, J. K., Capitano, B. R. and J. L. Kerrigan. 2008. The histopathology of *Phaeocryptopus gaeumannii* on Douglas-fir needles. Mycologia. 100: 431-444.

Stone, J. K., Coop, L. B. and D. K. Manter. 2008. Predicting the effects of climate change on Swiss needle cast disease severity in Pacific Northwest forests. Canadian Journal of Plant Pathology. 30: 169-176.

Watt, M. S., Stone, J. K., Hood, I. A. and D. J. Palmer. 2010. Predicting the severity of Swiss needle cast on Douglas-fir under current and future climate in New Zealand. Forest Ecology and Management (*in press*).

Forest Protection Issues

Kelsey, R. G. and D. K. Manter. 2004. Effect of Swiss needle cast on Douglas-fir stem ethanol and monoterpene concentrations, oleoresin flow, and host selection by the Douglas-fir beetle. Forest Ecology and Management. 190: 241-253.

Shaw, D. C., Filip, G. M., Kanaskie, A., Maguire, D. A. and W. Littke. 2011. Managing an epidemic of Swiss needle cast in the Douglas-fir region of Oregon: The Swiss Needle Cast Cooperative. Journal of Forestry (*in press*).

Genetic Resistance/Tolerance in Douglas-fir

Jayawickrama, K.J.S., D. Shaw, and T.Z. Ye. 2012. Genetic Selection in Coastal Douglas-fir for tolerance to Swiss Needle Cast Disease. Proceedings of the fourth international workshop on the genetics of host-parasite interactions in forestry: Disease and insect resistance in forest trees. Gen. Tech. Rep. PSW-GTR-240. Albany, CA: Pacific Southwest Research Station, Forest Service, U.S. Department of Agriculture. 372 p.

Johnson, G. R. 2002. Genetic variation in tolerance of Douglas-fir to Swiss needle cast as assessed by symptom expression. Silvae Genetica. 51: 80-86.

Kastner, W., Dutton, S. and D. Roche. 2001. Effects of Swiss needle cast on three Douglas-fir seed sources on a low-elevation site in the northern Oregon Coast Range: Results after five growing seasons. Western Journal of Applied Forestry. 16 (1): 31-34.

Temel, F., Johnson, G. R. and J. K. Stone. 2004. The relationship between Swiss needle cast symptom severity and level of *Phaeocryptopus gaeumannii* colonization in coastal Douglas-fir (*Pseudotsuga menziesii var. menziesii*). Forest Pathology. 34: 383-394.

Temel, F., Johnson, G. R. and W. T. Adams. 2005. Early genetic testing of coastal Douglas-fir for Swiss needle cast tolerance. Canadian Journal of Forest Research. 35: 521-529.

Wilhelmi, N.P., Shaw D.C., Harrington C.A., St. Clair J.B., Ganio L.M. 2017. Climate of seed source affects susceptibility of coastal Douglas-fir to foliage diseases. Ecosphere. 8(12):e02011.

Genetics of Nothophaeocryptopus gaeumannii

Bennett P, Hood P.I, Stone J.K.. 2018. The genetic structure of populations of the Douglas-fir Swiss needle cast fungus *Nothophaeocryptopus gaeumannii* in New Zealand. Phytopathology. 109:446-455.

Bennett P, Stone J.K.. 2019. Environmental variables associated with *Nothophaeocryptopus gaeumannii* population structure and Swiss needle cast severity in Western Oregon and Washington. Ecology and Evolution. 9(19):11379-11394.

Herpin-Saunier, N.Y., Sambaraju, K.R., Yin, X., Feau, N., Zeglen, S., Ritokova, G., Omdal, D., Côté, C. and Hamelin, R.C.. 2022. Genetic lineage distribution modeling to predict epidemics of a conifer disease. Frontiers in Forests and Global Change. 4:229-243.

Winton, L. M., Hansen, E. M. and J. K. Stone. 2006. Population structure suggests reproductively isolated lineages of *Phaeocryptopus gaeumannii*. Mycologia. 98 (5): 781-791.

Winton. L. M., Stone, J. K. and E. M. Hansen. 2007. The systematic position of *Phaeocryptopus gaeumannii*. Mycologia. 99: 240-252.

Hydrology

Bladon KD, Bywater-Reyes S, LeBoldus JM, Keriö S, Segura C, Ritóková G, Shaw D.C.. 2019. Increased streamflow in catchments affected by a forest disease epidemic. Science of The Total Environment. 691:112-123.

Mensuration and growth effects

Lee, E.H., Beedlow P.A., Waschmann R.S., Tingey D.T., Cline S., Bollman M., Wickham C., Carlile C. 2017. Regional patterns of increasing Swiss needle cast impacts on Douglas-fir growth with warming temperatures. Ecology and Evolution. 7(24):11167–11196.

Maguire D. A., Kanaskie, A., Voelker, W., Johnson, R. and G. Johnson. 2002. Growth of young Douglas-fir plantations across a gradient in Swiss needle cast severity. Western Journal of Applied Forestry. 17: 86-95.

Maguire, D. A. and A. Kanaskie. 2002. The ratio of live crown length to sapwood area as a measure of crown sparseness. Forest Science. 48: 93-100.

Maguire, D. A., Mainwaring, D. B. and Kanaskie A. 2011. Ten-year growth and mortality in young Douglas-fir stands experiencing a range in Swiss needle cast severity. Can. J. For. Res. 41: 2064-2076.

Weiskittel, A. R., Garber, S. M., Johnson, G. P., Maguire, D. A. and R.A. Monserud. 2007. Annualized diameter and height growth equations for Pacific Northwest plantation-grown Douglas-fir, western hemlock, and red alder. Forest Ecology and Management. 250: 266-278.

Weiskittel, A. R., Maguire, D. A., Garber, S. M. and A. Kanaskie. 2006. Influence of Swiss needle cast on foliage age class structure and vertical distribution in Douglas-fir plantations of north coastal Oregon. Canadian Journal of Forest Research. 36: 1497-1508.

Weiskittel, A. R., Maguire, D. A. and R. A. Monserud. 2007. Modeling crown structural responses to competing vegetation control, thinning, fertilization, and Swiss needle cast in coastal Douglas-fir of the Pacific Northwest, USA. Forest Ecology and Management. 245: 96-109.

Weiskittel, A. R., Maguire, D. A. and R. A. Monserud. 2007. Response of branch growth and mortality to silvicultural treatments in coastal Douglas-fir plantations: Implications for predicting tree growth. Forest Ecology and Management. 251: 182-194.

Weiskittel, A. R. and D. A. Maguire. 2007. Response of Douglas-fir leaf area index and litterfall dynamics to Swiss needle cast in north coastal Oregon, USA. Annals of Forest Science. 64: 121-132.

Weiskittel, A. R. and D. A. Maguire. 2006. Branch surface area and its vertical distribution in coastal Douglas-fir. Trees. 20: 657-667.

Weiskittel, A. R., Temesgen, H., Wilson, D. S. and D. A. Maguire. 2008. Sources of within and between-stand variability in specific leaf area of three ecologically distinct conifer species. Annals of Forest Science. 65: 103-112.

Zhao, J., Maguire, D. A., Mainwaring, D. B., Kanaskie, A. 2012. Climatic influences on needle cohort survival mediated by Swiss needle cast in coastal Douglas-fir. Trees 26: 1361-1371

Zhao, J., Mainwaring, D. B., Maguire, D. A., Kanaskie, A. 2011. Regional and annual trends in Douglas-fir foliage retention: Correlations with climatic variables. For. Ecol. And Management 262: 1872-1886

Zhao, J, Maguire DA, Mainwaring DB, Kanaskie A. 2015. The effect of within-stand variation in Swiss needle cast intensity on Douglas-fir stand dynamics. Forest Ecology and Management. 347:75-82.

Zhao, J., Maguire, D. A., Mainwaring, D. B., Wehage, J., Kanaskie, A. 2013. Thinning Mixed Species Stands of Douglas-Fir and Western Hemlcok in the Presence of Swiss Needle Cast: Guidelines Based on Relative Basal Area Growth of Individual Trees. For. Sci. 60 (1): 191-199.

Nutrition and soil interactions

El-Hajj, Z., Kavanagh, K., Rose, C., and Z. Kanaan-Atallah. 2004. Nitrogen and carbon dynamics of a foliar biotrophic fungal parasite in fertilized Douglas-fir. New Phytologist. 163: 139-147.

Lan Y-H, Shaw D.C., Ritóková G, Hatten J. 2019. Associations between Swiss Needle Cast Severity and Foliar Nutrients in Young-Growth Douglas-Fir in Coastal Western Oregon and Southwest Washington, USA. For. Sci. 65(5):537-542.

Mulvey, R.L., Shaw, D.C., Maguire, D.A. 2013. Fertilization impacts on Swiss needle cast disease severity in Western Oregon. Forest Ecology and Management 287: 147-158.

Perakis, S. S., Maguire, D. A., Bullen, T. D., Cromack, K., Waring, R. H. and J. R. Boyle. 2005. Coupled nitrogen and calcium cycles in forests of the Oregon Coast Range. Ecosystems. 8: 1-12.

Waring, R. H., Boyle, J., Cromack, K. Jr., Maguire, D. and A. Kanaskie. 2000. Researchers offer new insights into Swiss needle cast. Western Forester. 45 (6): 10-11.

Pathology and physiological host effects

Bennett, P., Stone, J. 2016. Assessments of Population Structure, Diversity, and Phylogeography of the Swiss Needle Cast Fungus (*Phaeocryptopus gaeumannii*) in the U.S. Pacific Northwest. Forests: 7, 14.

Black, B. A., Shaw, D. C. and J. K. Stone. 2010. Impacts of Swiss needle cast on overstory Douglas-fir forests of western Oregon Coast Range. Forest Ecology and Management. 259: 1673-1680.

Gervers, K. A., Thomas, D. C., Roy, B. A., Spatafora, J. W. and Busby, P. E. 2022. Crown closure affects endophytic leaf mycobiome compositional dynamics over time in *Pseudotsuga menziesii* var. *menziesii*. Fungal Ecology. 57–58:101155.

Lee, E.H., Beedlow, P.A., Waschmann, R.S., Cline, S., Bollman, M., Wickham, C. and Testa, N., 2021. Tree-ring history of Swiss needle cast impact on Douglas-fir growth in Western Oregon: correlations with climatic variables. J Plant Sci Phytopathol. 5:076-087.

Lee, E.H., Beedlow, P.A., Brooks, J.R., Tingey, D.T., Wickham, C. and Rugh, W., 2022. Physiological responses of Douglas-fir to climate and forest disturbances as detected by cellulosic carbon and oxygen isotope ratios. Tree Physiology, 42(1):5-25.

Lee, H.E., Beedlow, P.A., Waschamnn, R.S., Burdick, C.A., Shaw, D.C. 2013. Tree-ring analysis of the fungal disease Swiss needle cast in western Oregon coastal forests. Can Journal of For. 43(8):677-690.

Manter, D. K., Bond, B. J., Kavanagh, K. L., Rosso, P. H. and G. M. Filip. 2000. Pseudothecia of Swiss needle cast fungus, *Phaeocryptopus gaeumannii,* physically block stomata of Douglas-fir, reducing CO_2 assimilation. New Phytologist. 148 (3): 481-491.

Manter, D. K. 2002. Energy dissipation and photoinhibition in Douglas-fir needles with a fungal-mediated reduction in photosynthetic rates. Phytopathology. 150: 674-679.

Manter, D. K., Bond, B. J., Kavanagh, K. L., Stone, J. K. and G. M. Filip. 2003. Modeling the impacts of the foliar pathogen, *Phaeocryptopus gaeumannii*, on Douglas-fir physiology: net canopy carbon assimilation, needle abscission and growth. Ecological Modeling. 164: 211-226.

Manter, D. K. and Kavanagh, K. L. 2003. Stomatal regulation in Douglas-fir following a fungal-mediated chronic reduction in leaf area. Trees. 17: 485-491.

Manter, D. K., Kelsey, R. G., and J. K. Stone. 2001. Quantification of *Phaeocryptopus gaeumannii* colonization in Douglas-fir needles by ergosterol analysis. Forest Pathology. 31: 229-240.

Manter, D. K., Winton, L. M., Filip, G. M. and J. K. Stone. 2003. Assessment of Swiss needle cast disease: temporal and spatial investigations of fungal colonization and symptom severity. Phytopathology. 151: 344-351.

Saffell, B.J., Meinzer, R.C., Voelker, S.L., Shaw, D.C., Brooks, R.J., Lachenbruch, B, McKay, J. 2014. Tree-ring stable isotopes record the impact of a foliar fungal pathogen on CO_2 assimilation and growth in Douglas-fir. Plant, Cell & Environment. doi: 10.1111/pce.12256

Winton, L. M., Manter, D. K., Stone, J. K. and E. M. Hansen. 2003. Comparison of biochemical, molecular and visual methods to quantify *Phaeocryptopus gaeumannii* in Douglas-fir foliage. Phytopathology. 93: 121-126.

Winton, L. M., Stone, J. K., Watrud, L. S. and E. M. Hansen. 2002. Simultaneous one-tube quantification of host and pathogen DNA with real-time polymerase chain reaction. Phytopathology. 92: 112-116.

Winton, L. M., Stone, J. K. and E. M. Hansen. 2007. Polymorphic microsatellite markers for the Douglas-fir pathogen *Phaeocryptopus gaeumannii*, causal agent of Swiss needle cast disease. Molecular Ecology. 7: 1125-1128.

Silviculture and Control

Filip, G., Kanaskie, A., Kavanagh, K., Johnson, G., Johnson, R. and D. Maguire. 2000. Research Contribution 30, Forest Research Laboratory, College of Forestry, Oregon State University, Corvallis, Oregon.

Mainwaring, D. B., Maguire, D. A., Kanaskie, A. and J. Brandt. 2005. Growth responses to commercial thinning in Douglas-fir stands with varying intensity of Swiss needle cast. Canadian Journal of Forest Research. 35: 2394-2402.

Stone, J. K., Reeser, P. W. and A. Kanaskie. 2007. Fungicidal suppression of Swiss needle cast and pathogen reinvasion in a 20-year-old Douglas-fir stand. Western Journal of Applied Forestry. 22: 248-252.

Wood Quality

Grotta, A. T., Leichti, R. J., Gartner, B. L. and G. R. Johnson. 2004. Effect of growth ring orientation and placement of earlywood and latewood on MOE and MOR of very-small clear Douglas-fir beams. Wood and Fiber Science. 37: 207-212.

Johnson, G. R., Gartner, B. L., Maguire, D. and A. Kanaskie. 2003. Influence of Bravo fungicide applications on wood density and moisture content of Swiss needle cast affected Douglas-fir trees. Forest Ecology and Management. 186: 339-348.

Johnson, G. R., Grotta, A. T., Gartner, B. L. and G. Downes. 2005. Impact of the foliar pathogen Swiss needle cast on wood quality of Douglas-fir. Canadian Journal of Forest Research. 35: 331-339.

Lachenbruch, B., Johnson, G.R. 2020. Different radial growth rate effects on outerwood properties of coastal Douglas-fir in healthy trees vs. trees impacted by Swiss Needle Cast. Canadian Journal of Forest Research. https://doi.org/10.1139/cjfr-2020-0199